Technical Report

INSTITUTES FOR ENVIRONMENTAL RESEARCH IER 1-ITSA 1

Predicting Statistical Performance Indexes for High Frequency Ionospheric Telecommunications Systems

DONALD L. LUCAS

GEORGE W. HAYDON

THE INSTITUTES FOR ENVIRONMENTAL RESEARCH

The mission of the Institutes is to study the oceans, and inland waters, the lower and upper atmosphere, the space environment, and the earth, seeking the understanding needed to provide more useful services. These research Institutes are:

- The Institute for Earth Sciences
  conducts exploratory and applied research in geomagnetism, seismology, geodesy, and related earth sciences.

- The Institute for Oceanography
  works to increase knowledge and improve understanding of the ocean and its interaction with the total physical environment of the globe.

- The Institute for Atmospheric Sciences
  seeks the understanding of atmospheric processes and phenomena that is required to improve weather forecasts and related services and to modify and control the weather.

- The Institute for Telecommunication Sciences and Aeronomy
  supports the Nation's telecommunications by conducting research and providing services related to radio, infrared, and optical waves as they travel from a transmitter to a receiver. The Institute is also active in the study and prediction of periods of solar activity and ionospheric disturbance.

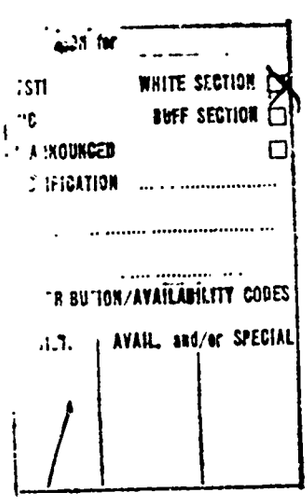

Environmental Science Services Administration

Boulder, Colo.

U. S. DEPARTMENT OF COMMERCE
John T. Connor, Secretary
ENVIRONMENTAL SCIENCE SERVICES ADMINISTRATION
Robert M. White, Administrator
INSTITUTES FOR ENVIRONMENTAL RESEARCH
George S. Benton, Director

ESSA TECHNICAL REPORT IER 1-ITSA 1

Predicting Statistical Performance Indexes for High Frequency Ionospheric Telecommunications Systems

DONALD L. LUCAS

GEORGE W. HAYDON

INSTITUTE FOR TELECOMMUNICATION SCIENCES AND AERONOMY
BOULDER, COLORADO
August, 1966

FOREWORD

Staff, Frequency Utilization Section:

R.M. Davis, Jr.
Gerald G. Gilbert
Rodney A. Hanson
John D. Harper, Jr.
Stephen R. McCammon
Robert S. Rauschenberger
Olaf D. Remmler
Charles O. Stearns
Kenneth K. Tagawa

This work was sponsored by the Department of the Navy, Naval Electronics Systems Command (NESC), Bailey's Crossroads, Virginia, Project Order No. 6-0034 under the SS-267 Program (Task 7040).

Table of Contents

	Page
List of Tables	vi
List of Figures	x
Abstract	xiii
1. Introduction	1
2. Philosophy of Prediction Method	2
3. Basic Ionospheric Data	3
3. 1. F2-Region Ionization	3
3. 2. F1-Region Ionization	8
3. 3. Regular E-Region Ionization	8
3. 4. Height of Maximum Ionization of the F2 and E Layers	9
3. 5. Quasi-Empirical Determination of F2-and E-Layer Semithickness (y)	19
4. Basic Noise Data	22
4. 1. Median and Decile Value of Man-Made Noise	22
4. 2. Median and Decile Value of Galactic Noise	22
4. 3. Median and Decile Value of Atmospheric Radio Noise (3-30 MHz)	24
4. 4. Combination of the Noise	27
5. General Problem of Predicting Sky-Wave Radio System Performance	30
5. 1. Likelihood of a Sky-Wave Path	30
5. 2. The Maximum Frequency Corresponding to a Specified Probability of Propagation	31
5. 3. The Loss in the Communication System (L_s)	31
5. 4. Available Signal at the Receiver	32
5. 5. Available Signal-to-Noise Ratio at the Receiver	33
5. 6. Likelihood that a Specified Signal-to-Noise Ratio will be Exceeded	33
5. 7. The Minimum Operating Frequency	33

Page

6. Theoretical Basis for Communication Path Geometry ----- 34

6.1. Brief Description of Model ---------- 34

6.2. Vertical-to-Oblique Transformation ---------- 34

6.3. The Equivalence Theorem ---------- 36

6.4. Parabolic Assumption ---------- 36

7. Calculation of Sky-Wave Paths ---------- 41

7.1. Theoretical Method for Computing Virtual Height of Reflection and Angles of Arrival for Obliquely Incident Ray Paths through Parabolic Layers ---------- 45

7.2. Method for Incorporating the Bending in the E Layer in Predicting Ray Paths by Way of the F2 Layer ----- 53

8. Transmission Losses ---------- 57

8.1. Absorption in Lower Layers (L_l) ---------- 57

8.2. Theoretical/Empirical Determination of Lower Region Absorption ---------- 58

8.3. Losses Due to Ground Reflections (L_g) ---------- 62

8.4. Free Space Loss Between Isotropic Radiators (L_{bf}) --- 63

8.5. Theoretical Antenna Power Gain Equations (G_T, G_R) -- 63

8.5.1. Reflection Coefficients ---------- 64

8.5.2. Power Gain Definition ---------- 67

8.5.3. Radiation Vector Method and Ground Reflection Factor ---------- 67

8.6. Antenna Efficiencies ---------- 68

9. Upper Limits of Frequencies ---------- 70

9.1. Empirical Distribution of F2(3000)MUF ---------- 71

9.2. Empirical Distribution of Transmission Loss (Y_p) ---- 72

10. Reliability, $q(R_h)$ ---------- 73

11. Grade of Service (g_r) and Required Signal-to-Noise Ratios (R_h) ---------- 80

Page

12. Time Availability (q_r) and Service Probability (Q_T) ------ 81

12.1. Calculation of the Protection Factor (C) for a Specified Time Availability (q_r) ---------- 82

12.2. Calculation of Service Probability (Q_T) ---------- 83

13. Multipath Considerations ---------- 88

14. Comparisons of Predictions with Observations ---------- 89

15. High Frequency Sky-Wave Computer Prediction Routine --- 98

16. Conclusions ---------- 119

16.1. Long Term Predictions ---------- 119

16.2. Short Term Predictions ---------- 120

17. Recommendations ---------- 121

18. References ---------- 124

19. Bibliography ---------- 128

Appendix A. Theoretical Antenna Power Gain Equations ------ 132

Appendix B. Tables of the Distribution of F2(3000)MUF ------ 141

Appendix C. Tables of the Distribution of Transmission Loss -- 150

Appendix D. Tables of Prediction Errors in Excess System Loss Above Quasi-Minimum (dB) ---------- 162

Appendix E. Tables of the Prediction Errors in the Atmospheric Radio Noise Levels ---------- 165

Appendix F. High Frequency Sky-Wave Computer Prediction Routine. Computer program listing and instructions for use of routine for predicting the performance of high frequency ionospheric telecommunication systems. (See Section 15)

List of Tables

		Page
3.1.	Predicted Coefficients D_{sk} Defining the Function $\Gamma(\lambda, \theta, t)$ for Monthly Median M(3000)F2 - December 1958	4
3.2.	Predicted Coefficients D_{sk} Defining the Function $\Gamma(\lambda, \theta, t)$ for Monthly Median foF2 (MHz) - December 1958	5
3.3.	Geographic Functions $G_k(\lambda, \theta)$	7
4.1.	Fourier Coefficients Representing the 1 MHz World-wide Distribution of Atmospheric Radio Noise, December-January-February (0000-0400 Local Mean Time)	28
4.2.	Power Series Coefficients Representing the Frequency Dependence and Distribution of Atmospheric Noise - Winter	29
10.1.	Sample Computer Print-Outs Using the Described Method of Prediction - Hawaii-San Francisco, June SSN 75 - 30 kW - Curtain Array and Rhombic	77
10.2.	Sample Computer Print-Outs Using the Described Method of Prediction - Hawaii-San Francisco, June - SSN 75 - 1 kW - Curtain Array and Rhombic	78
10.3.	Sample Computer Print-Outs Using the Described Method of Prediction - Hawaii-San Francisco, June - SSN 75 - 1 kW - Horizontal Dipole and 5 dB Antenna	79
12.1.	Sample Computer Print-Out Showing Service Probability for a Chosen Time Availability of 0.90 Using Described Prediction Model	86
12.2.	Sample Computer Print-Out Showing Service Probability for a Chosen Time Availability of 0.80 Using Described Prediction Model	87
15.1.	Sample Computer Print-Out of MUF (0.50) and FOT Only Using Described Prediction Model	103

Page

15.2. Sample Computer Print-Out of MUF (0.50), Mode, Angle, Delay, Fraction of Days, Signal-to-Noise Ratio, Circuit Reliability and Fraction of Days Multipath Using Described Prediction Model ---------- 105

15.3. Sample Computer Print-Out of LUF and FOT Using Described Prediction Model ---------- 107

15.4. Sample Computer Print-Out of MUF (0.50), Mode, Angle, Fraction of Days and System Loss Using Described Prediction Model ---------- 109

15.5. Sample Computer Print-Out of MUF (0.50), Mode, Angle, Delay, Fraction of Days, Field Strength and Received Power Using Described Prediction Model ---------- 111

15.6. Sample Computer Print-Out of MUF (0.50) and Circuit Reliability Using Described Prediction Model ---------- 113

15.7. Sample Computer Print-Out of MUF (0.50), Mode, Angle, Delay, Fraction of Days, Signal-to-Noise Ratio and Received Power Using Described Prediction Model ----- 114

15.8. Sample Computer Print-Out of MUF (0.50), Mode, Angle, Delay, Fraction of Days, Signal-to-Noise Ratio and Service Probability Using Described Prediction Model---------- 117

B.1. MUF Exceeded 0.10 and 0.90 of Hours (Ratio of MUF to Monthly Median) High SSN - Winter ---------- 141

B.2. MUF Exceeded 0.10 and 0.90 of Hours (Ratio of MUF to Monthly Median) High SSN - Equinox ---------- 142

B.3. MUF Exceeded 0.10 and 0.90 of Hours (Ratio of MUF to Monthly Median) High SSN - Summer ---------- 143

B.4. MUF Exceeded 0.10 and 0.90 of Hours (Ratio of MUF to Monthly Median) Medium SSN - Winter---------- 144

B.5. MUF Exceeded 0.10 and 0.90 of Hours (Ratio of MUF to Monthly Median) Medium SSN - Equinox ---------- 145

Page

B. 6. MUF Exceeded 0. 10 and 0. 90 of Hours (Ratio of MUF to Monthly Median) Medium SSN - Summer ---------- 146

B. 7. MUF Exceeded 0. 10 and 0. 90 of Hours (Ratio of MUF to Monthly Median) Low SSN - Winter---------- 147

B. 8. MUF Exceeded 0. 10 and 0. 90 of Hours (Ratio of MUF to Monthly Median) Low SSN - Equinox---------- 148

B. 9. MUF exceeded 0. 10 and 0. 90 of Hours (Ratio of MUF to Monthly Median) Low SSN - Summer---------- 149

C. 1. Expected Excess System Loss above Quasi-Minimum (Winter - Paths Less than 2500 km, 01-13 LMT) ------- 150

C. 2. Expected Excess System Loss above Quasi-Minimum (Winter - Paths Less than 2500 km, 13-01 LMT) ------- 151

C. 3. Expected Excess System Loss above Quasi-Minimum (Winter - Paths More than 2500 km, 01-13 LMT) ------- 152

C. 4. Expected Excess System Loss above Quasi-Minimum (Winter - Paths More than 2500 km, 13-01 LMT) ------- 153

C. 5. Expected Excess System Loss above Quasi-Minimum (Equinox - Paths Less than 2500 km, 01-13 LMT)------- 154

C. 6. Expected Excess System Loss above Quasi-Minimum (Equinox - Paths Less than 2500 km, 13-01 LMT)------- 155

C. 7. Expected Excess System Loss above Quasi-Minimum (Equinox - Paths More than 2500 km, 01-13 LMT) ------ 156

C. 8. Expected Excess System Loss above Quasi-Minimum (Equinox - Paths More than 2500 km, 13-01 LMT) ------ 157

C. 9. Expected Excess System Loss above Quasi-Minimum (Summer - Paths Less than 2500 km, 01-13 LMT) ------ 158

C. 10. Expected Excess System Loss above Quasi-Minimum (Summer - Paths Less than 2500 km, 13-01 LMT) ------ 159

Page

C. 11. Expected Excess System Loss above Quasi-Minimum (Summer - Paths More than 2500 km, 01-13 LMT) ------ 160

C. 12. Expected Excess System Loss above Quasi-Minimum (Summer - Paths More than 2500 km, 13-01 LMT) ------ 161

D. 1. Prediction Errors in Excess System Loss above Quasi-Minimum (dB) for Winter Months ---------- 162

D. 2. Prediction Errors in Excess System Loss above Quasi-Minimum (dB) for Summer Months ---------- 163

D. 3. Prediction Errors in Excess System Loss above Quasi-Minimum (dB) for Equinox Months ---------- 164

E. 1. Numerical Coefficients for Use in Evaluation of the Standard Deviation of the Median Value of the Atmospheric Radio Noise (σ_{FAM}) ---------- 165

E. 2. Numerical Coefficients for Use in Evaluation of the Standard Deviation of the Lower Decile Value of the Atmospheric Radio Noise (σ_{DL}) ---------- 166

E. 3. Numerical Coefficients for Use in Evaluation of the Standard Deviation of the Upper Decile Value of the Atmospheric Radio Noise (σ_{Du}) ---------- 167

List of Figures

		Page
3.1.	Empirical Relationship Between E(2000)MUF and Absorption Index "I"	10
3.2.	Effect of Height and Shape of Ionogram upon Scaled M(3000)F2	12
3.3.	Comparison Between the Daily Variation Curves of h_pF2 Calculated from M(3000)F2 and those Observed	13
3.4.	Effect of Lower Layer Retardation on the h_pF2 and Scaled M(3000)F2	16
3.5.	Correction to h_pF2 Due to Retardation in E-Region (Vertical Incidence)	18
3.6.	Contour Chart of the Ratio $h_mF2/yF2$ for High Solar Activity (SSN = 125)	20
3.7.	Contour Chart of the Ratio $h_{..}F2/yF2$ for Low Solar Activity (SSN = 25)	21
4.1.	Typical Man-Made Noise Relative to Population of Receiving Area	23
4.2.	Expected Value of 1 MHz Atmospheric Radio Noise December-January-February (0000-0400 Local Mean Time)	25
4.3.	Frequency Dependence and Variability of Atmospheric Radio Noise December-January-February (0000-0400 Local Mean Time)	26
6.1.	Ionospheric Curvature Correction Factor (N. Smith)	35
6.2.	Vertical-to-Oblique Transformation	37
6.3.	Equivalence Theorem for a Plane Ionosphere and Plane Earth	38
6.4.	Rawer's Range Equation for Two Parabolic Layers	40

Page

7.1. Sample Types of Sky-Wave Paths Inspected ---------- 44

7.2. Geometry of One Hop Propagation Via the Ionosphere----- 47

7.3. Logarithmic Transmission Curves for Curved Ionosphere ---------- 49

7.4. Geometry of E-Region Bending for Rays Propagating by the F2 Layer ---------- 54

8.1. Efficiency of the Inverted "L" and Grounded Vertical Antennas ---------- 69

14.1. Fort Monmouth - Palo Alto Smooth MOF (0.50) Data Versus Predicted MUF (0.50)(November SSN 65)-------- 90

14.2. Predictions and Observations of the Elmendorf-McClellan Oblique Sounder January 1963 - 12 kW - SSN 29---------- 91

14.3. WWV Monitoring Versus Predictions Beltsville-Crowborough (December - SSN 12 - 15 MHz) ---------- 92

14.4. WWV Monitoring Versus Predictions Beltsville-Crowborough (December - SSN 180 - 20 MHz) --------- 93

14.5. WWV Monitoring Versus Predictions Beltsville-Crowborough (June - SSN 14 - 10 MHz) ---------- 94

14.6. WWV Monitoring Versus Predictions Beltsville-Crowborough (March - SSN 201 - 5 MHz)---------- 95

14.7. WWV Monitoring Versus Predictions Beltsville-Crowborough (March - SSN 19 - 5 MHz)---------- 96

14.8. Predicted Versus Observed Relative Received Voltage Taipei - Tokyo - 1145 N. M. - June - SSN 161 - 200 Watts - Rhombics---------- 97

15.1. Sample Graphical Computer Print-Out of MUF (0.50) and FOT Using Described Prediction Model (London-Madrid, December - SSN 75)---------- 104

Abstract

Methods for predicting the performance of high frequency ionospheric telecommunication systems are revised to include recent improvements in the basic ionospheric and geophysical data. Revised techniques for the processing of this data by high speed electronic computers is described in detail with emphasis on better statistical descriptions of the expected performance of radio systems depending upon ionospheric propagation of radio waves. The application of the prediction techniques to communication problems is illustrated and the concept of service probability in ionospheric telecommunication systems is introduced. Comparisons between predictions and circuit operations are shown.

PREDICTING STATISTICAL PERFORMANCE INDEXES FOR HIGH FREQUENCY IONOSPHERIC TELECOMMUNICATION SYSTEMS

by

Donald L. Lucas, George W. Haydon

and

Staff, Frequency Utilization Section:

R. M. Davis, Jr.
Gerald G. Gilbert
Rodney A. Hanson
John D. Harper, Jr.
Stephen R. McCammon
Robert S. Rauschenberger
Olaf D. Remmler
Charles O. Stearns
Kenneth K. Tagawa

1. Introduction

Recent improvements in basic ionospheric and geophysical data and the increased availability of electronic computers to process these data have made it possible to improve previous methods of predicting the performance of ionospheric telecommunication circuits. It is the purpose of this report to outline a revised prediction method based on an assumed parabolic distribution of the electron density in the ionosphere.

Much has been written on parabolic approximations to the ionospheric layers, ionospheric radio wave propagation, and computer programming. Specific reference is made to a number of articles and books and others are listed as additional references.

It is not the intent of this report to review the above, but to outline a method of predicting the performance of high frequency ionospheric telecommunications systems employing those methods from the literature which are consistent with available world-wide data and which can be used economically while maintaining flexibility to easily incorporate advances in ionospheric research and data collection techniques.

The sections to follow will outline (1) philosophy of the method, (2) basic ionospheric data available, and (3) methods for predicting circuit performance.

2. Philosophy of Prediction Method

The need for high frequency prediction methods in the past few years has resulted in the development of many diverse models to represent the factors affecting the propagation of high frequency signals.

The models range from very simple ones, using only a few variables, to very elaborate ray-tracing techniques which require a precise detailed knowledge of geophysical and ionospheric parameters to yield a satisfactory result.

The model described in this report is intended to be as sophisticated as the basic data will permit and is designed to use all data available on a world-wide basis to predict an average profile of electron density versus virtual height for the path being considered. This model retains the equivalence theorem and transmission curve concept to remain consistent with the methods used to scale and predict ionospheric information. The electron density profile along the path is assumed to be adequately represented by two parabolic layers. The height of maximum ionization, thickness and electron density are derived from locations near the points of actual reflection along the path instead of the classical "two-control-point" method previously used in the calculation of the upper limit of frequencies and transmission loss.

Averaging of geophysical and ionospheric variables is effected along the path to yield monthly median values of critical frequencies and losses at specific frequencies. These values are combined with the day-to-day distributions to predict the signal level exceeded any fraction of the days within the month (or the likelihood of a given level being exceeded on a randomly chosen day).

In this report the convention is adopted of using lower case letters to denote power in watts, or power ratios and capital letters are used to denote their decibel equivalents. Thus w watts may be expressed as $W = 10 \log_{10} w$ decibels relative to one watt. This convention sometimes makes it impracticable to follow the recommendation that abbreviations for units based directly on proper names be capitalized. However, when no confusion will arise the recommendation will be followed, e.g., MHz (the H is obviously not in decibel units).

3. Basic Ionospheric Data

The ionosphere has four principal regions, or layers, which affect the propagation of high frequency radio waves. They are the D, E, F1, and F2 layers in order of increasing height above the earth's surface and increasing ionization. Either the E or F2 region totally reflect radio waves having a sufficiently low frequency or angle of incidence while most of their attenuation occurs during their passage through the upper D region and the lower E region. Basic atmospheric density and ionization data for these main layers is thus required and used in this model to predict the strength of high frequency sky-wave signals.

3.1. F2-Region Ionization

The ionization density of the F2 region is very unstable and exhibits marked variations with geographic latitude and longitude, local time, season of the year, and solar activity.

The Institute for Telecommunication Sciences and Aeronomy predicts the characteristics of the F2 region in terms of the vertical incidence critical frequency (foF2) and the M(3000)F2 factor as determined from vertical ionosonde records [Ostrow 1962].

The foF2 may be scaled directly from the vertical ionogram (figure 3.2). Through the use of transmission curves [Smith 1939] the vertical

Table 3.1.

TIME VARIATION:

GEOGRAPHICAL VARIATION

Harmonic		0	1		2		3	
	K \ S	0	1	2	3	4	5	6
I	0	2.4597045E 00	-2.7864561E-01	-2.0356853E-01	2.3461928E-02	-7.6179242E-02	3.2068893E-02	-3.2689627E-02
	1	3.6954687E-01	-1.8391149E-02	-1.2754253E-01	-1.5806746E-01	8.4492028E-02	-1.2135539E-01	-8.3682467E-02
	2	1.7629436E 00	8.8885969E-01	9.5534900E-01	-4.6495117E-01	3.3450422E-01	-4.4479275E-01	-2.4594132E-01
	3	4.4937205E-02	4.2120877E-02	8.8807715E-01	2.2096053E-01	-3.3338858E-01	2.0295692E-01	2.3496002E-01
	4	-5.4440793E 00	1.5063822E-01	-3.1809667E-01	7.0890932E-01	-1.4431769E 00	1.3843947E 00	8.6857817E-01
	5	6.0006863E-01	1.4744394E-02	-6.3039878E-01	-1.5046852E-01	3.0635701E-01	-8.8043374E-02	-1.9979359E-01
	6	6.7451826E 00	-1.3532918E 00	-1.0804226E 00	-4.9387181E-02	2.5417657E 00	-1.9422786E 00	-5.5254013E-01
	7	3.4695590E-01	-4.5053890E-02	-1.1137213E-01	1.1862618E-01	-2.8149233E-02	2.4925547E-02	5.2938817E-02
	8	-3.0666148E 00	6.0030538E-01	6.4208925E-01	-2.1531846E-01	-1.3797404E 00	1.0119923E 00	-5.7694210E-02
II	9	7.6215219E-03	-1.4952843E-02	9.2220060E-03	1.7373093E-02	1.9521040E-03	1.2557834E-02	2.4517395E-04
	10	-8.6248538E-02	3.9951287E-03	8.9846530E-03	2.1299871E-02	-3.9493725E-02	4.6963555E-02	1.4939295E-02
	11	1.3116686E-02	-3.6824179E-02	6.2515870E-02	-6.3571962E-05	1.8724717E-02	3.5390121E-02	-1.8339332E-02
	12	-2.9158792E-01	-6.3511761E-01	-1.8566048E-01	3.5302817E-01	-2.3466288E-01	7.6185253E-03	1.3288638E-01
	13	-5.6047089E-03	1.7272247E-02	-1.7549958E-01	1.9310906E-02	-6.8180130E-03	-8.0042152E-02	1.1169360E-02
	14	5.2549593E-01	-2.7285330E-02	-6.6125262E-01	-1.5278838E-01	2.2032028E-01	-6.2997752E-01	2.7349260E-02
	15	-1.9611105E-01	-8.5644186E-03	-4.0172087E-02	1.7888334E-01	-4.3772657E-02	-1.2270745E-01	1.5044717E-02
	16	2.0560703E 00	4.6495761E 00	1.4818957E 00	-1.9121817E 00	1.6249525E 00	-1.2032931E-01	-8.5532446E-03
	17	1.0345496E-02	-9.5678610E-02	3.8659861E-01	-8.2966511E-02	5.1813095E-02	-4.5166591E-02	-2.5326822E-02
	18	1.2496830E-01	-2.4561137E-01	3.3380832E 00	-1.1601990E-01	-9.5382241E-01	3.1154308E 00	-6.3513430E-02
	19	5.0870426E-01	-3.1294876E-01	-6.1709802E-02	-3.7130666E-01	-3.7149905E-02	1.7771534E-01	-7.0192923E-03
	20	-5.1198447E 00	-9.7591153E 00	-2.7327168E 00	3.3748487E 00	-3.2455807E 00	2.2450502E-01	1.5462864E 00
	21	9.2945119E-02	-5.3925217E-02	-4.8140595E-01	1.3339700E-01	-1.9650605E-01	2.9338350E-01	1.4836907E-02
	22	-9.8967094E-01	9.2055483E-01	-6.4649473E 00	5.3845559E-01	1.1124675E 00	-5.2129884E 00	4.1918286E-02
	23	-3.4868085E-01	3.2589110E-01	7.7423149E-02	2.2646917E-01	7.1522920E-02	-1.2589389E-01	-4.2114294E-03
	24	3.5455681E 00	6.2567248E 00	1.9184216E 00	-1.9352055E 00	1.8365364E 00	-1.3177885E-01	-8.6572829E-01
	25	-1.3643478E-01	1.3335468E-01	3.4164304E-01	-5.4899275E-02	1.6122415E-01	-1.6834600E-01	
	26	5.0289852E-01	-7.0687903E-01	3.8330904E 00	-2.5710703E-01	-3.2586023E-01	2.6988180E 00	
III	27	1.7577056E-03	2.8339747E-04	3.9620170E-04	-1.1928093E-03	1.1323065E-03	-3.8325585E-04	
	28	-1.7199886E-04	2.5405724E-02	-1.4097031E-04	-8.4594524E-04	1.0420042E-03	7.3792368E-03	
	29	-6.0263882E-02	-1.1798609E-01	4.4274451E-03	3.4380887E-02	-4.3196892E-02	-1.6411811E-02	
	30		-1.0068053E-01	1.0509565E-03	5.7696413E-02	-5.1688339E-02		
	31		-2.8248769E-02	-1.4250337E-01	2.2878611E-03	-1.1179516E-02		
	32		-2.3730302E-02	3.5673183E-03	8.4789476E-03	-1.0958673E-02		
	33		3.3189850E-01	-2.9969407E-02	1.0567941E-02	1.2241141E-01		
	34		2.8326480E-01	-1.0279279E-02	-1.6039630E-01	1.4685266E-01		
	35			3.8839197E-01				
	36							

GEOGRAPHICAL VARIATION

Harmonic		4		5		6	
	K \ S	7	8	9	10	11	12
I	0	2.0321863E-02	4.4910491E-03	1.0773362E-02	2.5578273E-02	-4.8214887E-03	1.2555835E-03
	1	4.4199712E-02	-8.7826320E-02	2.0691925E-02	-3.1163440E-03	4.3740110E-03	1.8809402E-02
	2	-3.1068542E-02	9.8289336E-04	-1.6551957E-02	-1.2071578E-01	4.1033049E-03	-3.7992496E-03
	3	-6.2312560E-02	1.0633776E-01	-2.7050457E-02	-2.1341972E-03		-2.6559583E-02
	4				9.8221246E-02		

I - Main latitudinal variation Mixed latitudinal and longitudinal variation II - First order in longitude, III - Second order in longitude.

Notation: For each entry the number given by the first eight digits and sign is multiplied by the power of ten defined by the last two digits and sign.

COEFFICIENTS D_{sk} DEFINING THE FUNCTION $\Gamma(\lambda,\theta,t)$ FOR MONTHLY MEDIAN F2-M 3000
DECEMBER 1958

Table 3.2.

TIME VARIATION:

Harmonic		0	1		2		3		4	
	K \ S	0	1	2	3	4	5	6	7	8
I	0	1.0975529E 01	1.7027571E 00	1.4862860E 00	-7.5606564E-01	7.6257150E-01	-2.7180890E-01	-5.5354336E-01	1.8953986E-01	-2.1906067E-01
	1	-1.7012024E 00	1.6448708E-01	2.5329333E 00	-2.7034453E 00	1.8156968E-01	-1.4224915E 00	-2.3583061E 00	-3.3616213E-01	-9.5059532E-01
	2	4.2770728E 00	9.3584328E 00	3.8619406E 00	-2.0455995E 00	-1.1351002E 00	1.0673727E 00	-6.8313993E-01	2.0678045E 00	-1.9993110E 00
	3	2.2543303E 01	3.4320387E 01	-1.4448591E 01	1.7876342E 01	2.6415675E 00	7.1083783E 00	1.6761376E 01	8.5148646E 00	4.6742557E 00
	4	-8.7023281E 01	-8.9283786E 01	5.0441217E 01	1.8679793E 01	7.7832181E 00	-7.9094652E 00	9.4932253E 00	-1.4594041E 01	1.4739242E 01
	5	-1.2697548E 02	-2.1021881E 02	1.0850153E 02	-4.3286481E 01	-2.1369857E 01	-2.5631759E 01	-4.9815283E 01	-1.6448317E 01	-1.6058546E 01
	6	3.3194980E 02	2.6762136E 02	-3.0061563E 02	-6.8039322E 01	-2.9353597E 01	4.2629441E 00	-2.3926843E 01	2.1681693E 01	-3.4825963E 01
	7	2.9398724E 02	4.9989017E 02	-2.5305406E 02	6.6123591E 01	6.7410372E 01	3.4701817E 01	7.2922651E 01	3.0152924E 01	2.5685517E 01
	8	-6.2864316E 02	-3.7050085E 02	6.5117434E 02	1.4214614E 02	6.2977137E 01	3.0199225E 01	1.9111568E 01	-4.2070195E 00	3.2328641E 01
	9	-2.9553332E 02	-5.1807641E 02	2.4061109E 02	-5.5248716E 01	-7.5580178E 01	-8.2885423E 00	-4.8029592E 01	-2.1621980E 01	-1.4334149E 01
	10	5.7812739E 02	2.4288284E 02	-5.3014296E 02	-1.4026740E 02	-6.3059824E 01	-4.3739870E 01	8.8887490E 00	-8.4759525E 00	-6.2703856E 00
	11	1.0728381E 02	1.9451654E 02	-8.4266973E 01	1.7395313E 01	2.6734065E 01	-6.5989668E 00	1.0488517E 01	-3.2576519E-01	2.9815755E 00
	12	-2.0465868E 02	-6.1672124E 01	2.2402565E 02	5.0565827E 01	2.2056101E 01	1.6441509E 01	-1.2472386E 01	3.2337783E 00	-3.9441097E 00
II	13	1.8253447E-01	-3.0897393E-01	-1.7134542E-01	-6.8267239E-02	2.2101744E-01	1.2034706E-01	4.3879483E-02	9.8065099E-03	-2.9474481E-02
	14	-2.7817490E-01	-2.4616947E-01	-5.2836371E-01	7.9224710E-01	-1.9317761E-01	-1.0721080E-01	2.2021524E-01	-8.8178408E-02	-4.4758748E-02
	15	-4.4723618E-01	-1.1510026E 00	-2.0885526E-01	6.7929192E-01	1.5771487E 00	2.1633874E-01	1.2565549E-01	3.8882741E-01	3.1735651E-01
	16	-4.1727904E 00	-8.3497413E 00	2.7795444E 00	2.5485381E 00	-5.8212114E-01	-2.2192447E 00	8.0045419E-02	-3.2292146E-02	-2.7617327E-02
	17	-9.1404111E 00	-6.1804598E-01	4.5093232E 00	-6.9523931E-01	-6.9972273E 00	-4.6429499E 00	-9.8506230E-01	-6.6326894E-02	1.1306202E 00
	18	1.2242684E 01	7.0345864E 00	-1.0043306E 01	-1.3412635E 01	1.7224812E 01	4.6672130E 00	-1.3309710E 00	1.6479981E 00	7.7601019E-03
	19	1.0127541E 01	1.5802478E 01	-1.0402084E 01	3.1921534E-01	-3.6087130E 01	-2.7518425E-01	6.0082695E-01	-6.2766758E 00	-1.8810184E 00
	20	1.3692289E 02	1.6502871E 02	-7.2863230E 01	-4.6039074E 01	1.6797187E 01	2.6934572E 01	-2.9434578E 00	4.0602687E 00	-6.7998774E-01
	21	6.1376760E 01	2.3823115E 01	-2.9387898E 01	1.3798739E 01	4.5257363E 01	3.3083965E 01	2.2576369E 00	4.9560452E-03	-7.0812981E 00
	22	-7.5134997E 01	-4.0703020E 01	1.2722517E 02	7.3901458E 01	-2.1298590E 02	-6.0032408E 01	4.1048784E 00	-5.3080921E 00	-4.4847116E-01
	23	-4.2678511E 01	-5.7403102E 01	6.3441706E 01	-1.0699640E 01	1.8860612E 02	3.9099306E-03	-1.3549511E 01	2.7534093E 01	2.9763668E 00
	24	-7.3474996E 02	-8.3837042E 02	4.6625933E 02	2.7487080E 02	-1.0501047E 02	-9.7848264E 01	1.7680123E 01	-1.0423073E 01	4.6347538E 00
	25	-1.3542068E 02	-9.5678871E 01	1.1218257E 02	-6.0150149E 01	-1.1361036E 02	-9.4025106E 01	-6.5297469E 00	2.5356720E-03	2.2912621E 01
	26	1.3588736E 02	7.0017204E 01	-4.1588927E 02	-2.2190408E 02	1.0106482E 03	2.9822517E 02	-1.6746828E 01	5.4490803E 00	2.2811089E 00
	27	6.6506710E 01	7.3650686E 01	-1.5071120E 02	2.7581728E 01	-4.8708670E 02	-2.3170511E 00	4.2250249E 01	-4.5925300E 01	-2.3007317E 01
	28	1.6004726E 03	1.7165541E 03	-1.1943014E 03	-6.8555969E 02	2.6207012E 02	1.4589258E 02	-4.5178688E 01	[illegible].0483167E 00	-1.2840969E 01
	29	1.2941161E 02	1.6905857E 02	-2.2417788E 02	1.1161972E 02	9.7296709E 01	1.2551122E 02	2.2378222E 01	-1.0174850E-01	-4.3421563E 01
	30	-1.4560894E 02	-2.1773458E 01	5.3643370E 02	3.4252456E 02	2.1409547E 03	-6.5663503E 02	4.7150726E 01	-1.5946963E 00	-4.0316450E 00
	31	-3.6146227E 01	-2.2681355E 01	1.5252939E 02	-3.3499210E 01	5.5134596E 02	4.7428764E 00	-4.8291029E 01	2.2551577E 01	1.6601351E 00
	32	-1.5217490E 03	-1.5436575E 03	1.3184717E 03	7.4570659E 02	-2.8001628E 02	-9.8419338E 01	4.9689458E 01		1.5125641E 01
	33	-7.6340763E 01	-1.5396956E 02	2.0957641E 02	-9.2436357E 01	1.9322647E 01	-7.2318683E 01	-3.1349616E 01		4.1260099E 01
	34	1.1984987E 02	-1.9887089E 01	-2.1895422E 02	-2.3280115E 02	2.1513221E 03	6.5328470E 02	-5.0107861E 01		2.8144535E 00
	35	2.5633815E 00	-8.9765286E 00	-5.5255212E 01	1.4662282E 01	-2.2688478E 02	-2.8998729E 00	1.9715753E 01		-4.2475979E-01
	36	5.2219397E 02	5.0781178E 02	-5.7367100E 02	-2.9317565E 02	1.0722054E 02	2.6733115E 01	-1.9521694E 01		-6.3189466E 00
	37	3.3476761E 01	5.7096434E 01	-7.4110801E 01	2.7676970E 01	-4.3072069E 01	1.1099980E 01	1.4804017E 01		-1.4512384E 01
	38	-4.8817652E 01	2.5019247E 00	-1.9992678E 01	4.9954472E 01	-7.8687621E 02	-2.3962078E 02	1.6999020E 01		-6.3592226E-01
III	39	-6.9022242E-03	-2.3726618E-02	-3.3863767E-01	2.4[illegible]50787E-01		1.1885768E-02	4.9183183E-02		6.0306707E-03
	40	2.3235672E-02	1.5689547E-01	-1.3921852E-01	8.43[illegible]702E-02		-6.4377151E-02	9.8777164E-02		-3.9878624E-02
	41	2.4512497E-02	-1.0729051E-02	2.5190540E-01	-4.0894723E-02		3.0240182E-03	2.9543621E-02		2.7270377E-03
	42	-5.6014360E 01	1.0909216E-01	-1.6336312E-01	1.3507879E 00		4.9721852E-02	4.4322462E-02		-2.7728304E-02
	43		2.6653873E-01	5.4411260E 00	-3.6560385E-01		-2.3472665E-01	-3.5234130E-01		-6.7747008E-02
	44		-2.4129488E 00	4.8272459E 00	-1.6109489E 00		1.8468230E 00	-5.9923277E-01		6.1330695E-01
	45		-2.2568523E-02	8.4226443E-01	2.9548096E-01		3.9690866E-02			5.7363140E-03
	46		-3.1946334E-01	1.2057747E 00	-5.6112505E 00		3.5356301E-01			8.1199026E-02
	47		-4.0274389E-01	-1.7344368E 01	-3.4528911E-01		7.9117051E-01			1.0236671E-01
	48		4.1000685E 00	-1.6958222E 01	2.7032396E 00		-7.3707471E 00			1.0421276E 00
	49			-1.1247104E 00	-4.2169459E-01		-7.9710127E-02			
	50			-1.5741791E 00	6.5178954E 00		-4.4173399E-01			
	51			1.6668546E 01			-7.2557599E-01			
	52			1.8444390E 01			6.9247085E 00			

GEOGRAPHICAL VARIATION

Harmonic		5		6		7		8	
	K \ S	9	10	11	12	13	14	15	16
I	0	1.9667511E-01	2.4664364E-01	-9.6199269E-02	9.6732820E-02	-8.4860413E-02	-9.1234739E-02	6.5003374E-02	-2.0512594E-02
	1	3.8972554E-01	-8.4171342E-03	1.8619000E-01	2.0956517E-01	-7.9410625E-02	[illegible].2109727E-02	-8.0547124E-02	-5.5247232E-02
	2	-4.4712581E-01	-1.2903891E 00	6.1299201E-01	-1.3439200E-01	2.9634734E-01	5.2667627E-01	-3.5176336E-01	2.5616074E-02
	3	-5.0140063E-01	-6.5880308E-02	-2.1470110E-01	-2.0893537E-01	9.4144408E-02	-6.6127658E-02	1.2508225E-01	6.7799408E-02
	4	1.9107307E-01	1.0919535E 00	-5.7498534E-01	7.2332078E-01	-2.1764221E-01	-4.8065190E-01	3.4288950E-01	

GEOGRAPHICAL VARIATION

I - Main latitudinal variation Mixed latitudinal and longitudinal variation II - First order in longitude, III - Second order in longitude

Notation: For each entry the number given by the first eight digits and sign is multiplied by the power of ten defined by the last two digits and sign

COEFFICIENTS D_{SK} DEFINING THE FUNCTION $\Gamma(\lambda,\theta,t)$ FOR MONTHLY MEDIAN f_oF2 (MHz)

DECEMBER 1958

ionogram also yields the M(3000)F2 which relates the vertical incident (foF2) frequency to the oblique 3000-km frequency as

$$\text{F2(3000) MUF} = \text{foF2} \cdot \text{M(3000)F2} \tag{3.1}$$

Tables 3.1 and 3.2 are examples of monthly median world-wide numerical coefficient representations of these two parameters for a given month. The "numerical" maps represented by these coefficients denote a function, $\Gamma(\lambda, \theta, t)$, of the three variables: latitude (λ), longitude (θ), and local time (t). The function $\Gamma(\lambda, \theta, t)$ is obtained by fitting appropriate mathematical functions to the observed ionospheric sounding data collected from a world-wide net of vertical sounders.

The general form of $\Gamma(\lambda, \theta, t)$ is the Fourier time series

$$\Gamma(\lambda, \theta, t) = a_o(\lambda, \theta) + \sum_{j=1}^{H} [a_j(\lambda, \theta) \cos j t + b_j(\lambda, \theta) \sin j t] \tag{3.2}$$

[Ostrow 1962].

H denotes the number of harmonics retained to represent the diurnal variation. The Fourier coefficients, $a_j(\lambda, \theta)$ and $b_j(\lambda, \theta)$, which vary with the geographic location, are represented by a series

$$\sum_{k=0}^{K} D_{s,k} G_k(\lambda, \theta), \tag{3.3}$$

where the $G_k(\lambda, \theta)$ are shown in table 3.3. The index (s) denotes which Fourier coefficient is represented, in the order

$D_{s,k}$ = Fourier coefficients defining $\Gamma(\lambda, \theta, t)$

$s = 2j$, for $a_j(\lambda, \theta)$, $j = 0, 1, 2 \ldots\ldots H$

$s = 2j - 1$ for $b_j(\lambda, \theta)$, $j = 1, 2, 3 \ldots\ldots H$

The above function (Γ) has the same form for both the foF2 and the M(3000)F2 which are utilized by this method [Jones and Gallet 1962a]. A revised method for the generation of foF2 and M(3000)F2 will be used in the near future [Jones, et al 1966].

Table 3.3.

MAIN LATITUDINAL VARIATION		MIXED LATITUDINAL AND LONGITUDINAL VARIATION			
		FIRST ORDER IN LONGITUDE		SECOND ORDER IN LONGITUDE	
k	$G_k(\lambda,\theta)$	k	$G_k(\lambda,\theta)$	k	$G_k(\lambda,\theta)$
0	1	k_0+1	$\cos\lambda\cos\theta$	k_1+1	$\cos^2\lambda\cos 2\theta$
1	$\sin\lambda$	k_0+2	$\cos\lambda\sin\theta$	k_1+2	$\cos^2\lambda\sin 2\theta$
2	$\sin^2\lambda$	k_0+3	$\sin\lambda\cos\lambda\cos\theta$	k_1+3	$\sin\lambda\cos^2\lambda\cos 2\theta$
		k_0+4	$\sin\lambda\cos\lambda\sin\theta$	k_1+4	$\sin\lambda\cos^2\lambda\sin 2\theta$
k_0	$\sin^{q_0}\lambda$				
			$\sin^{q_1}\lambda\cos\lambda\cos\theta$	$K-1$	$\sin^{q_2}\lambda\cos^2\lambda\cos 2\theta$
			$\sin^{q_1}\lambda\cos\lambda\sin\theta$	K	$\sin^{q_2}\lambda\cos^2\lambda\sin 2\theta$

Geographic Functions $G_k(\lambda, \theta)$

3.2. F1-Region Ionization

The F1 layer also affects HF propagation especially in the daytime. However the geographic, time and solar activity dependence described above for the F2-layer parameters is not presently available for the F1 layer. This layer is therefore not included as a separate layer in the present method although the effect of F1-layer retardation on waves propagated via the F2 layer is partially accounted for (see section 3.4. on layer heights).

3.3. Regular E-Region Ionization

The regular E layer does not exhibit irregularities as complex as those associated with the F2 region since its ionization is controlled primarily by the sun's zenith angle. Based on the Chapman theory and using the best current estimates of the rates of electron production and loss, the following semiempirical equation has been derived (Knecht 1962),

$$foE = 0.9\,[(180 + 1.44\,S)\cos\psi]^{\frac{1}{4}} \qquad (3.4)$$

where

S = 12 month running Zurich sunspot number

ψ = zenith angle of the sun - degrees

foE = monthly median critical frequency of E layer - MHz.

Although the above equation adequately represents the E-region electron density during most daylight hours, it fails to predict E-layer critical frequencies during the twilight hours ($\psi > 90°$) since an foE of zero at a sun's zenith angle of 90 degrees is clearly unreasonable, e.g., E-layer critical frequencies below 700 KHz have seldom been observed (Watts and Brown 1954).

Since the D-region ionospheric absorption is closely correlated with the critical frequency of the E region, it is convenient to relate foE to the index of ionospheric absorption which is also a function of solar

activity and the zenith angle of the sun. The ionospheric absorption index is expressed as

$$I = (1 + .0037\,S)\cos(K\,\psi)^{1.3} \qquad (3.5)$$

where

S = 12 month running average Zurich sunspot number

ψ = sun's zenith angle - degrees

K = 90°/102° = 0.881 (102° is sunset at 110 km height of the E layer).

The above value of I is related to the E(2000)MUF by figure 3.1 which is mathematically represented by a polynomial:

$$E(2000)\,MUF = 3.41 + 38.43 \cdot I - 68.07 \cdot I^2 + 89.97 \cdot I^3 - 70.97 \cdot I^4 + 29.51 \cdot I^5 - 4.99 \cdot I^6 \ (MHz) \qquad (3.6)$$

The above equation yields an E(2000)MUF of 3.41 MHz during the nighttime hours corresponding to an foE of 0.7 MHz (Watts and Brown 1954). The regular E layer is assumed to be very predictable and its associated distribution is considered negligible.

3.4. Height of Maximum Ionization of the F2 and E Layers

The height of maximum ionization of the F2 region (h_mF2) is needed in practical communication problems and geophysical research. Unfortunately, direct measurement of h_m is impossible from vertical incidence ionograms. Although accurate computer methods of determining electron density profiles from virtual height curves are available [Wright and Paul 1963], this information is not currently available on a world-wide basis and another way of estimating the h_m of the F2 region is required. As an interim method it is proposed to use the existing world-wide numerical maps of M(3000)F2 and a linear conversion formula developed by Shimazaki [1955] to obtain the necessary estimates of h_m. There has been some criticism of Shimazaki's formula [Wright and McDuffie 1960] but its use in practical prediction methods is considered to be justified as is explained later in the discussion.

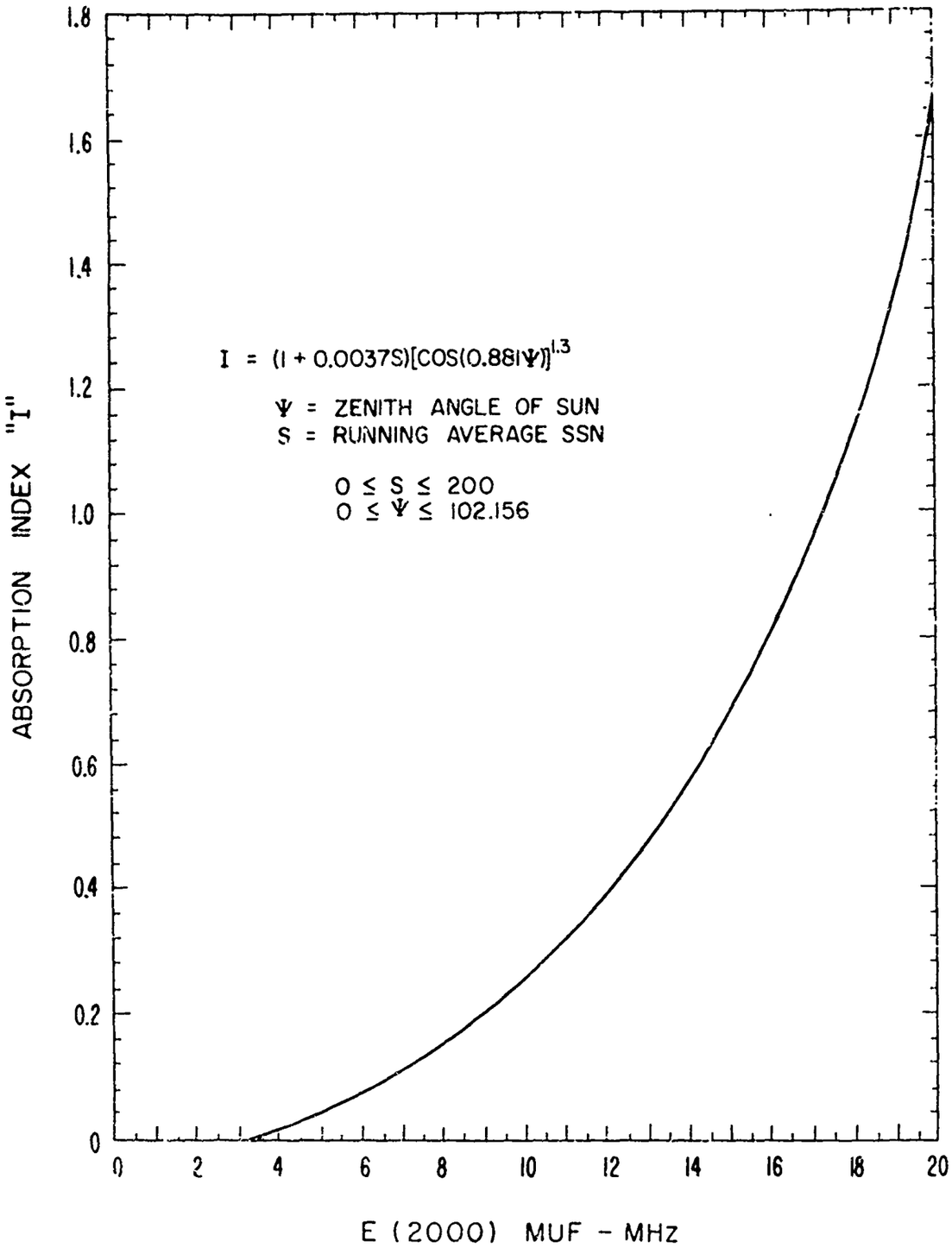

Figure 3.1. Empirical Relationship Between E(2000)MUF and Absorption Index "I"

In practical prediction methods, such as this, it is not always possible to justify rigorously every technique and parameter employed, e.g., it should be restated that transmission via the F1 region on oblique paths is not considered in this method; however, some adjustment to h_mF2 needs to be considered when using vertically incident ionograms which include F1 layer retardation. Improvements depend in a large part on the improvements in basic data, scaling methods, and basic research. Additional background for this material can be found in Davies [1965].

The maximum usable frequency factor, M(3000)F2, for propagation by way of the F2 layer over a 3000-kilometer path is regularly scaled from ionograms on a world-wide basis. Another parameter sometimes scaled regularly is h_pF2, the virtual height on the ionogram at a frequency equal to 0.834 foF2. This frequency was selected for scaling because in parabolic layer theory, the virtual height at 83.4 % of the critical frequency of the layer is equal to the true height (h_m) of maximum ionization (see figure 3.2). Shimazaki [1955] has demonstrated that these two parameters are approximately related by the following linear equation:

$$h_pF2 \cong -176 + \frac{1490}{M(3000)F2} \qquad (3.7)$$

This formula was derived theoretically using plausible approximations for the layer shape. Shimazaki also compared values of h_pF2 calculated from M(3000)F2 by the formula with the corresponding scaled values of h_pF2 for 18 stations for the months of March, June, September, and December 1952, and for Tokyo for the same months and the years 1949 through 1954 (see figure 3.3). The daily mean difference between the two values rarely exceeded 6.0 %, thus showing good agreement for all seasons, geographic locations and levels of solar activity.

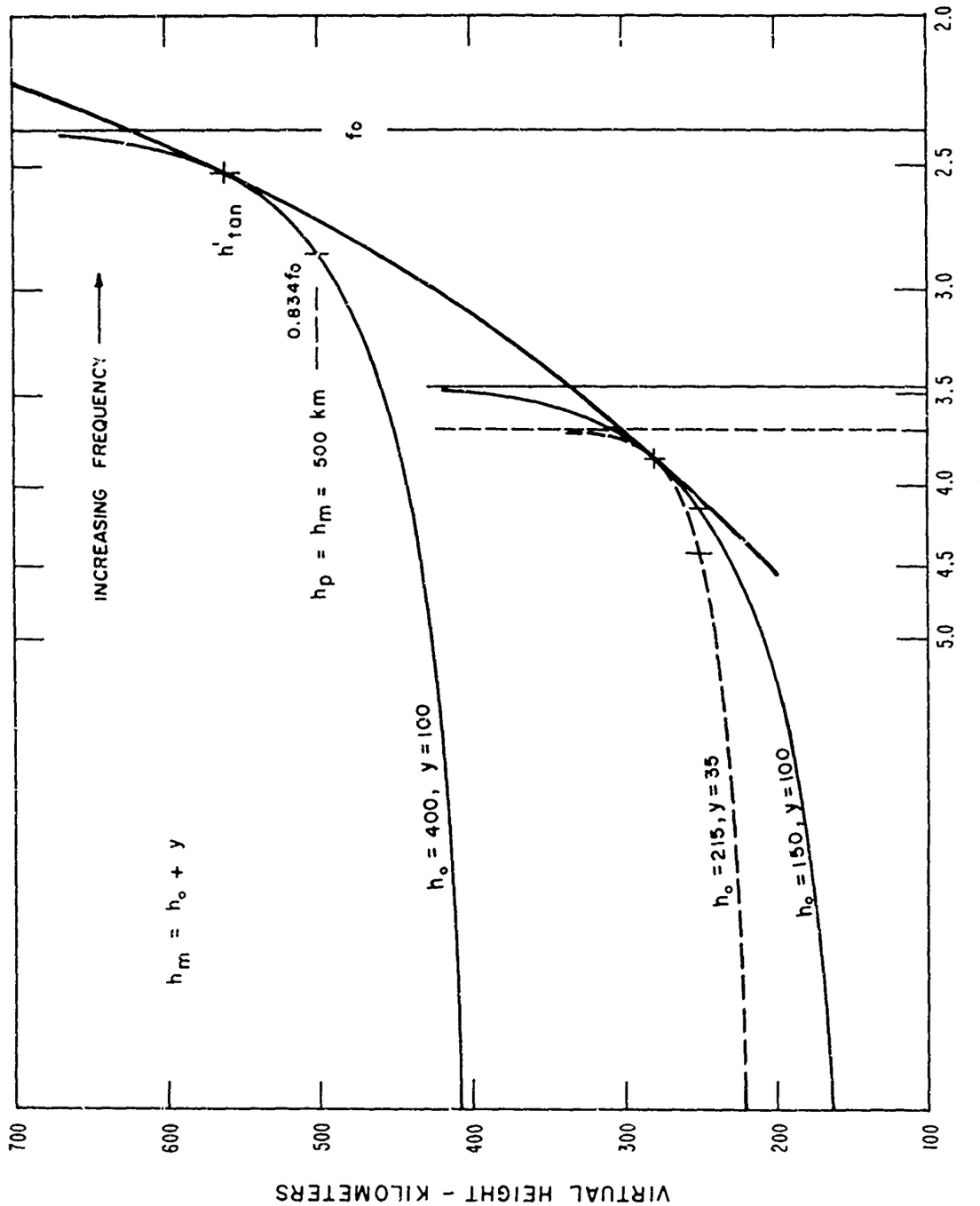

Figure 3.2. Effect of Height and Shape of Ionogram upon Scaled M(3000)F2

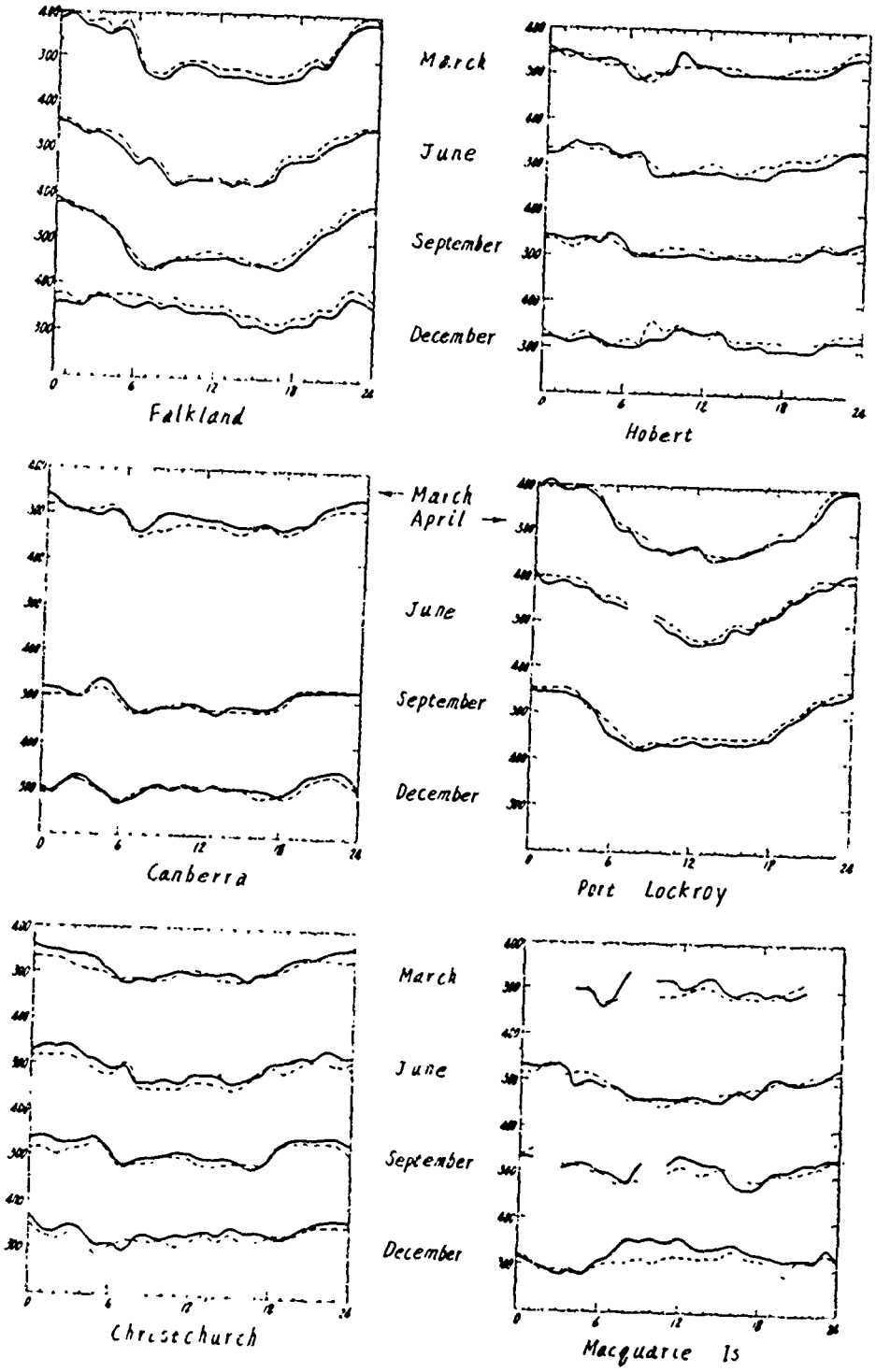

Figure 3.3. Comparison Between the Daily Variation Curves of h_pF2 Calculated from M(3000)F2 and those Observed

The MUF factor, M(3000)F2, is scaled from the ionograms along with foF2, and both are mapped using a numerical method on a world-wide basis. Since h_pF2 is not mapped world-wide, the present prediction program finds it from Shimazaki's formula (3.7).

In 1960 Wright and McDuffie reconsidered Shimazaki's formula (along with other methods of inferring the height of the F-region peak) in the light of h_m values obtained from the computer methods of deriving N(h) profiles from ionograms. Their analysis showed that h_pF2 was "free from bias at night at low and medium latitudes, but that systematic differences are significant in the daytime and at high latitudes at all times." For these latter times and latitudes, h_m is significantly less than h_pF2 as deduced from Shimazaki's formula, but an empirical linear relationship between h_m and M(3000)F2 which fits the data quite well can usually be found though the slope and intercept values may be a function of time, location, etc.

Wright [1964] later indicated that h_pF2 as inferred from M(3000)F2 would be preferable to h_m for prediction purposes even at the times when h_pF2 is greater. This is because the M(3000)F2→h_p theory does not take into account the effects of the daytime E and F1 layers on M(3000)F2. The virtual height of the observed F2 trace includes the effects of retardation in the lower layers. Therefore the application of the 3000-km transmission curve to such an ionogram results in an M(3000)F2 smaller than that for the F2 layer alone. The smaller M(3000)F2 yields a greater h_pF2 than would be obtained for the F2 layer alone. While this effect is a disadvantage for deducing true heights for geophysical research, it is an advantage in computing elevation angles for communication paths via the F2 layer when independent information on the F1 layer parameters is not otherwise available.

Figure 3.2 illustrates how changes in the virtual height (vertical scale) and semithickness of the F2 layer affect the values of M(3000)F2

factors scaled from ionograms. The thick solid line is the 3000-kilometer transmission curve with MUF factor marked on a logarithmic horizontal scale. The MUF factor increases with decreasing values of the virtual height, but must by definition be read where the h'-f curve becomes vertical, i.e., at the critical frequency (long vertical lines). Note that the factor is not read at the point of tangency to the transmission curve. The short vertical lines on the h'-f curves correspond to 83.4% of the critical frequency and thus intersect the h'-f curves at a virtual height equal to the true height of maximum, h_m, of a single parabolic layer. Note that h_m is not necessarily equal to the height of tangency of the transmission curve, h'_{tan} (crosses).

Since the frequency scale of the ionogram is logarithmic, the MUF factor scaled is independent of the absolute value of the critical frequency (at least as far as the scaling procedure is concerned). The two thin solid lines are h'-f curves for parabolic layers of equal semithickness (100 km) but at different heights illustrating the increase of MUF factor with decreasing height. The increase of MUF factor with decreasing semithickness is illustrated by the dotted h'-f curve which is tangent at the same virtual height (crosses) but has a semithickness of 35 km instead of 100 km.

Since scaling the MUF factor is strictly a mechanical procedure, it makes no distinction between increases in the true height of the F2 layer and apparent height increases due to the retardation in the F1 layer beneath. Therefore, when the F1 layer is present during the daytime hours, neither MUF factors nor values of h_pF2 scaled from the same ionogram (at 0.834 foF2) will correspond to the true height of the F2 layer. However, they may still be linearly related to a good approximation through Shimazaki's formulas as his figures demonstrate.

Figure 3.4 illustrates the relationship between an observed ionogram (solid line) when both F1 and F2 layers are present and an ionogram

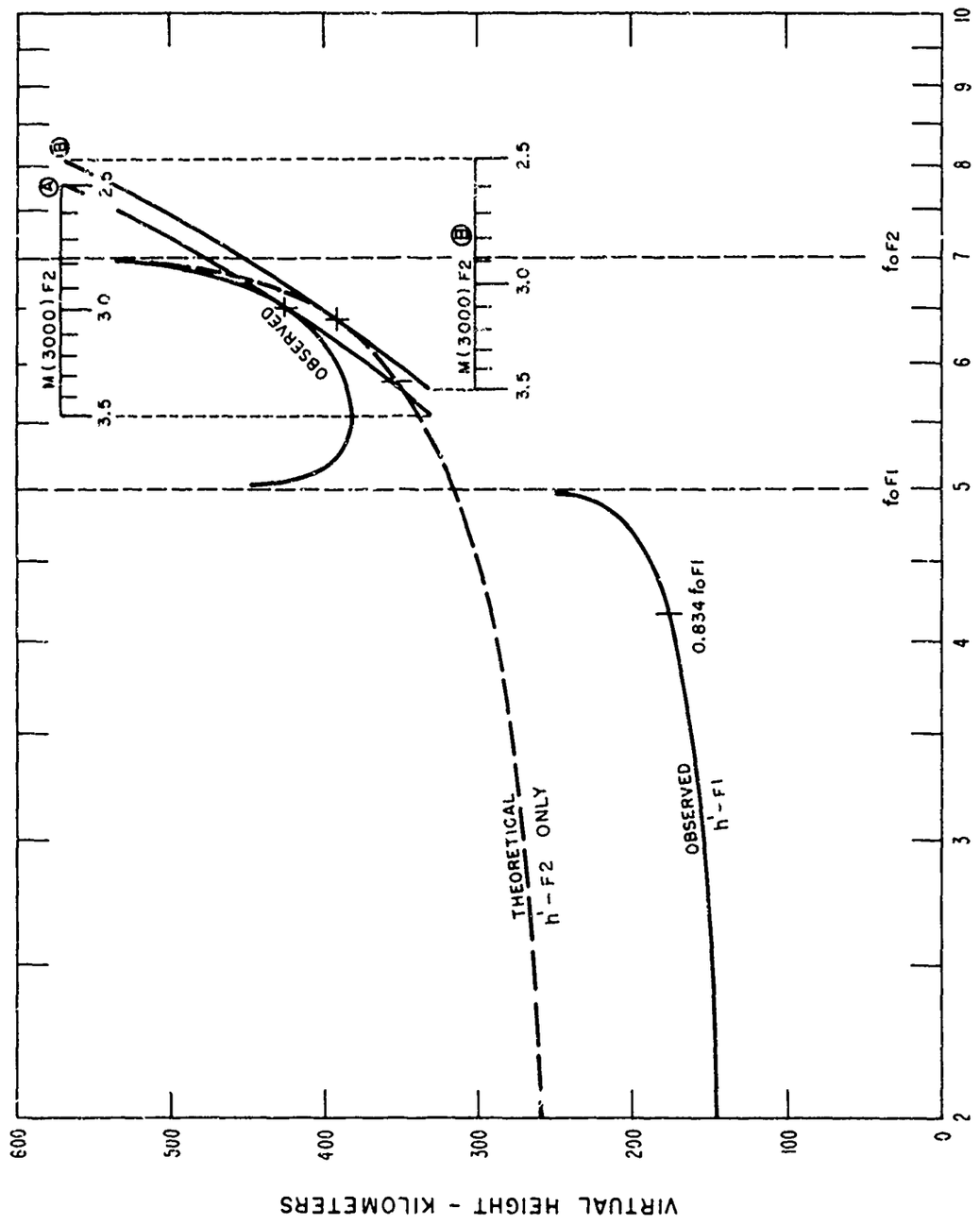

Figure 3.4. Effect of Lower Layer Retardation on the h_pF2 and Scaled M(3000)F2

calculated from the true height, h_mF2, of the F2 layer (dotted curved line). Portions of the 3000-kilometer transmission curves (marked A and B) are shown tangent to each ionogram. The M(3000)F2 factors may be read from the scales at the critical frequency of the F2 layer. Note that the MUF factor (scale A) for the observed ionogram is less than that (scale B) for the h'-f curve corresponding to h_mF2 (marked $h'F2$ only).

In this case h_mF2 was 350 kilometers, while the values of h_pF2 obtained by Shimazaki's formula were 341 km for the larger MUF factor (scale B) and 360 km for the small (scale A). Thus a h'-f curve corresponding to $h_pF2 = 360$ would everywhere be 10 km higher than the dotted curve and would, therefore, fit the observed ionogram somewhat better at least for frequencies above the critical frequency of the F1 layer.

Virtual heights found in the above manner should, therefore, yield more accurate elevation angles (by means of the iterative process discussed elsewhere in this report) than would virtual heights based on the actual true heights from which the F1 retardation had been removed. Of course, if the F1 layer were explicitly included as a separate layer, the unretarded true F2-layer heights would be preferred.

The E region is considered as a separate layer in this method; thus some allowance is made for the effect of the retardation in the E region upon the calculated value of h_pF2 derived from the M(3000)F2 scaled at vertical incidence. The formula to follow is a general formula which could be used to calculate the retardation in any underlying parabolic layer.

The amount of retardation expected when a vertical ray penetrates the E region ($f > f_c$) assuming a parabolic distribution of electron density with height is

$$-\Delta h = \left\{ f/f_c \log \left[\frac{f/f_c + 1}{f/f_c - 1} \right] - 2 \right\} - y$$

where f = frequency at which h_pF2 was scaled (= 0.834 foF2)

f_c = critical frequency of the E region (f_oE)

y_E = semithickness of E region.

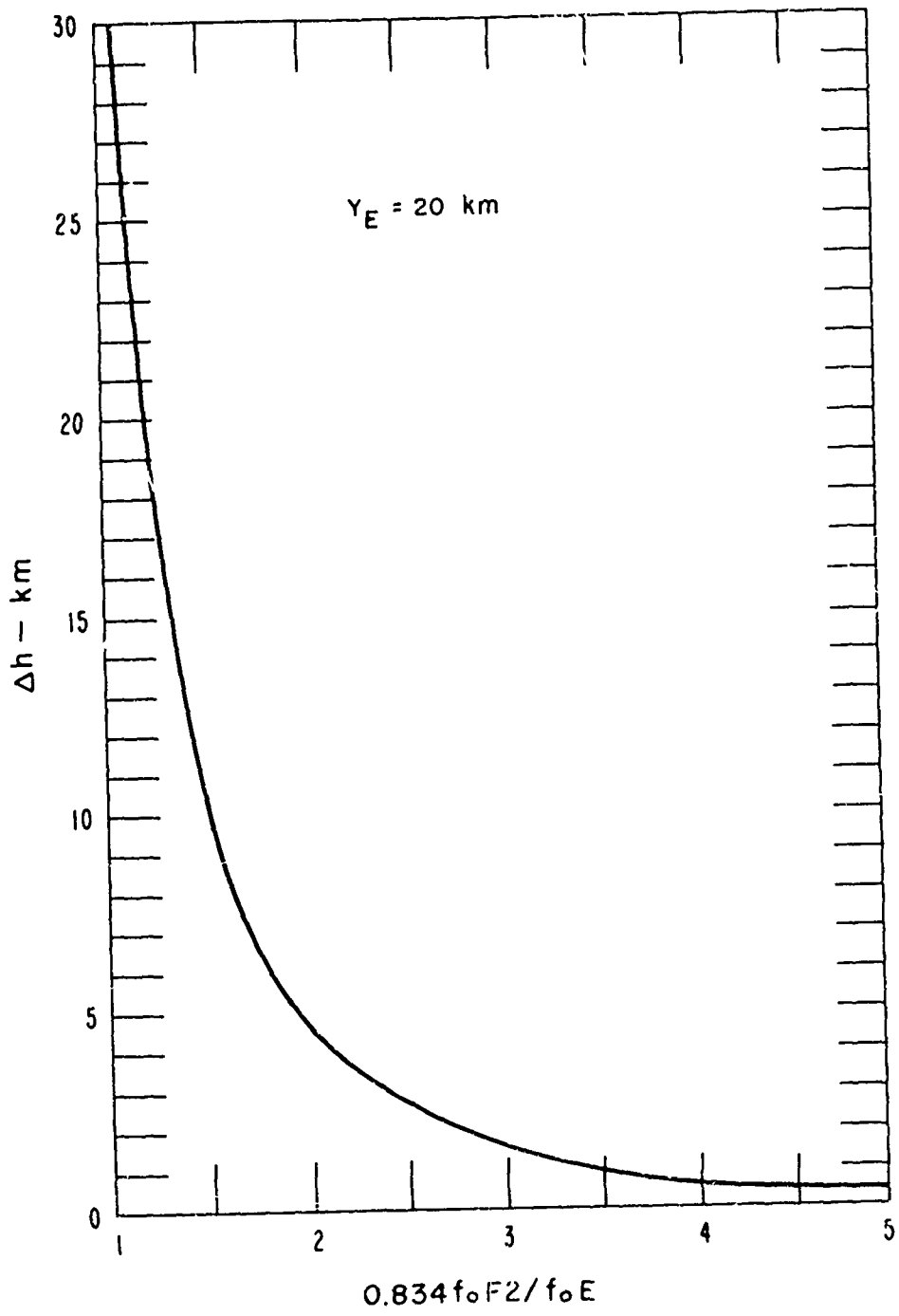

Figure 3.5. Correction to $h_p F2$ Due to Retardation in E-Region (Vertical Incidence)

Figure 3.5 shows some typical values of vertical retardation as a function of foF2/fo(E). A complete derivation of the above relationship is available [Kelso 1964], in terms of group path and the parabolic layer assumption.

The maximum height of the E region, $h_m(E)$, is taken to be constant for all hours and seasons at 130 km [Al'pert 1960].

3.5. Quasi-Empirical Determination of F2-and E-Layer Semithickness (y)

The height of maximum ionization of the F2 layer h_mF2 in units of the semithickness y is mapped as a function of geomagnetic latitude and solar zenith angle (figure 3.6 and 3.7) for high and low solar activity. The contour plots were generated by using smoothed values of the height of maximum electron density and quarter-thickness (SCAT = y/2) from observations primarily along the 75th meridian [Wright, Wescott, and Brown 1960].

June and January data were used to estimate extreme values of the zenith angle of the sun at specific geographic latitudes. A scatter plot of h_m/SCAT versus sun's zenith angle produced average regression lines with little scatter.

Stations off the 75th meridian, varying in geomagnetic latitude, were checked against values on the 75th meridian to verify the relationship with geomagnetic latitude. The values compared favorably, thus geographic longitudes and latitudes were replaced by geomagnetic latitudes. The ratio (h_m/y) depends somewhat on solar activity. Therefore contour charts were prepared for high (125) and low (25) twelve month running average Zurich sunspot numbers [Lucas and Remmler 1966].

The ratio h_m/y is overestimated when h_pF2 is used as an approximation to h_mF2, especially during the daylight hours in the summertime. The reasons for this are as explained in the preceding section. However, until the F1 layer is represented separately, the values of semithickness,

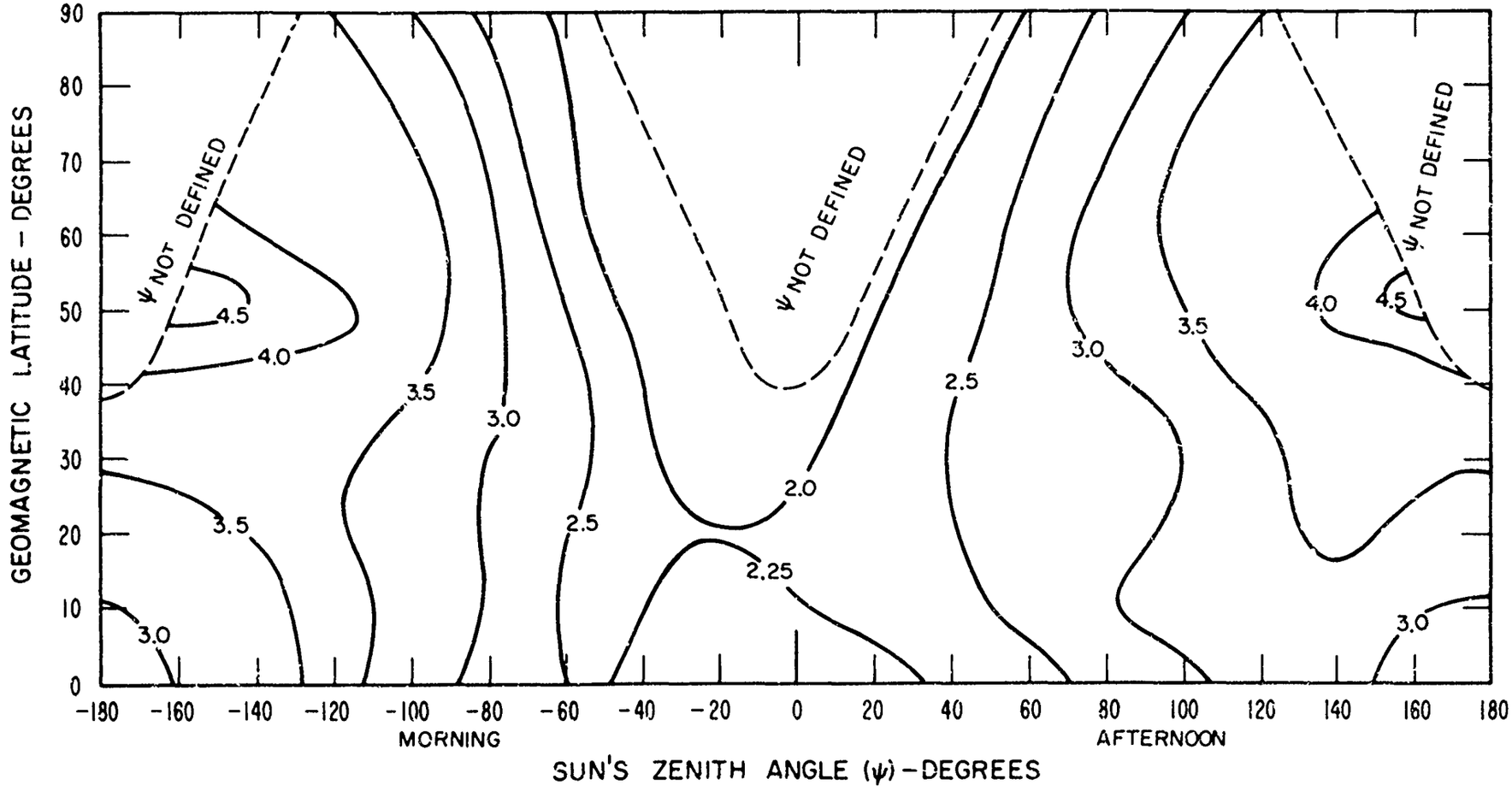

Figure 3.6. Contour Chart of the Ratio $h_m F2 / yF2$ for High Solar Activity (SSN = 125)

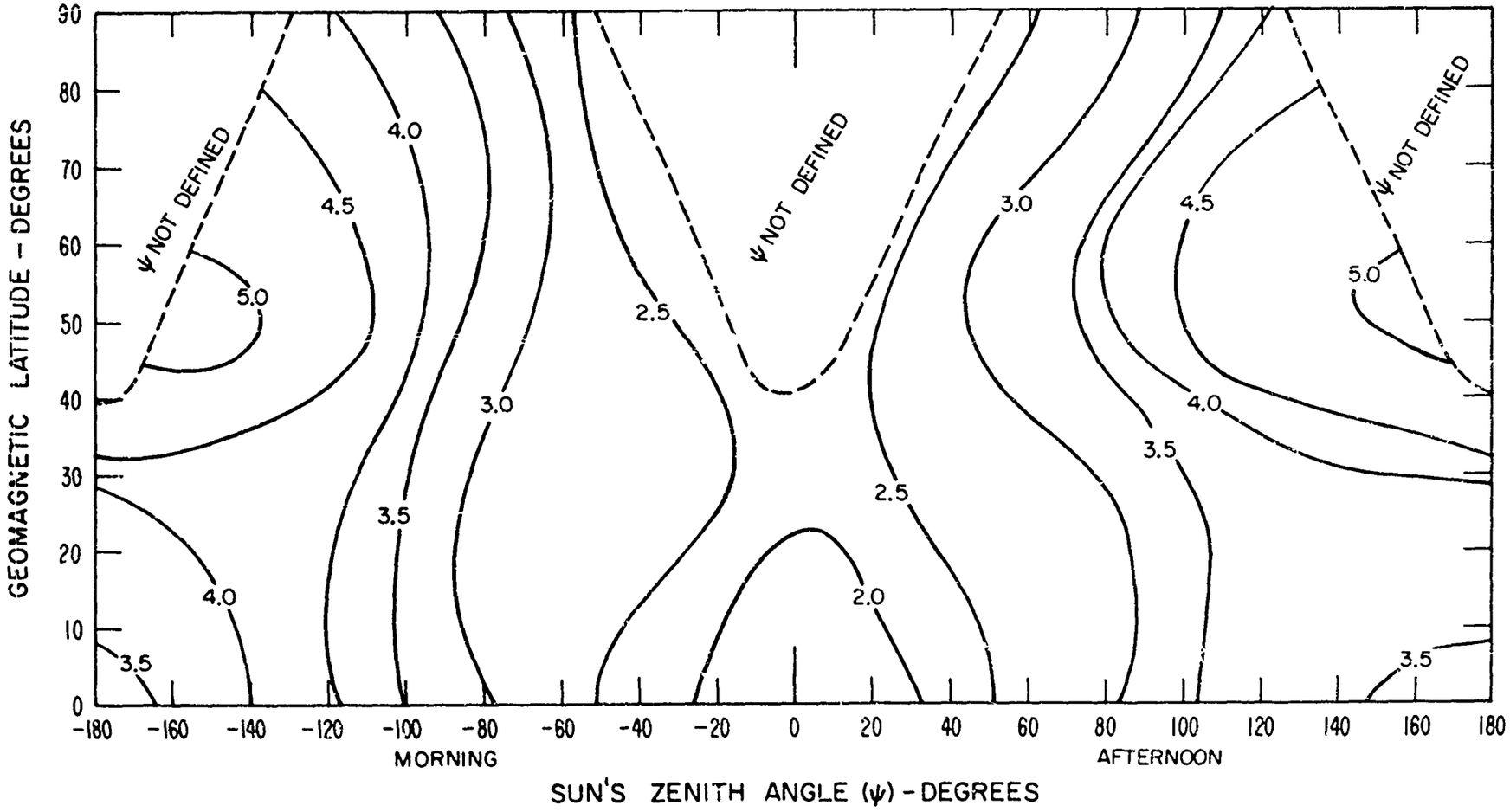

Figure 3.7. Contour Chart of the Ratio $h_m F2 / yF2$ for Low Solar Activity (SSN = 25)

using h_pF2 as an estimate of h_mF2, yield a more realistic description of the complete F layer than values estimated from the true height of the F2 region. This is especially true in a practical prediction routine that relies upon the equivalence theorem and the sec ϕ "corrected" law.

The semithickness of the E region is taken to be stable throughout the day and for all seasons as 20 km [Al'pert 1960].

4. Basic Noise Data

4.1. Median and Decile Values of Man-Made Noise

The available man-made noise power at the input of an equivalent loss-free receiving antenna used in this model is assumed to vary as

$$N_a = V + 12.60 \log_e (f/3)$$

where

N_a = man-made noise power in 1 Hz band - dB < 1 watt

V = measured value of man-made noise power at 3 MHz in 1 Hz band-dB <1 watt

f = operating frequency (3-30 MHz)

If measured values of man-made noise are not available, an estimate may be obtained from the population of the area about the receiving site as shown in figure 4.1. The upper and lower decile values, D_u and D_ℓ, are taken to be 9 dB and 7 dB from the graphical values which are the medians, respectively [Spaulding 1965].

4.2. Median and Decile Value of Galactic Noise

The galactic noise estimates and the associated distributions are those levels extrapolated to 3 MHz from Cottony and Johler [1952], and verified using a vertical antenna [Crichlow and Spaulding 1965].

The median galactic noise is represented by

$$N_g = 165 + 9.555 \log_e (f/3)$$

where

N_g -- expected median value of the galactic noise in a 1 Hz band - dB < 1 watt

f = operating frequency - MHz.

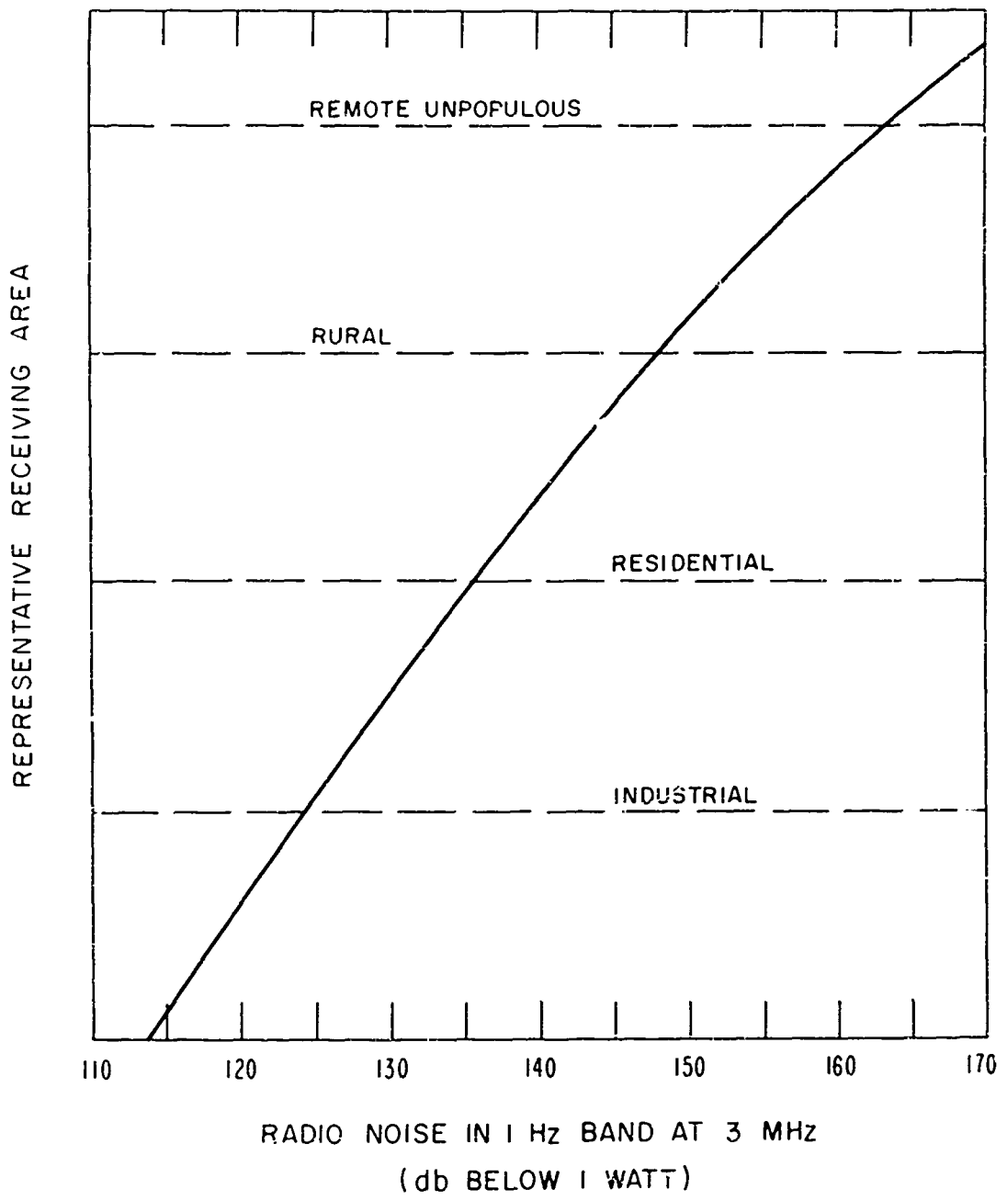

Figure 4.1. Typical Man-Made Noise Relative to Population of Receiving Area

The variability (D_u and D_ℓ) is taken to be 2 dB about the median [CCIR 322] at times when it is possible to see the galaxy at the operating frequency. The ionosphere above the receiving locations is examined to determine whether ionospheric penetration is likely and galactic noise present.

4.3. Median and Decile Value of Atmospheric Radio Noise (3-30 MHz)

The values of atmospheric radio noise used in these methods are taken from the world-wide 1 MHz noise maps, frequency dependencies (3-30 MHz), and variability charts (3-30 MHz), found in CCIR Report 322.

The world-wide (1 MHz) atmospheric noise maps are for discrete four-hour time blocks for four seasons of the year. The values from two adjacent maps are used and an interpolation made on time. A frequency dependence and variability accompanies each four-hour time block and adjacent values are used to interpolate for a given time.

Methods of mapping the noise and the accuracy to which it was mapped are explained by Lucas and Harper [1965]. A sample numerical world-wide map, frequency dependence, and variability chart appear in figures 4.2 and 4.3 (k, Boltzmann's constant; t, 288° Kelvin; b, effective noise bandwidth).

The numerical coefficients of table 4.1 which describe the world-wide distribution of the 1 MHz atmospheric noise (dB > ktb) are evaluated by the function

$$F(\lambda, \theta) = \left\{ \sum_{\kappa} \left[\left(\sum_{k} b_{k,\kappa} \sin^{k} \theta \right) + \chi \right] \sin^{\kappa} \lambda \right\} + \xi, \quad (4.3)$$

where

χ = normalizing coefficient in longitude

$\xi = \alpha + \beta\lambda$,

$\alpha = F(0, \theta)$

$\beta = \dfrac{F(\pi, \theta) - F(0, \theta)}{\pi}$

θ = geographic latitude - degrees (north positive, south negative)

λ = geographic longitude - degrees (east of Greenwich).

(Contours in Tens of Decibels above ktb at 1 MHz

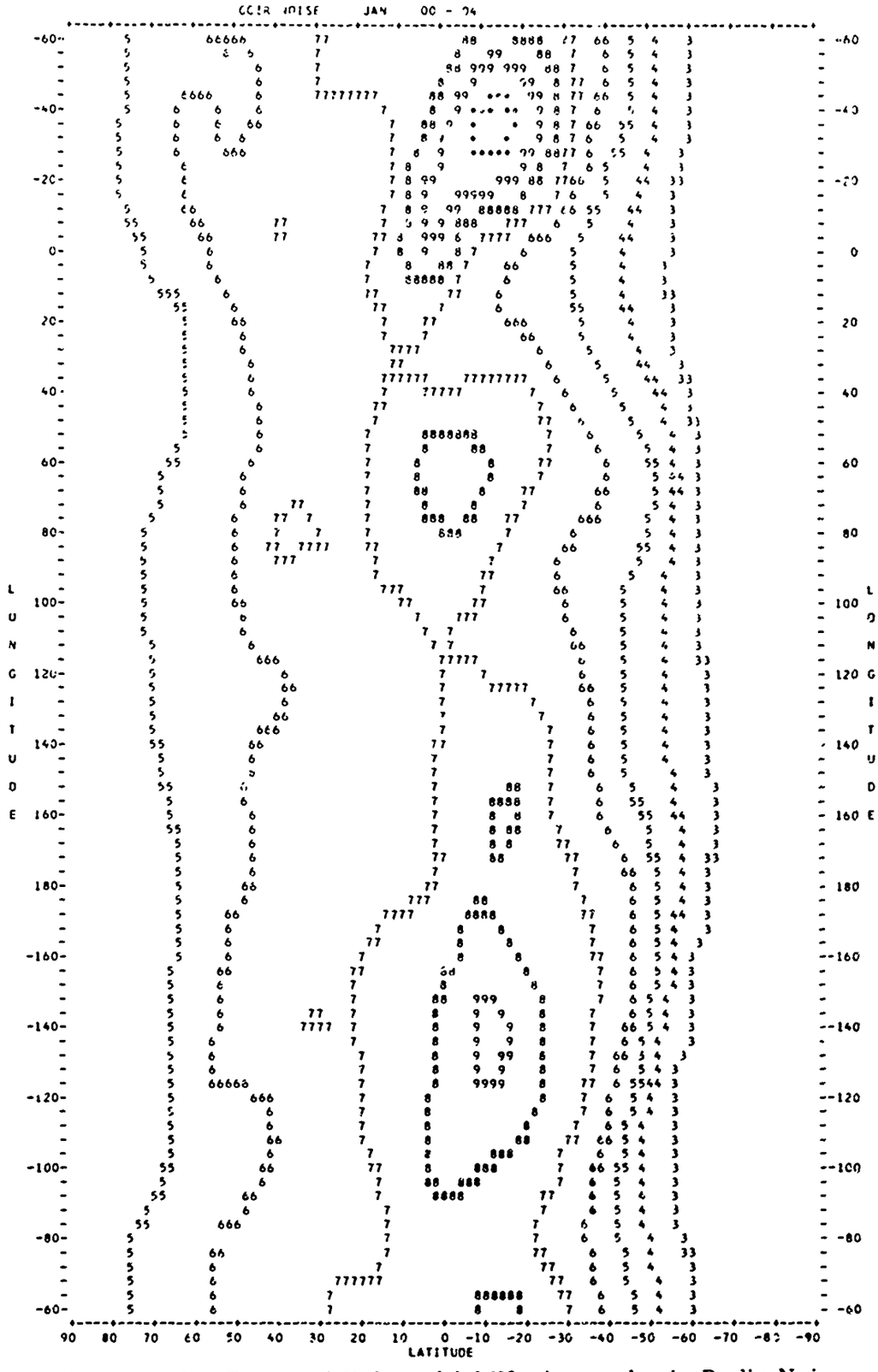

Figure 4.2. Expected Value of 1 MHz Atmospheric Radio Noise December-January-February (0000-0400 Local Mean Time)

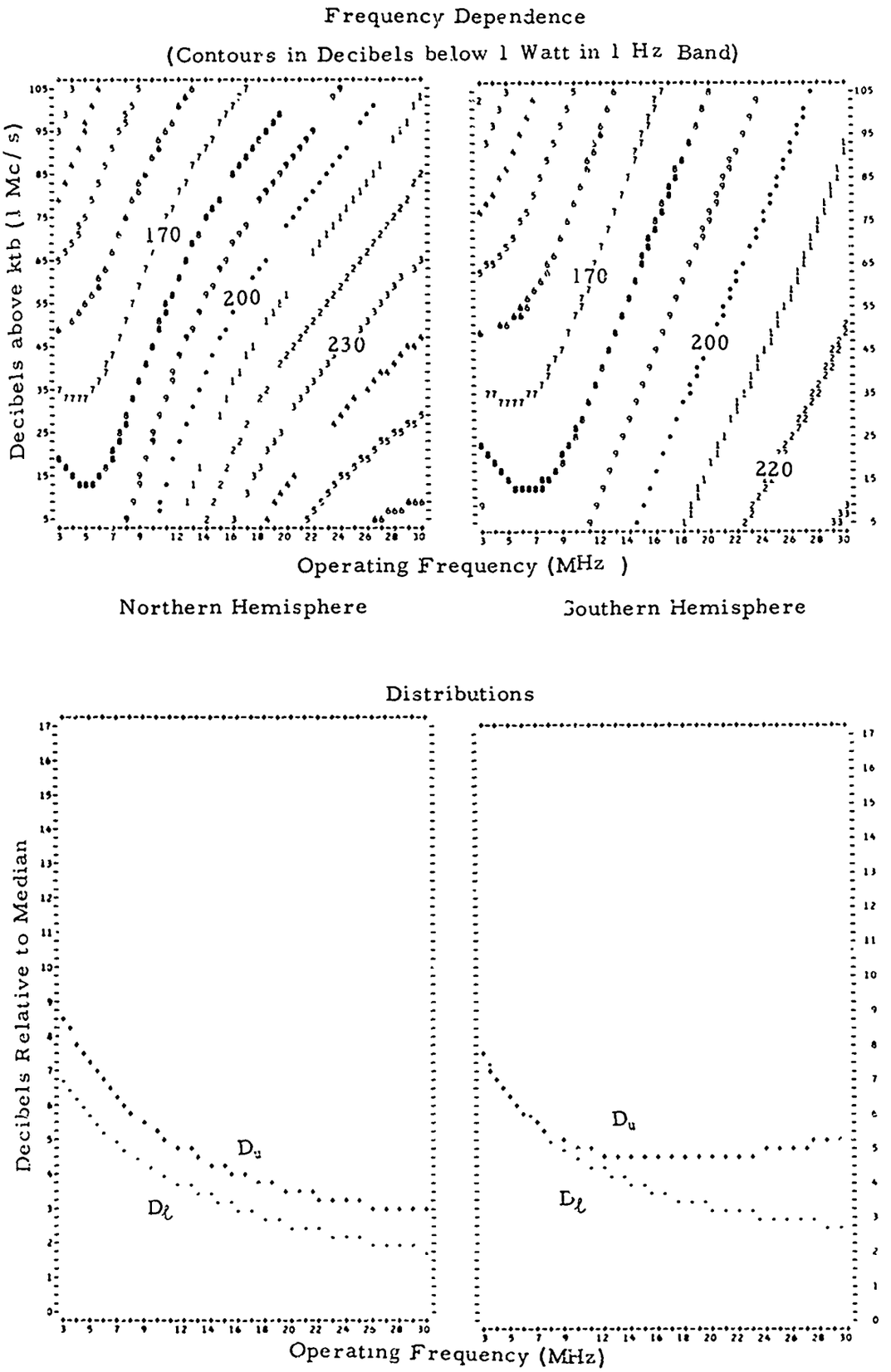

Figure 4.3. Frequency Dependence and Variability of Atmospheric Radio Noise December-January-February (0000-0400) Local Mean Time

The coefficients χ, α, and β appear on the top of table 4.1. The $b_{k,n}$ seen in the above table are in ascending order in k.

The "numerical" representation of the frequency dependence of the atmospheric noise (figure 4.3) is evaluated by

$$Y(X, N) = A_1(N) + A_2(N)\,X + A_3(N)\,X^2 + \ldots + A_7(N)\,X^6 \qquad (4.4)$$

where

$$A_i(N) = b_{i,1} + b_{i,2}\,N, \qquad i = 1, \ldots, 7$$

N = amplitude of the hourly median 1 MHz atmospheric radio noise (dB > ktb), and

$$X = \frac{8 \times 2^{\log_{10} f} - 11}{4}$$

where f is operating frequency - MHz.

The "numerical" coefficients shown in table 4.2 representing the day-to-day distribution (D_u & D_ℓ) of the atmospheric radio noise are evaluated by

$$Y(X) = A_1 + A_2\,X + A_3\,X^2 + A_4\,X^3 + A_5\,X^4\,, \qquad (4.5)$$

where

X = log (f), and

f = operating frequency - MHz .

All coefficients shown in tables 4.1 and 4.2 are listed in ascending order from left to right.

4.4. Combination of the Noise

The atmospheric, man-made, and galactic noises are evaluated at the receiving site and the predominant median noise and its associated distribution taken to be the prevailing noise power at all probability levels. Due to the uncertainties associated with the predicted values of noise, a negligible additional error is anticipated through the use of this assumption.

Table 4.1.

CHI (χ)	ALPHA (α) = 2.269999E 01		BETA (β) = 6.7163385E 00		
	MIXED LATITUDINAL AND LONGITUDINAL COEFFICIENTS ($b_{K,k}$)				
3.4641479E 01	4.1838363E 00	3.2114376E 00	8.9953179E-01	-1.6974557E-01	1.6158222E 00
	3.3186507E 00	2.7083092E-01	2.2331367E 00	-1.1209315E 00	4.8256665E-01
	2.0589997E-02	8.5821838E-02	-1.9583172E-01	-2.6686098E-01	6.4544409E-03
-7.5187851E 00	1.1590691E 01	6.2095144E-01	1.5535090E 00	-1.4273447E-01	2.4402036E 00
	1.1623971E 00	9.1016945E-01	1.0748580E 00	-1.9987696E-01	5.0635177E-01
	-8.5019631E-01	-1.8743569E-01	4.0717903E-02	-2.1692961E-01	7.7613309E-02
-8.6982949E 00	2.4657872E 00	-1.2486752E 00	-3.0897281E-01	8.0361975E-01	3.5433365E-01
	-4.6153469E-01	-7.6248726E-01	-1.1270536E 00	-6.9617344E-02	-4.6668957E-01
	8.5319638E-02	1.4724271E-01	2.3000628E-01	2.6034773E-01	-2.0105496E-01
-1.5436085E 00	-4.4117047E 00	-2.4024609E 00	-1.3466542E 00	-1.1570974E 00	-1.4608705E 00
	-1.4250866E 00	-1.6104781E 00	-1.4002871E 00	5.6879533E-02	-7.0556926E-01
	2.7420908E-01	-2.0364012E-01	-1.0327001E-01	-6.2937494E-02	6.7669654E-02
1.3706101E 00	-4.8005903E 00	2.2654845E-01	-4.7745761E-01	6.6932891E-01	-1.0071011E 00
	3.2000929E-02	-3.1236828E-02	7.1575443E-01	6.5738083E-02	5.5866561E-01
	6.0296925E-02	3.1414077E-02	1.1369560E-01	3.5426513E-02	2.1205742E-01
6.1284662E-01	1.9742792E-01	1.2945121E 00	2.7450939E-01	6.0511023E-01	4.3691183E-01
	5.6840682E-01	9.5418876E-01	8.3673636E-01	3.2128377E-01	1.7297205E-01
	3.1594925E-01	3.1201237E-01	-7.5862439E-02	-8.8055369E-02	-1.4125150E-01
-3.4068217E 00	4.2503302E 00	7.4010170E-01	1.5048757E 00	6.7479340E-01	9.6068445E-01
	-3.2817095E-01	1.0287417E 00	-1.1916623E-01	1.4891621E-01	-3.4761769E-01
	-3.2123270E-01	8.1785465E-04	-4.0498657E-01	8.6962527E-03	-1.4618824E-01
1.1255579E 00	-1.7440683E 00	5.9519903E-01	-8.8492602E-01	-2.2925416E-01	-1.0281412E 00
	-8.9691107E-01	-8.9222268E-02	-5.8161654E-01	-1.3910757E-01	-3.6209463E-02
	-2.3172602E-01	-2.5856530E-01	8.0749542E-02	2.3171104E-01	1.2793520E-01
2.6409014E 00	-2.7063663E 00	-3.0069564E-01	-7.7782393E-01	-8.6896805E-01	-1.0232958E 00
	3.0471668E-01	-7.3099355E-01	-9.4490529E-02	8.6539656E-02	2.2454228E-01
	4.0407534E-01	8.4599663E-02	2.8447475E-01	4.7984049E-03	5.1451579E-02
1.1584860E-03	9.6304939E-01	6.4538500E-01	3.8107366E-01	-5.5120395E-02	5.0567412E-01
	6.4151160E-01	-3.0330572E-02	3.1470300E-01	-1.8471400E-01	-1.2524988E-01
	-9.3014406E-02	-2.3877290E-02	-2.3222978E-02	-1.7396925E-01	-1.0074406E-01
-2.1746216E 00	3.2683047E 00	-2.8430077E-01	4.2815639E-01	-2.3733925E-01	9.5019515E-01
	8.1716286E-02	4.4815574E-01	-1.8116413E-01	-8.8720208E-03	-2.2963195E-01
	-8.5179273E-02	5.9392298E-02	-6.0480731E-02	3.0063088E-02	4.8716214E-02
1.5946736E 00	-2.1562011E 00	-4.3744873E-01	-2.0611041E-01	2.0493224E-01	4.1234136E-02
	1.6107755E-01	-1.8079664E-01	-3.1419422E-02	-1.0448193E-01	1.1934572E-01
	1.2976262E-01	7.3347365E-02	-1.3326478E-01	2.0672675E-03	-4.5910547E-02
1.1699423E 00	-1.5792550E 00	-2.5449755E-01	-3.9909337E-01	8.8875179E-03	-3.0585724E-01
	-2.2256739E-01	-2.4563146E-01	1.2344014E-01	-9.1622903E-02	2.5872564E-01
	-4.5232101E-02	-1.3863005E-01	7.2964433E-02	-2.3786612E-02	2.5091340E-02
-9.3058598E-01	9.3483422E-01	-4.4868054E-01	3.2631055E-01	3.2173563E-02	1.1614085E-01
	1.0990906E-01	-4.2361338E-02	-2.7248545E-02	1.4352324E-01	4.2833887E-02
	-1.9052193E-03	-9.7036332E-03	1.6940341E-01	5.3340090E-02	9.2850770E-02
-7.8763641E-01	1.0738458E 00	8.7518213E-02	2.3873042E-01	7.0959565E-02	1.4078416E-01
	-8.1726638E-02	1.4819878E-01	1.2792732E-04	5.9923285E-02	-1.4252998E-01
	-1.2760729E-02	-8.2424253E-02	-1.0705708E-01	-9.5950598E-02	-1.1751129E-01
2.1600585E-02	-3.4387323E-02	2.3900788E-02	-1.5753577E-01	-2.3969109E-02	-4.7808595E-02
	-2.8907470E-01	5.7093941E-02	-1.5396938E-02	-2.1983922E-02	-3.8343917E-02
	-8.8688895E-02	1.2479780E-01	-2.7908701E-02	3.7739315E-02	9.2389973E-02
9.7669928E-01	-1.3490050E 00	-2.8223188E-02	-2.7278056E-01	6.0496410E-02	-3.9363531E-01
	-2.1260647E-01	-1.6107881E-01	1.1953866E-01	-2.3542236E-02	3.5194042E-02
	-3.6814155E-02	3.8382035E-02	-6.9230825E-02	5.3093469E-02	4.6383966E-02
-6.5701414E-01	8.1954885E-01	1.6195972E-01	2.7439178E-01	-1.3938923E-02	8.1943864E-02
	1.9195054E-02	1.0059547E-01	4.7303112E-02	1.2326524E-01	2.9068188E-02
	5.6146145E-02	-1.0025152E-01	2.4888263E-02	-1.9454892E-02	-1.1748289E-01
-5.6786439E-01	6.6199526E-01	9.9584180E-02	2.0509375E-01	-2.6008622E-02	1.5919285E-01
	2.2144167E-01	7.2422233E-02	-1.3792194E-01	1.0992916E-02	-8.7341417E-02
	1.8219609E-02	4.4138992E-02	7.5539654E-02	2.9724226E-02	-2.1267013E-02
3.0983446E-01	-2.2143902E-01	2.2173144E-01	-1.5246169E-01	-5.5985320E-02	-8.4307539E-02
	3.9864458E-02	9.2259294E-02	6.9509510E-02	4.4085193E-03	-5.0679226E-02
	6.3213329E-02	6.7632990E-02	2.0457405E-02	-2.2398057E-02	-1.9804921E-02
6.1626999E-01	-7.9372652E-01	4.4471113E-02	-2.4837638E-01	2.3627989E-02	-1.6684577E-02
	8.5042124E-02	-2.6746383E-02	2.1112916E-02	-1.4285335E-01	2.4136366E-02
	-1.2796140E-02	3.9184040E-02	-2.4318395E-02	-5.0749759E-02	3.7884517E-02
-5.2788065E-01	5.4866268E-01	-1.4587637E-01	2.0014451E-01	-1.7658861E-02	2.7867115E-02
	-5.2869652E-02	-5.0788510E-02	-7.8505645E-02	-6.7707503E-02	5.4139685E-02
	7.9882280E-02	1.0060148E-02	-3.9806549E-04	4.3656200E-02	1.6215308E-02
-2.3633683E-01	3.4599479E-01	-1.1544026E-02	1.1531503E-01	1.5346203E-03	1.2147482E-01
	6.9448562E-02	4.5366562E-02	-2.6172943E-02	7.2743568E-02	2.0151228E-03
	-4.0376027E-02	-1.2215829E-01	-3.0504355E-02	-7.6822593E-03	-5.4943502E-03
4.9502340E-01	-6.9573006E-01	-1.9216791E-02	-2.3916905E-01	-3.4897467E-03	-9.6757020E-02
	2.5023650E-02	-1.2097344E-01	-1.1786556E-01	-1.1143765E-01	1.1913951E-02
	-6.5070303E-02	-5.2703794E-02	-2.4122529E-02	-3.7377777E-02	3.6064968E-02
7.1638407E-02	-4.2834280E-02	-1.5550874E-02	-5.2523381E-02	4.6603216E-02	-1.4820323E-02
	1.7613651E-02	8.2576052E-03	8.0537319E-02	9.4820329E-02	6.8962116E-02
	5.3437116E-02	6.0261269E-02	2.1590534E-02	2.5998014E-02	2.1318753E-02
-8.6970037E-02	1.0757427E-01	-1.6310197E-02	8.7720697E-02	8.0987113E-02	6.6522471E-02
	-1.3011668E-02	4.2576828E-03	1.0092393E-01	8.1283978E-02	1.6721611E-02
	-3.5087837E-02	8.2912921E-03	-8.7403171E-03	1.1464976E-02	1.2783808E-02
-2.4476871E-01	3.0481783E-01	-1.6271845E-02	8.8080128E-02	-2.1270840E-02	3.6942236E-02
	-1.3844983E-01	3.9015760E-02	-2.9462057E-03	3.1630345E-02	-1.7927796E-03
	-3.5014738E-03	5.6930228E-03	3.6207843E-02	2.6823764E-02	-1.1850161E-02
3.4911822E-01	-4.2152635E-01	-2.2881739E-02	-1.4902288E-01	-6.5884550E-02	-1.0852067E-01
	2.9210823E-03	-4.6913841E-02	-3.2959051E-02	-4.5102556E-03	-9.0507488E-02
	-8.0836468E-02	-3.1536205E-02	-1.7965888E-02	7.7461631E-03	-3.9183684E-02
4.4339446E-02	-4.0566724E-02	3.1462368E-02	2.1738124E-02	4.4431764E-03	-5.9557740E-02
	1.9843870E-02	-3.1133253E-02	1.7950980E-03	-4.7113091E-02	-2.8238736E-02
	2.2579070E-04	-8.0499197E-03	-3.5822563E-04	-3.6707798E-02	-3.7908193E-02

Fourier Coefficients Representing the 1 MHz World-wide Distribution of Atmospheric Radio Noise, December-January-February (0000-0400 Local Mean Time)

Table 4.2.

TIME BLOCKS

00 - 04	04 - 08	08 - 12	12 - 16	16 - 20	20 - 24
FREQUENCY DEPENDENCE (NORTHERN HEMISPHERE)					
5.1464396E-03	1.9578661E-03	6.4431812E-04	-7.7358635E-04	4.7935808E-03	7.5132148E-03
-2.1874073E-02	-3.1284123E-02	-2.1885861E-03	-1.2374851E-03	-2.0086448E-02	-3.1190486E-02
-5.3265774E-02	-5.7129856E-02	-3.8541876E-02	-1.0759584E-02	-5.2335115E-02	-7.0445139E-02
2.3485862E-01	2.6515074E-01	1.3823060E-01	1.1765277E-01	2.1836369E-01	2.9776482E-01
9.3090396E-02	3.4857854E-02	1.4159342E-01	3.0344274E-02	1.1949617E-01	1.4221385E-01
-5.2714667E-01	-4.8079920E-01	-5.3263597E-01	-5.4932964E-01	-5.2892510E-01	-5.9214756E-01
7.2661293E-01	8.1514313E-01	5.3700674E-01	6.1035067E-01	7.0268744E-01	6.9095528E-01
-4.0462420E-01	-4.8874449E-01	1.3336874E-01	2.5647958E-01	-2.4503308E-01	-5.1815356E-01
1.7321095E 00	2.0165651E 00	-1.5656420E-01	-9.6593907E-01	9.7256898E-01	2.1326680E 00
4.6754704E 00	4.5076702E 00	-4.5337248E-01	-1.7218062E 00	3.4270667E 00	5.4322478E 00
-2.1917779E 01	-2.1965428E 01	-9.0273744E 00	-5.8219453E 00	-1.5965903E 01	-2.4450892E 01
-6.2582144E 00	-9.8616028E-01	1.2710692E 01	1.6671449E 01	-1.8885631E 00	-7.4510769E 00
2.4616179E 01	2.1699456E 01	1.8181485E 01	1.3845789E 01	2.2249658E 01	2.9032140E 01
7.3174758E 00	2.1794727E 00	4.5146703E 00	2.2940871E 00	7.0567941E 00	9.7249165E 00
FREQUENCY DEPENDENCE (SOUTHERN HEMISPHERE)					
3.0143955E-03	-2.2845696E-03	-7.5274411E-04	-1.3997095E-03	-3.6564795E-03	3.3167374E-04
-1.3958785E-02	-1.1765908E-03	-3.7619833E-03	-1.5487762E-03	4.5869794E-03	-3.3206859E-03
-2.7567580E-02	2.4051259E-02	5.2770951E-03	4.8204224E-03	3.2040968E-02	-4.5952080E-04
1.6856721E-01	1.0463027E-01	1.2206943E-01	1.1480539E-01	6.0028845E-02	1.4311093E-01
-3.6980309E-02	-1.5088457E-01	-1.0070603E-01	-5.9997109E-02	-1.4929356E-01	-9.4815058E-02
-4.7263805E-01	-4.5339737E-01	-5.0750125E-01	-4.9003121E-01	-3.8420528E-01	-4.6252675E-01
8.2445444E-01	7.5110295E-01	7.0779588E-01	6.9604462E-01	7.7892180E-01	8.4676390E-01
-3.0476368E-01	5.2602189E-02	7.8407382E-02	1.9581196E-01	3.0842602E-01	-5.7306319E-02
1.3392726E 00	5.0137264E-01	2.8305843E-01	-1.5927426E-01	-4.4212906E-01	7.2664566E-01
3.1315548E 00	-6.8688268E-01	-1.2244095E 00	-1.6802038E 00	-2.6451535E 00	6.7443838E-01
-1.8412520E 01	-1.3906543E 01	-1.0959831E 01	-8.6921585E 00	-7.2818758E 00	-1.5076057E 01
3.8431763E 00	1.4617926E 01	1.9799508E 01	1.8380329E 01	1.8911183E 01	1.0063312E 01
2.4079279E 01	2.1927978E 01	1.4974221E 01	1.2803221E 01	1.4034052E 01	2.2037366E 01
1.0766247E 00	4.1730763E 00	-1.9565070E 00	-1.3030351E 00	2.0163780E-01	-1.5549285E 00
DU (NORTHERN HEMISPHERE)					
6.0209275E-01	2.1340638E-01	-1.9555985E 00	-1.6651338E 00	-2.8739800E-01	-1.8917620E-01
6.5778819E-01	8.5388710E-01	-2.1205268E-01	1.2117138E-01	4.4589695E-01	-6.3425864E-02
-4.1046134E 00	-4.0685837E 00	3.7298402E 00	3.2738994E 00	-2.4546834E 00	-2.0347731E 00
-2.5166600E 00	-3.9695986E 00	-2.6170116E 00	-2.8402774E 00	-3.2955722E 00	-1.6193680E 00
1.0600909E 01	1.3791575E 01	9.1979216E 00	9.3408259E 00	1.3676551E 01	1.0342979E 01
DU (SOUTHERN HEMISPHERE)					
1.0632049E 00	1.3976116E 00	1.4660566E 00	1.2005752E 00	1.2081916E 00	1.1392663E 00
1.1593890E 00	1.1515625E 00	1.9263401E 00	-2.3964122E-02	1.1658406E-01	2.0747147E 00
-4.3297605E 00	-7.8835601E 00	-7.2381649E 00	-8.4895499E 00	-8.0678885E 00	-3.2627040E 00
-2.5652402E 00	-3.6707661E 00	-4.6941070E 00	-9.2496518E-01	-1.1817305E 00	-3.8453463E 00
9.7716473E 00	1.6127013E 01	1.6370249E 01	1.8977912E 01	1.7165843E 01	8.2028161E 00
DL (NORTHERN HEMISPHERE)					
3.7486929E-01	1.7813529E-01	-1.8116861E 00	-1.7880262E 00	-7.1384400E-01	-5.4076995E-01
3.1564012E-01	3.2218151E-01	-1.4920878E 00	-1.6136066E 00	-8.5257655E-01	-7.3759924E-01
-3.0003346E 00	-3.8502192E 00	3.3302979E 00	3.4342778E 00	-1.4325795E 00	-6.8667439E-01
-1.8057770E 00	-2.9635462E 00	4.1285570E-01	8.9947309E-01	-9.8679343E-01	-3.1564179E-01
8.2776666E 00	1.1999329E 01	6.2525381E 00	5.8376649E 00	1.1112038E 01	7.8052481E 00
DL (SOUTHERN HEMISPHERE)					
5.6810469E-01	-9.8571727E-02	3.3805420E-01	1.6123230E 00	1.0424289E 00	4.3483636E-01
5.3066228E-01	-3.2132708E-01	1.3994567E 00	1.6955148E 00	1.9244705E-01	7.4837818E-01
-3.6617504E 00	-4.0435092E 00	-2.8583916E 00	-7.9285545E 00	-7.3462748E 00	-2.0943523E 00
-2.0830088E 00	-2.1118134E 00	-4.5804893E 00	-4.2703484E 00	-1.7737439E 00	-2.0550801E 00
9.4660861E 00	1.3757253E 01	1.1324406E 01	1.5791625E 01	1.6037100E 01	7.2837164E 00

Power Series Coefficients Representing the Frequency Dependence and Distribution of Atmospheric Noise - Winter

5. General Problem of Predicting Sky-Wave Radio System Performance

The performance of ionospheric telecommunication circuits varies markedly with frequency, geographic location, time of operation, equipment parameters, etc. Much of this variation is directly related to changing ionospheric conditions which (among other things) dictate the likelihood of long-distance communications. The changes affect the attenuation of the radio signal and control the vertical angles of arrival and departure.

Predictions of ionospheric telecommunication system performance can be expressed in many ways. This report expresses the expected performance as follows:

(1) the probability that a sky-wave path exists for a given frequency (q_f);

(2) the maximum frequency corresponding to a specified probability of propagation MUF (q_f);

(3) the loss in the communication system (L_s);

(4) available median signal at the receiving system input ($\bar{s}$);

(5) available signal-to-noise ratio at the receiver ($\bar{s}/\bar{n}$);

(6) likelihood that a specified signal-to-noise ratio will be exceeded ($q_{s/n}$);

(7) probability that a specified grade of service (gr) will be equalled or exceeded for a specified fraction of days within the month (service probability, Q_T)[Barsis et al 1961; Norton 1962; Rice et al. 1965]; and

(8) the minimum operating frequency for a specified fraction of days within the month (LUF).

5.1. Likelihood of a Sky-Wave Path

The detailed considerations in the determination of sky-wave paths and the associated probability of the existence of a sky-wave path are given in section 10. In general, the probability is estimated as a function

of frequency, for a specified path length, at a given geographic location and time. The probability depends upon the maximum ionization level and the corresponding height in the various ionospheric regions. Probability predictions involve both estimates of median ionospheric conditions and estimates of the distribution about the median and are expressed as the fraction of days within the month that some sky-wave path is expected to exist at a given hour.

5.2. The Maximum Frequency Corresponding to a Specified Probability of Propagation

The maximum frequency corresponding to a specified probability of propagation involves the same considerations outlined in section 5.1 above, except that the probability is fixed and the corresponding frequency is determined rather than the frequency being fixed and the probability determined. Normally the probability is fixed at 0.5 and the frequency corresponding to this probability is referred to as the monthly median Maximum Usable Frequency or MUF (0.5). Note that MUF(q) is the quantile of order q of the distribution, i.e., MUF $<$ MUF(q) with probability q. As q varies from 0 to 1 the quantile of order q, MUF(q), will increase from zero to its maximum value.

5.3. The Loss in the Communication System (L_s)

System loss for a particular propagation path in high frequency communication circuits may be defined as follows:

$$L_s = L_{bf} + L_i + L_e - G_t - G_r + Y_p, \text{ (dB)} \qquad (5.1)$$

where:

L_s = system loss (signal power available at the receiving antenna terminals relative to that available at the transmitting antenna terminals in decibels)

L_{bf} = free space transmission loss based on ray path distance of the path being considered and the radio frequency (decibels)

L_i = losses due to ionospheric absorption (decibels)

L_g = losses due to ground reflection (decibels)

G_t and G_r = the transmitting antenna and receiving antenna power gains in decibels relative to an isotropic antenna*

Y_p = loss associated with day-to-day variations in ionospheric and circuit parameters (statistically determined and dependent upon circuit location, time, path length, and fraction of days being considered).

In high frequency communication circuits, several propagation paths are often possible, e.g., a single reflection from the F region (1F); a single reflection from the E region (1E), multiple reflection from the E and F region (2F, 3F, 2E, etc.); or paths involving reflection from both regions (1E1F, 1F1E, etc.). The probable paths are dependent upon the geometry of the circuit involving layer heights and great circle distance and upon the relative ionization in the various regions.

For most systems applications, it is considered adequate: (1) to evaluate L_{bf}, L_i, L_g, G_t and G_r for each of the likely propagation paths, (2) to select the path with the minimum loss, and (3) to combine this loss with the empirically determined (Y_p) which includes the effect of the day-to-day variations in the parameters used in estimating L_{bf}, L_i, L_g, G_t and G_r, plus such factors as ionospheric focusing, deviative absorption, polarization mismatch at the receiving antenna, and the addition of signals via various paths.

5.4. Available Signal at the Receiver

The available signal level at the receiver requires only that the loss in the communication system as defined in section 5.3. be combined with the power available at the transmitting antenna terminals. The fraction of time a given signal level is exceeded is directly related to the fraction of time associated with Y_p in section 5.3.

* In this report G_t and G_r are in the direction of the propagation path and include all losses so that $G_t + G_r$ approximates the path antenna gain G_p [Rice, et al 1965].

5.5. Available Signal-to-Noise Ratio at the Receiver

An estimation of the available signal-to-noise ratio requires that the expected available signal power be combined with the expected noise power. The expected noise power includes estimates of atmospheric, cosmic, and man-made noise powers. Distributions as well as median values of both signal and noise are involved including seasonal, geographic, and frequency dependence. Normally the expected signal-to-noise ratio is expressed as a median of the hourly medians for those days some sky-wave path exists within the month.

5.6. Likelihood that a Specified Signal-to-Noise Ratio Will be Exceeded

The likelihood that a specified signal-to-noise ratio will be exceeded involves the same considerations as in section 5.3 except that signal-to-noise ratio is fixed and the likelihood determined plus a consideration of the probability that some sky-wave path exists. The likelihood that a specified signal-to-noise ratio is available at the receiver input is referred to as circuit reliability $q(R_h)$ and is obtained as a product of the likelihood that a given signal-to-noise ratio exists on the days a sky-wave path is expected ($q_{s/n}$) with the probability that a sky-wave path exists (q_f).

5.7. The Minimum Operating Frequency

As the operating frequency is decreased, the likelihood that a specified signal-to-noise ratio is equalled or exceeded also decreases. The minimum operating frequency, or Lowest Useful Frequency (LUF), is therefore the lowest frequency which can be expected to have a signal-to-noise ratio equal to or greater than that required for at least a given fraction of days (q_r) within the month (T). The required signal-to-noise ratio (R_h) is associated with the type and quality of communication required (grade of service, g_r) and is expressed as an hourly median signal-to-noise ratio. Unless otherwise specified the LUF is estimated

on the basis that the required signal-to-noise ratio be equalled or exceeded on 0.90 of the days of the month.

6. Theoretical Basis for Communication Path Geometry

6.1. Brief Description of Model

The propagation prediction model relies primarily upon vertical incidence ionosonde data to predict the performance on oblique incident communication paths. Probing at a given frequency through assumed parabolic layers (E and F2) is used to predict the virtual height of reflection on oblique paths. The data used for the above approximation are the monthly median foE, foF2, M-3000 factor, F2 and E semithickness, and probing frequency (f).

6.2. Vertical-to-Oblique Transformation

Since the basic data available on a world-wide basis are obtained from vertical ionosondes, a transformation must be effected in the application to an oblique path. The relation between the frequency (f) of an oblique incident wave reflected from the ionosphere and the frequency (f') of a vertical incident wave reflected from the same region is the point of interest. Since the two waves are reflected from the same virtual height, the relative electron density at the level of reflection must be the same for both.

Disregarding the terms due to the earth's magnetic field and also using Snell's law applied to a flat ionosphere for the refractive index of the ionosphere, the following relation is obtained:

$$f = f' \sec \phi, \tag{6.1}$$

where

ϕ = incident angle of the wave upon the ionosphere

f = oblique frequency at h'

f' = vertical incident frequency at h'

h' = virtual height of reflection.

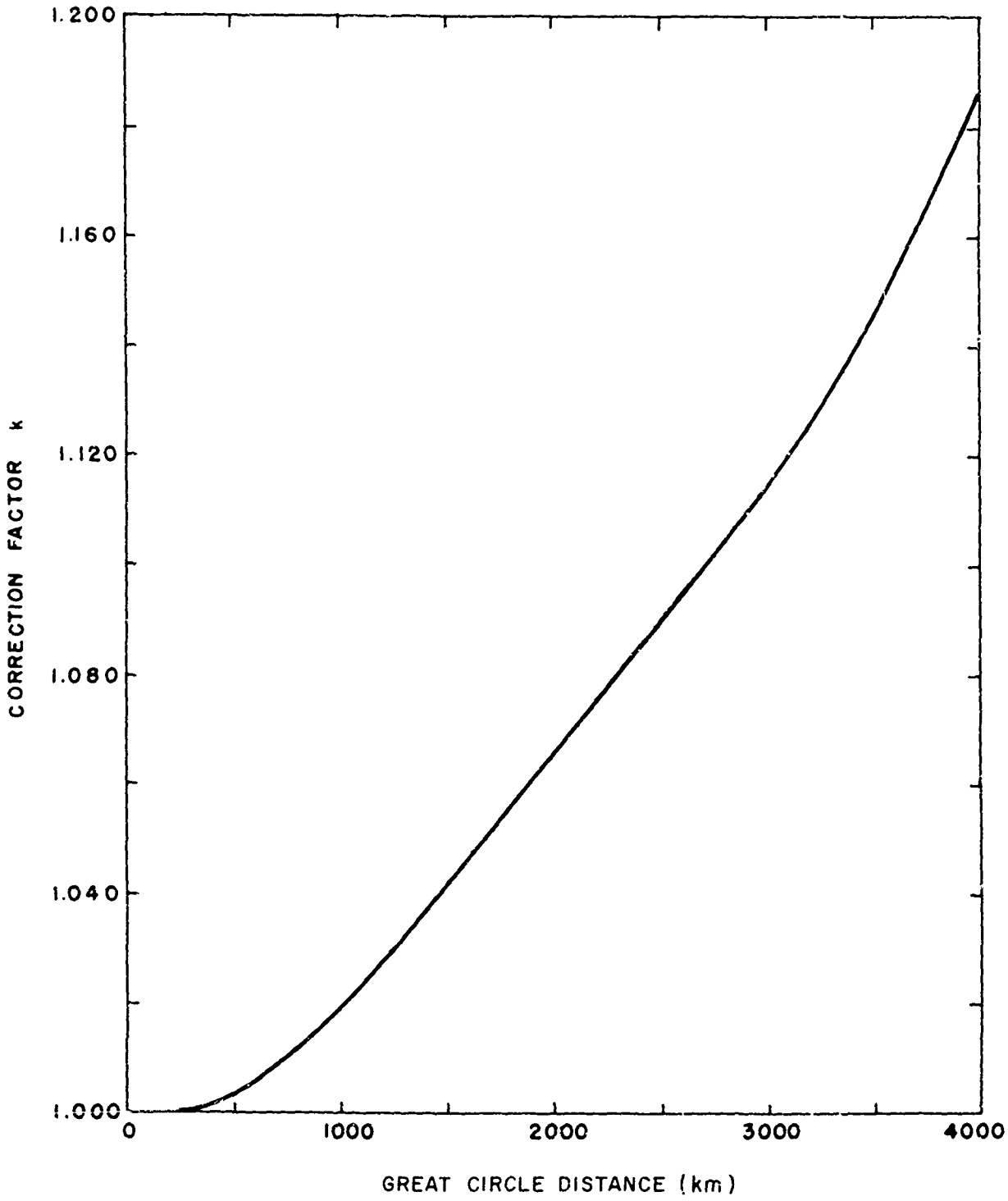

Figure 6.1. Ionospheric Curvature Correction Factor (N. Smith)

For the curved ionosphere the above relationship must be corrected to

$$f = f' \, k \sec \phi, \tag{6.2}$$

where k sec ϕ is referred to as secant ϕ (corrected). The ionospheric curvature correction factor, k, is shown as a function of the transmission distance in figure 6.1 and discussed in section 7.1.

Figure 6.2 shows the vertical-to-oblique transformation graphically. The dashed curve C, is the so-called transmission curve (given distance) by which vertical ionograms are scaled. The point at which the transmission curve C becomes tangent to the h'f curve is the scaled h' at (3) which corresponds to the same height (3) on the oblique ionogram only shifted by sec ϕ. The curves A and B illustrate how further points on the h'f curve may be obtained by shifting the transmission curve.

6.3. The Equivalence Theorem

Neglecting the earth's magnetic field and applying Snell's law, the concept of equivalent path for flat earth is shown in figure 6.3.

The equivalent path concept states that the time required for a signal to travel the assumed actual path TBR is the same as a wave traveling at the speed of light by the path TAR [Mitra 1952]. This concept then leads to an important relation between vertical and oblique incident propagation; i.e., the height of the equivalent path is the same as the vertical height, h', measured at the equivalent vertically incident frequency.

The above relationship, secant ϕ (corrected) and assumed parabolic distributions for two layers (E and F2), are the theoretical basis for ray path selections, time delays, and vertical angles of arrival.

6.4. Parabolic Assumption

The parabolic-layer method used is based on the equivalent path concept and the secant law for curved earth and ionosphere. The validity

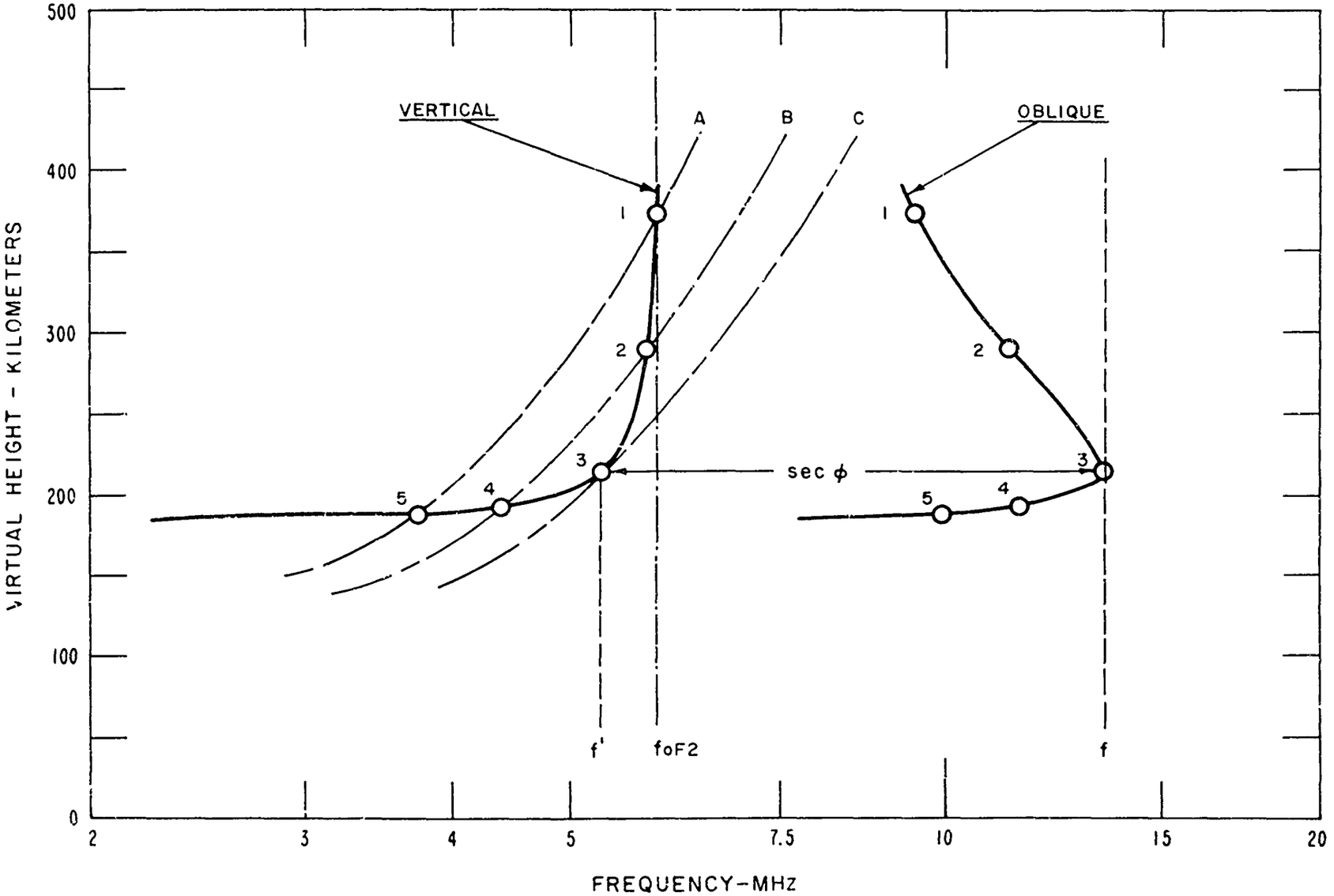

Figure 6.2. Vertical-to-Oblique Transformation

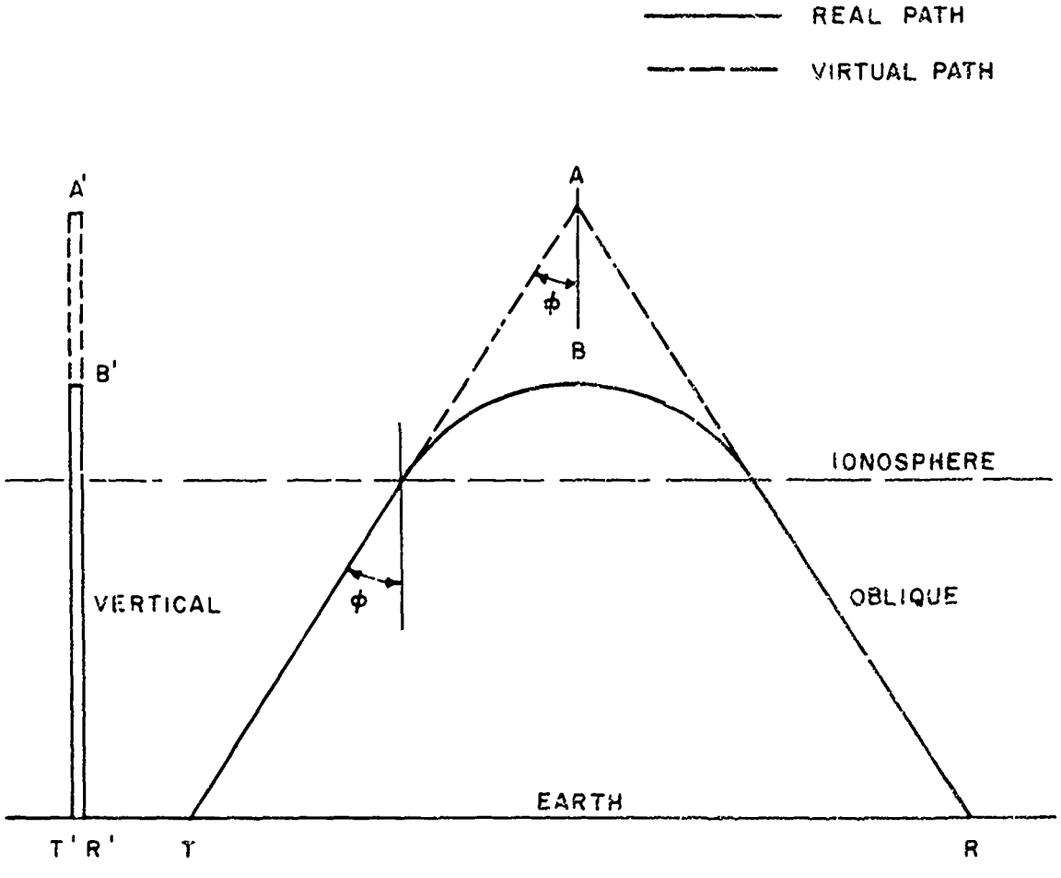

Figure 3. Equivalence Theorem for a Plane Ionosphere and Plane Earth

of this method is determined when one observes how well the shape of the ionosphere is approximated by two parabolas. It is believed that for average conditions, at frequencies of interest for long-distance HF propagation and considering the limiting factor of accurate world-wide data, the shapes of electron density versus true height profiles are adequately represented.

The model used in this method is patterned after the work of Newbern Smith [1939] and the transmission equations developed by Rawer [1948, 1950], [Bibl 1950] for parabolic ionospheric layers. The effect of the earth's magnetic field is neglected and the vertical ionization distribution is assumed to be parabolic. The earth and ionosphere are assumed concentric and the vertical ionization distribution taken to be constant over the area in which the radio ray is in the ionosphere. The angle-of elevation at the transmitter is therefore equal to the angle-of-arrival at the receiver.

The range equation developed by Rawer for two parabolic layers is (see figure 6.4)

$$D = 2 R_o \left\{ \left[\left(\frac{\pi}{2} - \Delta \right) - \alpha_F \right] + \left[\frac{y_F \tan \alpha_F}{R_F} \left(\frac{\text{arc coth } \mu_F}{\mu_F} - 1 \right) \right] + \left[\frac{2 y_E}{R_E} \tan \alpha_E \left(\frac{\text{arc tanh } \mu_E}{\mu_E} - 1 \right) \right] \right\} \qquad (6.3)$$

where

$$\mu_{E,F} = \frac{\sec \alpha_{E,F} \, f_{E,F}}{f}$$

D = great-circle distance - km

$\alpha_{E,F}$ = angle of incidence at the midpoint of the layer

$\alpha_{E,F} = \text{arc sin} \left[\frac{R_o}{R_{E,F}} \cos \Delta \right]$

R_o = earth's radius - km

Δ = angle of takeoff - degrees

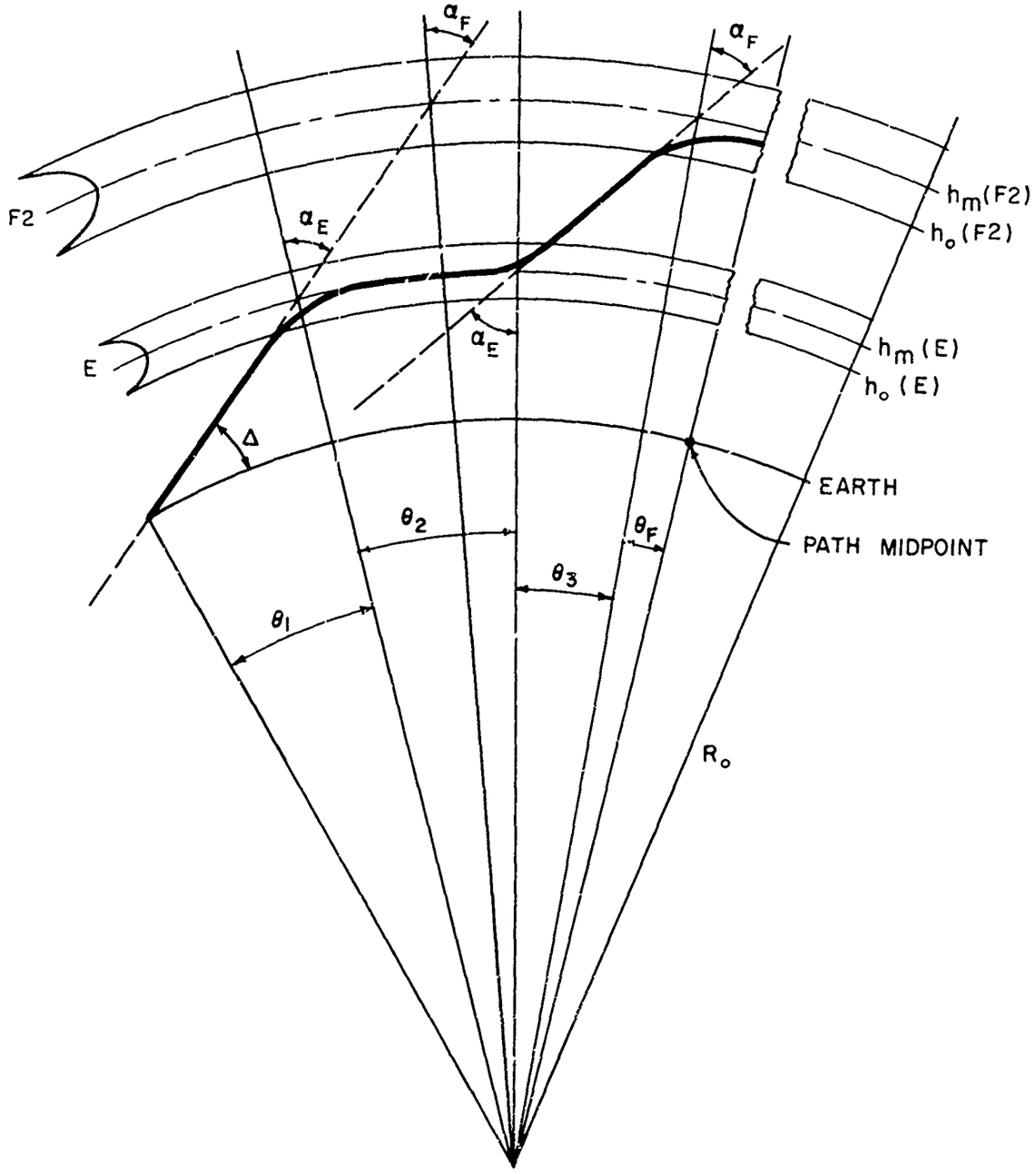

Figure 6.4. Rawer's Range Equation for Two Parabolic Layers

f = operating frequency - MHz

$f_{E,F}$ = critical frequency - MHz

$R_{E,F}$ = $R_o + h_{m(E,F)}$

$h_{m(E,F)}$ = true height of maximum ionization

$y_{E,F}$ = semithickness of the layer in kilometers.

The terms of the range equation (6.3) correspond to the angular distances as:

Term 1 is $\theta_1 + \theta_3$

Term 2 is θ_F

Term 3 is θ_2 (see figure 6.4)

The above range equations are derived for one hop via the reflecting region. In the case of multihop propagation the method applied is to convert the path parameters to an average profile along the path; thus equal hop lengths are assumed along with equal angles of elevation. Areas typical of actual reflection and retardation regions are inspected to generate the typical path profile.

Rawer's range equation and the transmission curve method of Newbern Smith are coupled together to yield a fast and economical method of selecting ray paths which is consistent with the scaled data.

7. Calculation of Sky-Wave Paths

The calculation of the upper limit of frequency and signal levels for a given circuit requires knowledge of the path and its associated ionospheric parameters as seen in the preceding sections. The total ground range (great-circle distance) of the circuit is calculated by knowing the geographic coordinates of the transmitter and receiver. The earth is considered a perfect sphere and the distance is calculated by

$$\cos(g) = \sin(x_1) \cdot \sin(x_2) + \cos(x_1) \cos(x_2) \cdot \cos(y_2 - y_1) \qquad (7.1)$$

where

g = great-circle distance - degrees

x_1 = transmitter latitude - degrees

y_1 = transmitter longitude - degrees

x_2 = receiver latitude - degrees

y_2 = receiver longitude - degrees.

Once this great-circle arc is defined the bearing from receiver to transmitter, degrees east of north ($0 \leq b \leq 360°$), is calculated by

$$b = 114.5916 \cdot \tan^{-1} \sqrt{\left| \sin (u - 90 + x_2) \cdot \sin (u-g) \right| / c} \qquad (7.2)$$

$$u = (180 - x_1 - x_2 + g)/2$$

$$c = \sin (u) \cdot \sin (u - 90 + x_1).$$

With the great-circle route and the associated bearings defined, the typical reflection and penetration areas of the ray in the ionosphere can be calculated by

$$\text{Reflection Lat} = 90 - \arccos (x'_1) \qquad (7.3)$$

where

$$x'_1 = \cos (p) \cdot \cos (90 - x_2) + \sin (p) \cdot \sin (90 - x_2) \cdot \cos (b)$$

p = great-circle distance in degrees from transmitter terminal to reflection latitude.

The geographic longitude of the reflection area is

$$y = y_2 - y' \qquad (7.4)$$

and

$$y' = \arccos \left[\cos (p) - \cos (90 - x_2) \cdot \cos (90 - x_3) / \sin (90 - x_2) \cdot \sin (90 - x_3) \right]$$

x_3 = reflection area latitude.

The zenith angle of the sun at any typical reflection or penetration area on the great circle can be calculated by

$$\cos(\psi) = \sin(z) \cdot \sin(s) + \cos(z) \cdot \cos(s) \cdot \cos\left[15 \times GMT - 180 - y\right] \quad (7.5)$$

where

ψ = sun's zenith angle - degrees

z = reflection area latitude - degrees = x_3

s = latitude of subsolar point of sun for middle of month in question - degrees.

The above parameters are needed for the development of a typical profile of electron density along the path.

The vertical angles of arrival, angles incident in the absorbing region, and angles of reflection are a function of the above profile, path length, and number of sky-wave hops involving reflection from either the E or F2 region.

Seven distinct ray paths are evaluated for each hour at each operating frequency. The ray paths must be geometrically possible with a takeoff angle Δ greater than any arbitrary values set by the user. The sky-wave paths evaluated are (a) two ray paths reflected by the regular E-region (b) three ray paths reflected by the F2 region, and (c) two mixed modes of the "N" type, i.e., E reflections occurring on either end with F2 reflections following.

The following section is devoted to defining the angles and slant range associated with the above ray paths using the transmission curve method and the parabolic range equations. Figure 7.1 illustrates some typical sky-wave paths which are evaluated by this method.

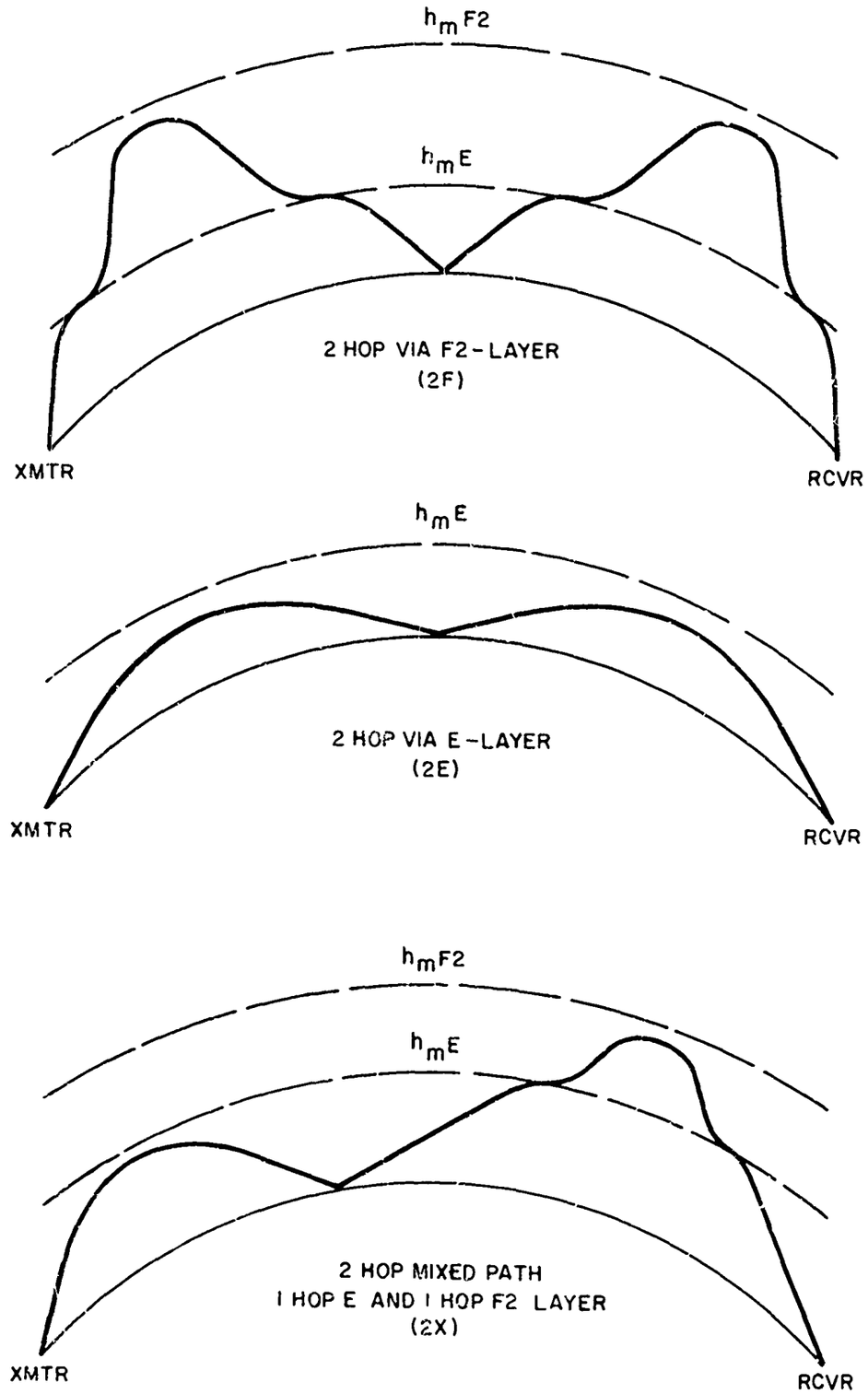

Figure 7.1. Sample Types of Sky-Wave Paths Inspected

7.1. Theoretical Method for Computing Virtual Height of Reflection and Angles of Arrival for Obliquely-Incident Ray Paths through Parabolic Layers

Effective communication by way of the ionosphere requires a knowledge of the range of frequencies that can be propagated between two points on the earth's surface.

A knowledge of the elevation angle at each frequency is also important when directive antennas are employed to permit reduced transmitter power. A transmission curve is "a simple, rapid graphical method of obtaining from vertical-incidence data, the maximum usable frequency over a given path, and the effective heights of reflection (hence elevation angles) of waves incident obliquely upon the ionosphere."

The quotation above is from a 1939 Proceedings of the I.R.E. paper in which Newbern Smith presented the geometrical basis and the mathematics of transmission curves for various combinations of flat and curved earth and ionosphere. The paper includes references to the earlier work of Breit and Tuve, Martyn, Eckersley, Berkner, Millington, and others. Transmission curves are also discussed in "Ionospheric Radio Propagation" NBS Monograph 80, [Davies 1965, Chapter 4].

This section shows how one of Smith's many equations may be rearranged to provide a rapidly convergent method which imitates the application of a transmission curve to a vertical incidence ionogram. At present the ionogram is assumed to be adequately represented by a parabolic distribution of electron density, but other models for empirical distributions could be incorporated in the routine. Several model distributions are considered in section 3.3.4 of "Ionospheric Radio Propagation," [Davies 1965].

Except for notation, Smith's equation giving an approximate* equivalence relation for curved earth and ionosphere is as follows:

* The approximation is that both $h' - h_o$ and $h - h_o$ be less than 400 km and hence much less than $R_o + h_o$.

$$f' = f \cos \phi \sqrt{1 - \frac{2\,(h'-h)}{R_o + h_o} \tan^2 \phi} \quad , \tag{7.6}$$

where (see figure 7.2):

f' = the equivalent vertical-incidence frequency, i.e., the frequency on the vertical incidence ionogram which correponds to f

f = the probing frequency at oblique incidence

ϕ = the half-vertex angle of the equivalent triangular path composed of the straight lines joining the transmitter and receiver locations with a point at the height h' above the midpoint

h' = the virtual height on the vertical incidence ionogram at the frequency f', measured above the earth's surface

h = the true height of reflection of the curved ray path in the ionosphere

h_o = the height of the bottom of the ionospheric layer

R_o = the earth's radius

D = the surface distance between the end points of the hop

Equation (7.6) is basically the well-known "secant law" which holds for a flat earth and ionosphere. The square root represents k, a "correction factor" resulting from the curved geometry. This equation is sometimes written as

$$f = k f' \sec \phi \quad , \quad \text{and} \tag{7.7}$$

comparison with equation (1) shows that this correction factor is

$$1/k = \sqrt{1 - \frac{2\,(h'-h)}{R_o + h_o} \tan^2 \phi} \quad . \tag{7.8}$$

The value of k ranges from unity for very short distances to about 1.2 for the maximum one-hop distance via the F layer of about 5000 km. Since k is a function of ϕ, h_o, and $h'-h$, it depends on the distance of

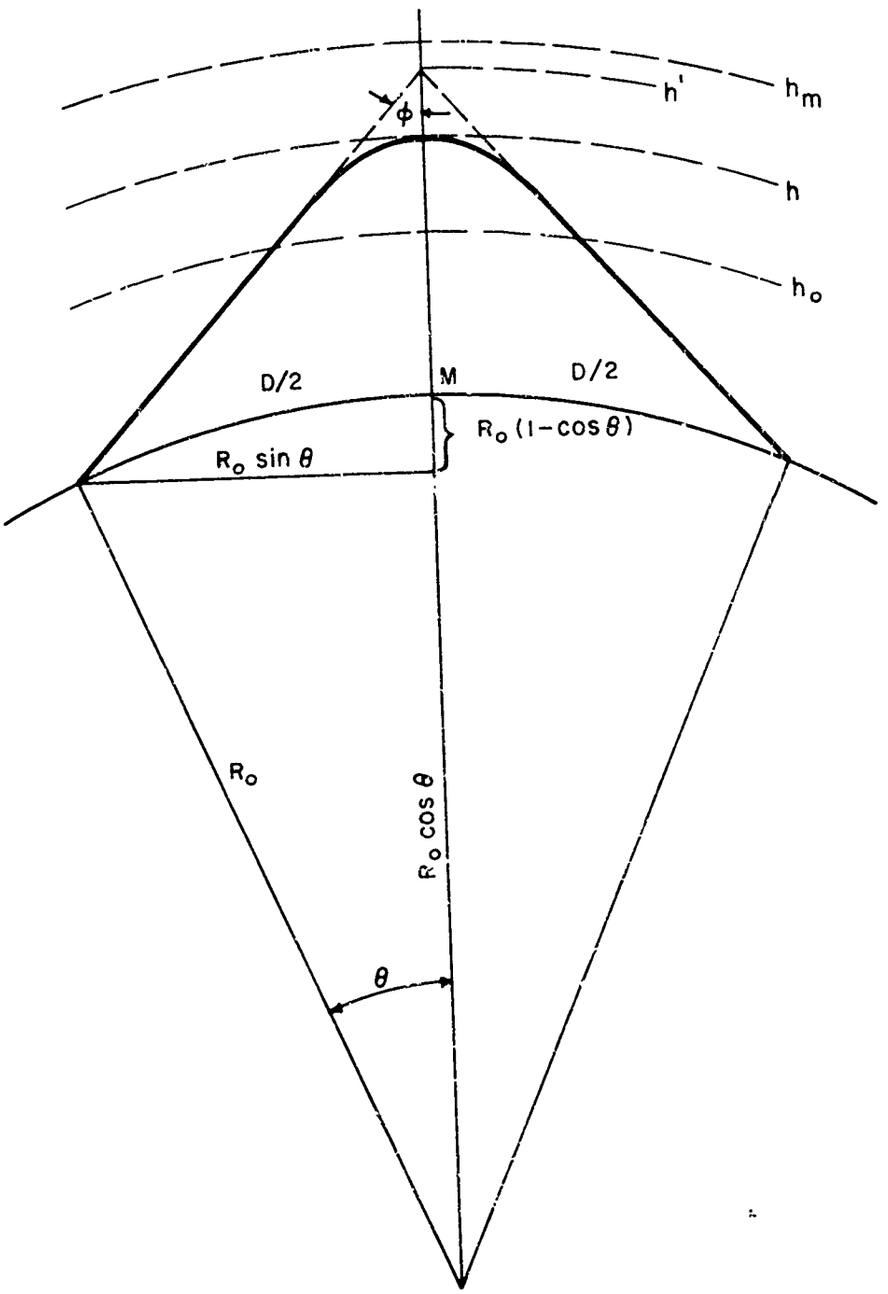

Figure 7.2. Geometry of One Hop Propagation Via the Ionosphere

transmission and the height and the electron density distribution of the ionosphere. In practice an approximate correction factor which depends only on the distance (figure 6.1) is used to simplify the construction of the transmission curves. A logarithmic transmission curve is illustrated in figure 7.3 taken from Davies [1965] which also describes the derivation and application of these transmission curves. Kobayashi [1961] has developed transmission curves using the explicit dependence of k on h'-h and showing how an ionogram may be corrected to allow for the effect of ionospheric curvature. The method described here also allows for the explicit dependence of k on h-h'.

The iterative formula for the computer routine is obtained from equation (7.6) as follows.

Given are the oblique incidence frequency, the distance between the end points of the hop and the critical frequency, maximum layer height and semithickness at the midpoint (M in figure 7.2). These parameters are sufficient to specify the midpoint vertical-incidence ionogram mathematically through parabolic layer theory. For the parabolic layer, the virtual height is given by

$$h' = h_o + y \times \text{arctanh}(x) \text{ [Appleton and Beynon 1947]}, \qquad (7.9)$$

where

$y = h_m - h_o$ = the semithickness

h_m = height of maximum electron density of the layer

$x = \frac{f'}{f_c}$, the vertical incidence sounding frequency normalized to the critical frequency

f_c = vertical incidence critical frequency (corresponds to maximum electron density).

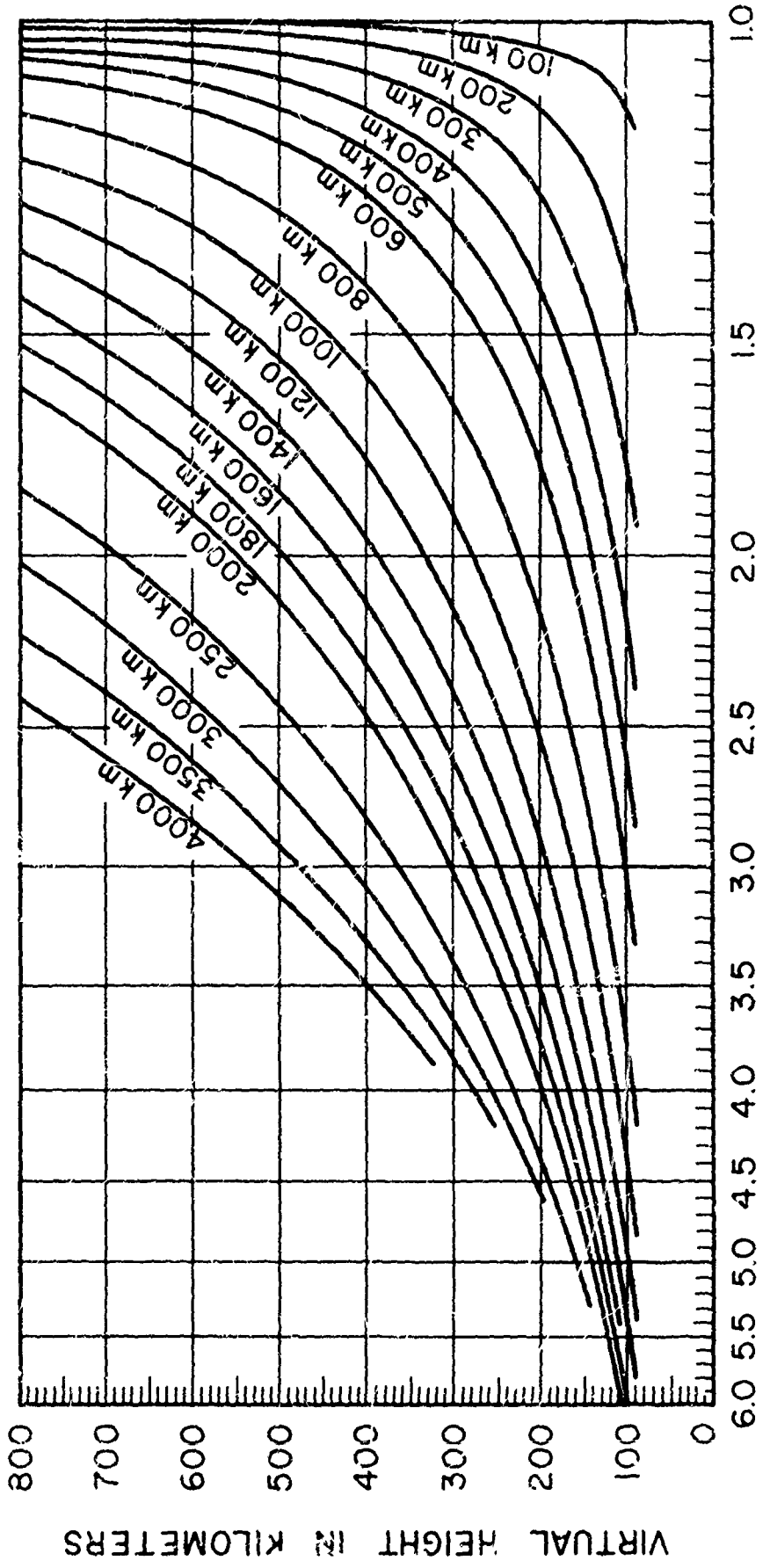

Figure 7.3. Logarithmic Transmission Curves for Curved Ionosphere

The true height of reflection in a parabolic layer is

$$h = h_o + y\,(1 - \sqrt{1 - x^2}\,)\,, \tag{7.10}$$

and the difference between the virtual and true height is

$$h' - h = y\,(\sqrt{1 - x^2} + x \operatorname{arctanh} x - 1) \equiv y\,\delta. \tag{7.11}$$

Both the above expressions refer to vertical incidence at the midpoint and involve $x = \frac{f'}{f_c}$, the quantity sought.

Now write $\frac{f'}{f} = \left(\frac{f'}{f_c}\right)\left(\frac{f_c}{f}\right)$ which normalizes both f' and f to the midpoint critical frequency. Rewriting equation (7.6) yields

$$\left(\frac{f'}{f_c}\right)\left(\frac{f_c}{f}\right) = \cos\phi \sqrt{1 - \frac{2\,y\,\delta}{R_o + h_o} \tan^2\phi}\,. \tag{7.12}$$

Multiplying both sides by $\frac{f}{f_c}$ and then squaring both sides yields

$$x^2 = \left(\frac{f'}{f_c}\right)^2 = \left(\frac{f}{f_c}\right)^2 \left(1 - \frac{2\,y\,\delta}{R_o + h_o} \tan^2\phi\right) \cos^2\phi\,. \tag{7.13}$$

For convenience in computing we express $\cos^2\phi$ in terms of $\tan^2\phi$: $\cos^2\phi = \frac{1}{1 + \tan^2\phi}$. From the geometry of figure 7.2, it is found that

$$\tan\phi = \frac{R_o \sin\theta}{R_o\,(1 - \cos\theta) + h'} = \frac{\sin\theta}{1 - \cos\theta + \frac{h'}{R_o}}\,, \tag{7.14}$$

where $\theta = \frac{D}{2R_o}$, the central angle between the midpoint and either end of the hop.

In drawing figure 7.2 with the ϕ vertex closed, it is assumed that the height of the equivalent triangular path is equal to the virtual height h' corresponding to f' on the ionogram. This is true for the flat ionosphere [Waterman 1952]. However, in this practical work, the error due to this difference is a second order effect.

Equation (7.14) for tan ϕ involves the distance of transmission and the virtual height which is given by equation 7.9. The complete equation to be iterated is

$$x_r^2 = \frac{\left(\frac{f}{f_c}\right)^2 \frac{1}{k^2}}{1 + \tan^2 \phi} = \frac{\left(\frac{f}{f_c}\right)^2 \left(1 - \frac{2 y \delta}{R_o + h_o} \tan^2 \phi\right)}{1 + \left(\frac{\sin \theta}{1 - \cos \theta + \frac{h_o + y x_o \operatorname{arctanh} x_o}{R_o}}\right)^2} \quad , \qquad (7.15)$$

where

$$\delta = x_e \operatorname{arctanh} x_e - 1 + \sqrt{1 - x_e^2} \text{ (from 7.11)} \qquad (7.16)$$

and

x_o = an estimate of x

x_r = the result of computing the r.h.s. of (7.15) using x_o
(Note that x_r depends mainly on θ and h_o).

To start the iterative procedure we use the limits $x_e = 0$ and $x_o = x_t$, where x_t represents the point on our mathematical h' - f ionogram tangent to a transmission curve positioned for finding the maximum usable frequency. This upper limit also assures that only values of h' corresponding to low angle rays are found by this method.

With the lower limit

$x_o \operatorname{arctanh} x_o = 0$, $\delta = 0$ (hence $k = 1$) and equation (7.15) reduces to

$$x_r^2 = \frac{\left(\frac{f}{f_c}\right)^2}{1 + \left(\frac{\sin \theta}{1 - \cos \theta + \frac{h_o}{R_o}}\right)^2} \qquad (7.17)$$

which depends only on the transmitter distance and the height of the bottom of the parabolic layer. The resulting x_r is already closer to but less than the true value which results from further iterations.

From some other work [Remmler 1965] it is found that the upper limit, x_t, depends only on y/h_o as follows:

$$x_t^2 = \frac{1}{1 + .93\frac{y}{h_o}} . \qquad (7.18)$$

Thus x_t decreases as $\frac{y}{h_o}$ increases. For the F layer, y/h_o varies between about 0.2 and 1.0; hence x_t varies between about 0.92 and 0.72, and the corresponding δ varies between 0.854 and 0.347, respectively. Therefore, for any reasonable value of y, the subtractive term in the numerator varies less than one-tenth as fast as the additive term in the denominator of equation (7.15). Alternatively, $\frac{1}{k^2}$ varies between 1 and 0.7 as k varies between its limits of 1 and 1.2. Finally, since tan ϕ varies from zero at vertical incidence to about 3 at the one-hop F limit the entire denominator can vary from 1 to about 11. Hence, x_r is determined principally by the transmission distance and layer height as indicated above.

If the upper limit x_t is used as an estimate of x in (7.15) the resulting value of x_r is closer to but greater than the true value. A second iteration using either of the above values of x_r gives a better approximation which always lies on the same side of the true value as the input estimate. Faster convergence occurs when the next estimate x_e is the average of the first two x_r's. Further estimates are obtained by averaging each new result with the closer of the two values just previously averaged. This procedure guarantees that the two values averaged straddle the unknown true value. Virtual heights are computed for each x_r and when the difference in successive virtual heights is less than 0.5 km the process is stopped. The average virtual height is then used to find the angle of elevation of the F-region ray.

Three or four iterations are usually sufficient to reduce the virtual height difference to 0.5 km. If x_r exceeds x_t when x_t is put into the r.h.s. of (7.15) the skip distance exceeds the transmitter-receiver distance, that is f exceeds the MUF for the path.

7.2. Method for Incorporating the Bending in the E Layer in Predicting Ray Paths by Way of the F2 Layer

Rawer [1960] and Woyk [1959] among others have discussed the refraction (or bending) of radio waves passing completely through a spherical ionized layer using a simple ray treatment. Figure 7.4 illustrates the ray geometry and the nomenclature employed.

The following formulas and data are supposedly given (at this point):

1. Rawer's formula for the bending β experienced by a ray passing entirely through a parabolic layer:

$$\beta = 2\,\epsilon \tan\alpha \left(\frac{\tanh^{-1} u}{u}\right), \tag{7.19}$$

where

$$\epsilon = \frac{y_E}{R_o + h_mE} : \quad y_E = \text{semithickness of E layer}$$

h_mE = height of maximum density of E layer

R_o = radius of earth

α = angle of incidence of the unrefracted ray extension at h_mE measured from vertical

$$u = \frac{f_E}{f} \sec\alpha$$

f_E = critical frequency of E layer

f = signal frequency.

Rawer and Woyk have shown that β can also be measured at the center of the earth, i.e., between perpendiculars to extensions of the rays above and below the layer penetrated (figure 7.4).

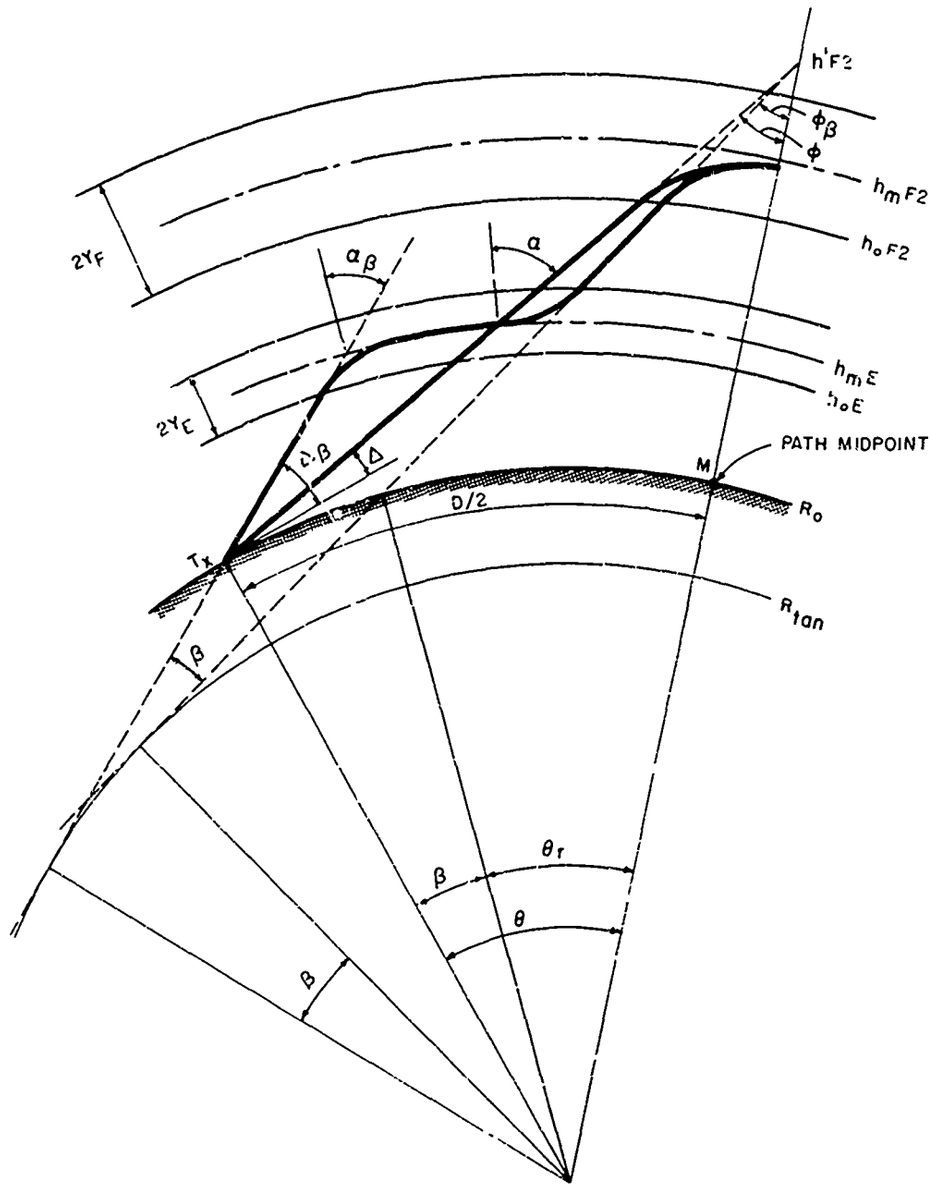

Δ = ELEVATION ANGLE AT Tx (NO BENDING)
$\Delta\beta$ = ELEVATION ANGLE AT Tx (WITH BENDING)
α = ANGLE OF INCIDENCE AT h_mE (NO BENDING)
α_β = ANGLE OF INCIDENCE AT h_mE (WITH BENDING)
ϕ = ANGLE OF INCIDENCE AT h'F2 (NO BENDING)
ϕ_β = ANGLE OF INCIDENCE AT h'F2 (WITH BENDING)
β = BENDING IN E-REGION
R_{tan} = RADIUS OF TANGENCY OF BENT RAY EXTENSIONS
R_o = RADIUS OF EARTH; ALL HEIGHTS (h, h') ABOVE EARTH'S SURFACE
Tx = TRANSMITTER
D/2 = DISTANCE BETWEEN Tx AND M
θ = $D/2R_o$, $\theta_r = \theta - \beta$

Figure 7.4. Geometry of E-Region Bending for Rays Propagating by the F2 Layer

2. The iterative routine finding the virtual height of reflection in the F layer as a function of the F-layer parameters and one hop path length. This routine is described in detail in section 7.1.

3. Snell's law for spherical layers [Woyk 1959; Rawer 1960]:

$$n \rho \sin \alpha = \text{const.}, \tag{7.20}$$

where n = index of refraction and ρ = radius of curvature where α is measured w.r.t. the vertical at that radius.

Whenever, n = 1, e.g., between layers, we have

$$\rho \sin \alpha = \text{const.}$$

This applies to straight line extensions into ionized regions also. The constant may be determined from any corresponding pair of values ρ and α, or $R_o + h'$ and ϕ, etc. Thereafter α can be found for any given ρ and vice versa.

4. The following parameters for both E and F2 layers:

   a. critical frequency, f_E, f_F

   b. height of bottom, $h_o E$, $h_o F$

   c. semithickness, y_E, y_F

   d. height of max density, $h_M = h_o + y$.

5. The signal frequency (f) and the hop length (D), expressed in radians and measured at the center of the earth, i.e.,:

$$\frac{D}{2} = R_o \theta \tag{7.21}$$

or

$$\theta = \frac{D}{2R_o}, \text{ the central angle from either endpoint to the midpoint.}$$

The iteration proceeds as follows:

A. Use the virtual height routine (2 above) with θ, f and the F layer parameters to determine the elevation angle (Δ) for propagation by the F layer alone. This angle can be found, for example, through application of (7.20) above as follows:

$$R_o \sin\left(\frac{\pi}{2} - \Delta\right) = (R_o + h'_F) \sin \phi \qquad (7.22)$$

or

$$R_o \cos \Delta = (R_o + h'_F) \sin \phi$$

$$\cos \Delta = \frac{R_o + h'_F}{R_o} \sin \phi .$$

B. The angle of incidence (α) at h_m of the E layer is obtained from (7.20) in the same manner:

$$(R_o + h_m E) \sin \alpha = R_o \sin (\pi/2 - \Delta)$$

or

$$\alpha = \arcsin\left(\frac{R_o \sin (\pi/2 - \Delta)}{R_o + h_m E}\right) \qquad (7.23)$$

or

$$\alpha = \arcsin\left(\frac{(R_o + h'_F) \sin \phi}{R_o + h_m E}\right) .$$

C. Next α from step B and the E layer parameters f_E, $h_m E$, and y_E are substituted into Rawer's formula (7.19) to get an initial value of the bending, β.

D. The ray which would reach the receiver by way of the F layer alone, is bent in passing through the E layer; it overshoots the receiver location. Now a ray leaving the transmitter at a somewhat greater elevation angle can be found for which the angular distance added by the bending is just compensated by the reduction in angular distance below and above the E layer caused by increasing the elevation angle (figure 7.4).

Because the bending is itself a function of the elevation angle as is the virtual height of reflection in the F layer, a successive approximation procedure is used. Steps A, B, and C initiated the process and similar steps are used in the iteration.

E. Subtract the total initial bending from θ to find the reduced half-hop distance:

$$\theta_r = \theta - \beta. \tag{7.24}$$

Repeat steps A, B, C with θ_r substituted for θ to find a new smaller bending corresponding to the decreased angle of incidence for the reduced distance. The subscript β in figure 7.4 indicates angles with some bending.

F. Since this bending is less than anticipated, the ray falls short of the receiver and the final bending lies between the two values computed thus far. Therefore, average these two values of bending, compute the corresponding reduced distance as in step E and iterate through steps A, B, C, and F until the F layer virtual height of reflection falls within the prescribed limits, (or possibly until the sum of the reduced distance and the bending is within a prescribed small angular increment of the desired distance).

8. Transmission Losses

8.1. Absorption in Lower Layers (L_l)

The main features of the structure and the diurnal, seasonal, and geographical variations of the D and E regions are adequately explained in terms of the ionization produced by absorption of ultraviolet solar radiation and the recombination of the ions, and are assumed to be related to the zenith angle of the sun. The absorption equation of section 8.2 is a semiempirical relationship derived from observations of operating high frequency circuits.

The mean effective height of the absorbing region is taken to be 100 km above the earth and the total absorption of a high frequency wave is directly related to the length of the trajectory within the absorbing region [Laitinen and Haydon 1962].

In this development of a semiempirical expression for absorption in the lower layers, it was assumed that there is negligible nighttime absorption in the range of frequencies 3 to 30 MHz so that the change in signal level throughout the day was the basis for the analysis. Likely propagation paths in the daytime were estimated from median ionospheric conditions without any adjustment for the likelihood of the various sky-wave paths. Comparison between circuit performance predictions based on monthly median ionospheric conditions and the observed circuit performance indicated that the median signal level was 8.9 dB below the quasi-maximum.

The prediction method presented in this report considers the probability of a sky-wave path and combines this probability with the expected day-to-day signal level variations during the days a sky-wave path is expected. Since the signal level distributions required in this report apply only to those days a sky-wave path is expected, the adjustment between the median calculated for these days, and the expected signal level should be somewhat less than previously required. Pending the completion of more detailed comparisons, the 8.9 dB is retained for the temperate regions. The values for other latitudes are shown in Appendix C.

8.2. Theoretical/Empirical Determination of Lower Region Absorption

The absorption that takes place in the lower E and upper D region (80-120 km) of the ionosphere is assumed to account for much of the loss encountered by a ray traveling between transmitter and receiver via the ionosphere. Nondeviative absorption ($u \cong 1$) is the only absorption explicitly dealt with in these calculations of monthly median transmission

losses. Deviative absorption is in part considered in the distributions (Y_p) about these monthly median values. The expression used for the absorption is semiempirical and a brief explanation of its origin is given. A complete explanation of data and analyses is contained in Technical Report No. 9 [Laitinen and Haydon 1962]. Appleton derived an expression for the total nondeviative lower region absorption for frequencies much greater than the collision frequency. The equation expressed in terms of the ionospheric reflection coefficient for vertical incidence is

$$- \log_e \rho = 4.13H \frac{4\pi^2 e^2 N_o \nu_o \cos^{1.5} \psi}{mc(\omega + \omega_L)^2} \qquad (8.1)$$

where ρ = the reflection coefficient

e = the electronic charge

m = the mass of the electron

c = the velocity of light

N_o = the electron density at the maximum ionization of the layer when the sun's zenith angle is zero

ν_o = the collisional frequency at the height of maximum ionization

H = the scale height

ψ = the zenith angle of the sun

ω = the angular frequency of the propagated radio wave

ω_L = the angular gyro-magnetic frequency due to the longitudinal component of the earth's magnetic field.

This equation, based on a Chapman distribution of ionization, shows the vertical incidence absorption for the ordinary component of the electromagnetic wave. The absorption varies directly with $\cos^{1.5} \psi$ and inversely with the square of the sum of the wave frequency and the longitudinal component of the gyro-frequency.

The above equation indicates that absorption would cease at a solar zenith angle of 90°. The data analyzed indicated that it in fact levels off

at sunset at the ionospheric height of 110 km or a zenith angle of 102°. The portion of the equation is then adjusted to be

$$(\cos K\,\psi)^m = (\cos 0.881\,\psi)^m \qquad (8.2)$$

K = constant of 90°/ 102.2° = 0.881

m = constant obtained from data = 1.3

ψ = zenith angle of the sun.

Analyses of the data over a period of several years indicated that an adjustment needs to be made to allow for the change in solar activity. Twelve-month running average sunspot numbers were used to analyze the data in an attempt to remove the seasonal trends of absorption.

The analysis produced a linear relationship with sunspot number:

$$A_S = A_o\,(1 + b\,S)\,, \qquad (8.3)$$

where

S = Twelve-month running average sunspot number

b = constant of 0.0037 obtained from the experimental data

A_o = absorption at sunspot number zero

A_S = absorption at sunspot S.

The total equation for the anticipated losses (A) due to the absorption in the lower regions on oblique paths is written as

$$A = \frac{615.5\,n \sec\phi\,[1 + 0.0037S]\,[\cos 0.881\,\psi]^{1.30}}{[f + f_H]^{1.98}}\,, \text{ (dB)} \qquad (8.4)$$

where

$\sec\phi$ = factor relating back to vertically incident waves

n = number of hops in the ray path from transmitter to receiver

f_H = gyro-frequency at 100 km above earth's surface - MHz.

The above equation has the same form as the Appleton equation, but contains the aforementioned correction in addition to the factor 615.5 determined from oblique observations and the f_H used in conjunction with the modified exponent of 1.98. Errors in the above equation can develop (a) because the frequency is not sufficiently greater than the collision frequency or (b) at those times when the $(f + f_H)^{1.98}$ expression does not sufficiently approximate $(f + f\ell)^2$ where $i\ell$ is the longitudinal component of the magnetic field for the path in question.

It has also been stated that the variation of absorption between winter and summer is less than that expected by theory based on solar zenith angle. It was found by the data analyzed that the absorption follows an inverse relationship with layer height. During the summer, layer heights are typically higher than in the winter; thus the ray angles at the absorbing regions are higher for a given ray path. This in turn tends to decrease absorption during the summer months relative to the values during the winter months; thus explaining the difference between seasons not accountable explicitly by the solar zenith angle dependence. Equation 8.4 is a reasonable fit to the data of Technical Report No. 9 [Laitinen and Haydon 1962] for values of $f + f_H$ in excess of 5 MHz; however, the equation fails to fit the data at lower values of $f + f_H$. A revised equation which yields similar results as equation 8.4 for values of $f + f_H$ greater than 5 MHz and also represents the data to a lower limit of 3 MHz is

$$A_{dB} = \frac{677.2\ n\ (\sec \phi)\ I}{(f + f_H)^{1.98} + 10.2} \qquad (8.5)$$

where

$$I = [1 + 0.0037S]\ [\cos .881\ \psi]^{1.30}.$$

The analysis of observations of nighttime field intensities has indicated that the lower region absorption does not in fact cease, but rather tends to level off as the absorption index (defined p. 8) I approaches a value of one-tenth. The above absorption equation is thus restricted to values of I greater than 0.1. This assumption checks well with the work of Wakai [1961] and unpublished comparisons with observations at The Institute for Telecommunication Sciences and Aeronomy (formerly CRPL).

For a complete explanation of the above analysis and data, refer to Technical Report No. 9 of the U. S. Army Radio Propagation Agency [Laitinen and Haydon 1962].

8.3. Losses Due to ground Reflections (L_g)

The ground reflection losses calculated in this method are for randomly polarized sky waves which are assumed to have equal amounts of energy in the horizontally and vertically polarized fields. The losses are represented by the following equation:

$$L_g = 10 \log_{10} \frac{K_V^2 + K_H^2}{2} \quad (dB), \qquad (8.6)$$

where

K_v = magnitude of the vertical reflection coefficient at the angle (Δ)

K_H = magnitude of the horizontal reflection coefficient at the angle (Δ)

K_v and K_H equations can be found in section 8.5.

It should also be mentioned here that "cutback factors" [Wait and Conda 1958] affecting the radiation at low angles are not at the present time included in the ground reflection losses, and it is assumed that the majority of the energy is reflected at an angle of reflection equal to the angle of incidence of the wave; plans are under way for improving this aspect of the predictions.

8.4. Free Space Loss Between Isotropic Radiators (L_{bf})

Consider isotropic radiators in free space which are radiating a power w (watts) which produce a field intensity of $w/4\pi d^2$ when d is much greater than λ. The absorbing area (a) of an isotropic radiator in free space is

$$a = \lambda^2 / 4\pi \ , \tag{8.7}$$

with

λ = free space wavelength.

The resulting power available from an isotropic radiator at a distance d from the isotropic transmitting antenna is

$$w_a = w\left(\frac{\lambda}{4\pi d}\right)^2 \tag{8.8}$$

and the resulting basic transmission [Norton 1959] between isotropic radiators can be expressed by

$$L_b = 10 \log_{10}\left(w/w_a\right) = 10 \log_{10}\left(\frac{4\pi d}{\lambda}\right)^2 \quad \text{or} \tag{8.9}$$

$$L_b = 32.45 + 20 \log_{10} d + 20 \log_{10} f$$

f = frequency - MHz

d = distance in kilometers along the ray path between the two antennas.

8.5. Theoretical Antenna Power Gain Equations (G_T , G_R)*

Equations are given for the power gain relative to a free space isotropic source for several antennas over finite earth in Appendix A.

* Some symbols appearing in this section and Appendix A may duplicate symbols used for different variables appearing in other sections of the report. It was necessary to do this when attempting to remain consistent with the symbols used in antenna theory.

This section contains a brief presentation of ground reflection coefficients, power gain definition, the radiation vector method and ground reflection factor.

8.5.1. Reflection Coefficients

If an electromagnetic wave in air is incident on the ground, then the reflection coefficient of the wave is defined as the ratio of the field strength of the reflected wave to the field strength of the incident wave. Since the incident and reflected waves have phase as well as amplitude, the reflection coefficient is, in general, a complex number. For waves polarized parallel to the plane of incidence of the wave (vertical polarization) the reflection coefficient is [Schelkunoff and Friis 1952]

$$K_V = \frac{(\epsilon_r - ix)\sin\Delta - \sqrt{(\epsilon_r - ix) - \cos^2\Delta}}{(\epsilon_r - ix)\sin\Delta + \sqrt{(\epsilon_r - ix) - \cos^2\Delta}} \quad , \tag{8.10}$$

and for waves polarized perpendicular to the plane of incidence (horizontal polarization)

$$K_H = \frac{\sin\Delta - \sqrt{(\epsilon_r - ix) - \cos^2\Delta}}{\sin\Delta + \sqrt{(\epsilon_r - ix) - \cos^2\Delta}} \quad , \tag{8.11}$$

where $\surd$ denotes the principal branch of the complex square root function, and

$\epsilon_r \equiv$ relative dielectric constant of earth,

$x \equiv \frac{\sigma}{\omega \epsilon_\nu} = 18 \times 10^3 \sigma / f$

$\epsilon_\nu \equiv$ dielectric constant of free space (farad/meter)

$\sigma \equiv$ conductivity of earth (mhos/meter)

$\omega \equiv$ angular frequency

$f \equiv$ frequency in megahertz

$\Delta \equiv$ angle of elevation in degrees, and

$i \equiv \sqrt{-1}$.

If, using the appropriate subscript V or H on K, one writes K in the form $K = |K| e^{i\gamma}$, then $|K|$ is the amplitude of the reflection coefficient and γ the phase. Since the function $e^{i\gamma}$ is periodic with $2\pi i$, the expression given here does not uniquely define the phase. It will, however, always be clear from the context which value of γ is being used. Letting $\psi = \gamma \pm \pi$,

$$K = - |K| e^{i\psi} . \tag{8.12}$$

It is the purpose of this section to obtain K and ψ for both vertically and horizontally polarized waves. Letting $A = (\epsilon_r - ix) - \cos^2 \Delta$, one finds that

$$A = \rho e^{i\alpha} , \tag{8.13}$$

where

$$\rho = [(\epsilon_r - \cos^2 \Delta)^2 + x^2]^{\frac{1}{2}} , \tag{8.14}$$

and

$$\alpha = -\mathrm{Tan}^{-1} \frac{x}{(\epsilon_r - \cos^2 \Delta)} \tag{8.15}$$

Equation (8.11) can now be written as

$$K_V = \frac{(\epsilon_r - ix) \sin\Delta - \rho^{\frac{1}{2}} e^{i\alpha/2}}{(\epsilon_r - ix) \sin\Delta + \rho^{\frac{1}{2}} e^{i\alpha/2}} \tag{8.16}$$

The reduction of (8.16) to the form (8.12) gives

$$K_V = \frac{\left[\rho^2 + (\epsilon_r^2 + x^2)^2 \sin^4 \Delta - 2\rho(\epsilon_r^2 + x^2) \sin^2 \Delta \cos\left(\alpha + 2 \sin^{-1} \frac{x}{(\epsilon_r^2 + x^2)^{\frac{1}{2}}}\right)\right]^{\frac{1}{2}}}{\left[\rho + (\epsilon_r^2 + x^2) \sin^2 \Delta + 2\rho^{\frac{1}{2}} (\epsilon_r^2 + x^2)^{\frac{1}{2}} \sin \Delta \cos\left(\frac{\alpha}{2} + \sin^{-1} \frac{x}{(\epsilon_r^2 + x^2)^{\frac{1}{2}}}\right)\right]} \tag{8.17}$$

The analysis of ψ_v yields the following three cases:

1. If $(\epsilon_r^2 + x^2)\Delta - \rho = 0$, then

   a. If $\sin\Delta \sin(\mathrm{Tan}^{-1}\frac{x}{\epsilon_r} + \frac{\alpha}{2}) = 0$, then $\psi_V = 0$. (8.18a)

   b. If $\sin\Delta \sin(\mathrm{Tan}^{-1}\frac{x}{\epsilon_r} + \frac{\alpha}{2}) > 0$, then $\psi_V = \frac{\pi}{2}$. (8.18b)

   c. If $\sin\Delta \sin(\mathrm{Tan}^{-1}\frac{x}{\epsilon_r} + \frac{\alpha}{2}) < 0$, then $\psi_V = -\frac{\pi}{2}$. (8.18c)

2. If $\rho - (\epsilon_r^2 + x^2)\sin^2\Delta > 0$, then

$$\psi_V = \mathrm{Tan}^{-1}\left[\frac{2\rho^{\frac{1}{2}}\sqrt{\epsilon_r^2 + x^2}\sin\Delta\sin(\tan^{-1}\frac{x}{\epsilon_r} + \frac{\alpha}{2})}{\rho - (\epsilon_r^2 + x^2)\sin^2\Delta}\right] \quad (8.18d)$$

3. If $\rho - (\epsilon_r^2 + x^2)\sin^2\Delta < 0$, then

$$\psi_V = \mathrm{Tan}^{-1}\left[\frac{2\rho^{\frac{1}{2}}\sqrt{\epsilon_r^2 + x^2}\sin\Delta\sin(\mathrm{Tan}^{-1}\frac{x}{\epsilon_r} + \frac{\alpha}{2})}{\rho - (\epsilon_r^2 + x^2)\sin^2\Delta}\right] + \pi \quad (8.18e)$$

A similar analysis leads to

$$|K| = \frac{[\rho^2 + \sin^4\Delta - 2\rho\sin^2\Delta\cos\alpha]^{\frac{1}{2}}}{[\rho + \sin^2\Delta + 2\rho^{\frac{1}{2}}\sin\Delta\cos\frac{\alpha}{2}]}, \quad (8.19)$$

and

$$\psi_H = \mathrm{Tan}^{-1}\left[\frac{2\rho^{\frac{1}{2}}\sin\Delta\sin\alpha/2}{\rho - \sin^2\Delta}\right]. \quad (8.20)$$

8.5.2. Power Gain Definition

Following Ramo and Whinnery [1960], the gain, g, relative to an isotropic source is defined as the ratio of power required from the isotropic source to produce the given intensity in the desired direction to that required from the actual antenna:

$$g = \frac{4\pi r^2 P_r}{w} = \frac{4\pi r^2 P_r}{\frac{1}{2} R I^2} \quad , \tag{8.21}$$

where

P_r = the time average Poynting vector,

r = the distance from the origin of the coordinate system to point in space,

w = the total radiated power in free space,

R = the radiation resistance of the antenna,

I = the input current to the antenna.

8.5.3. Radiation Vector Method and Ground Reflection Factor

Using the radiation vector approach introduced by Schelkunoff [Ramo and Whinnery 1960],

$$P_r = \frac{\eta}{8 \lambda^2 r^2} \left\{ |N_\theta|^2 + |N_\phi|^2 \right\} , \tag{8.22}$$

where

λ = the wave length in meters,

$\eta \cong 120 \pi$ = the intrinsic impedance of free space

N_θ and N_ϕ = the vertical and horizontal components, respectively, of the radiation vector in spherical coordinates.

N_θ is multiplied by

$$\mathcal{K}_v = K_v^2 + 1 - 2 K_v \cos (\psi_v - 2 kh \sin \Delta) \qquad (8.23a)$$

and N_ϕ by

$$\mathcal{K}_H = K_H^2 + 1 - 2 K_H \cos (\psi_H - 2 kh \sin \Delta) \qquad (8.23b)$$

to give the sum of the direct and ground reflected waves. Here, h is the height above ground, $k = \frac{2\pi}{\lambda}$, and $\mathcal{K}_v$ and $\mathcal{K}_H$ are the vertical and horizontal ground reflection factors, respectively. Equations (8.23a) and (8.23b) are valid for horizontal antennas only.

8.6. Antenna Efficiencies

The efficiency of an antenna or its ability to radiate the power supplied to it is assumed in these methods to be 100% for horizontal non-terminated antennas, and 67% (1.7 dB reduction) for terminated horizontal antennas. The efficiency (F_ℓ) of an inverted "L" antenna (figure 8.1) is represented by the following polynomial

$$F_\ell = 20 \log_{10} (6.335 X + 67.95 X^2 - 693.00 X^3 + 1600.00 X^4)$$

where

X = physical height/λ

λ = wavelength of the operating frequency (8.24)

F_ℓ = theoretical power gain to be reduced by this amount--dB.

The efficiency (F_v) of the grounded vertical antenna (figure 8.1) is represented by the following polynomial

$$F_v = 25.646 - 364.817 X + 2179.89 X^2 - 6091.33 X^3 + 6416.702 X^4 \qquad (8.25)$$

(variables are identical to above).

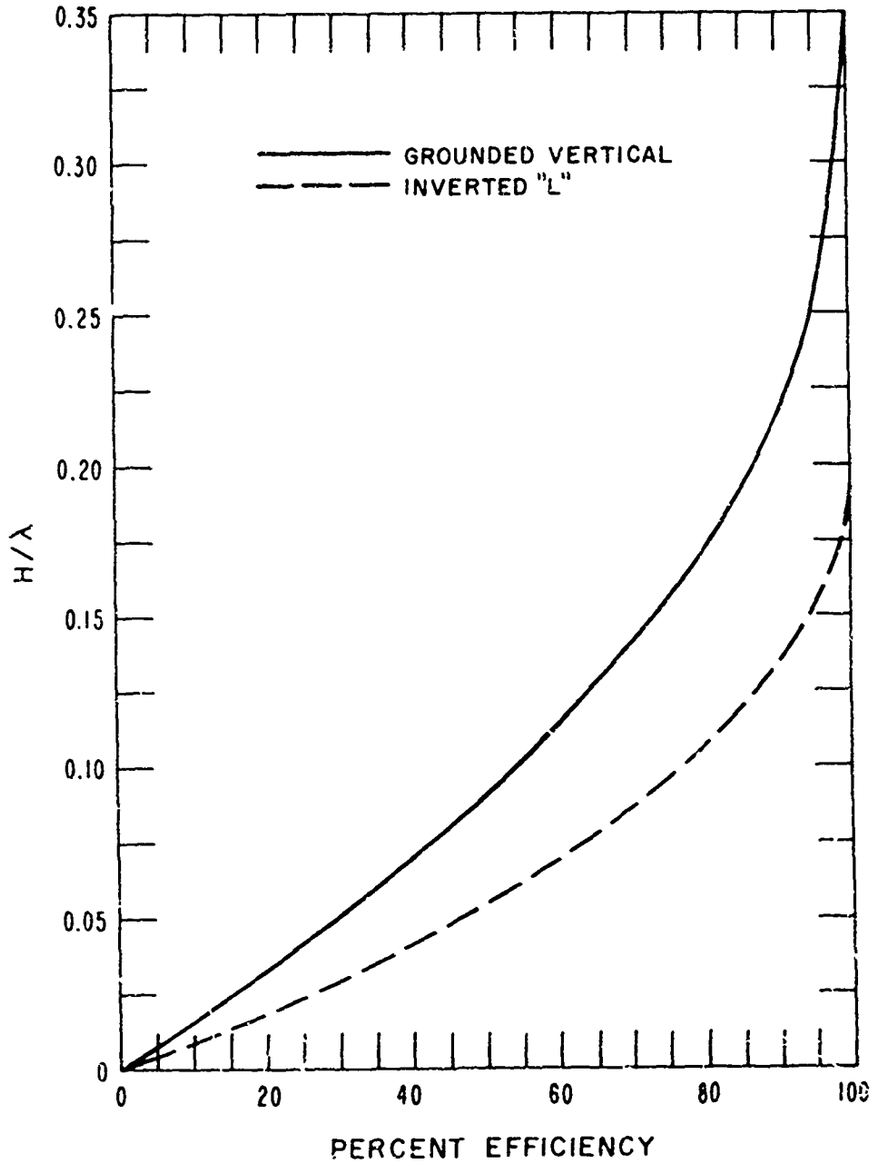

Figure 8.1. Efficiency of the Inverted "L" and Grounded Vertical Antennas

The above efficiencies are commonly used throughout the field [Laitinen 1957]; therefore, no further justification will be given for their acceptance.

For a complete explanation of the efficiencies used and the curves in figure 8.1, the reader is referred to the work of Laitinen [1957].

For the reception of high frequency signals, the ability of the antenna to discriminate between the signal and the noise is the important consideration, since the major noise sources, atmosphere, man-made and cosmic, are external to the antenna system. In the absence of better information, it is assumed that this external noise arrives equally from all directions, and the receiving antenna gain (performance of the antenna in the reception of this signal relative to its performance in the reception of noise) is the directive gain of the antenna; i.e., antenna efficiency is not considered in the receiving antenna gain.

The directive gain may be applied to signal-to-noise ratio predictions; however, power gain should be used when predicting system loss or receiver input power.

9. Upper Limits of Frequencies

The upper limits of frequencies are calculated from monthly median values of foF2, the maximum height of electron density which is derived from the M-3000 factors, and the thickness of the parabolic layer (y).

Conditions along the path are estimated from the above variables averaged from areas of reflection along the path to yield a typical profile of height and electron density associated with the parabolic layers. The Maximum Usable Frequency, MUF (0.50), is the highest operating frequency (f) that is still reflected by the layer for 0.50 of the days within the month when the electron density, height, and thickness are monthly median values. Only the low-angle ordinary rays are considered. The probability of reflection associated with frequencies equal to or greater

than the monthly median MUF is approximated by knowing its height of reflection, relation to the MUF (0.50) and associated distribution of the MUF's as seen in the tables contained in Appendix B.

Paths are not considered to be long (4000 km or greater) or short in the calculation of the upper limits since one hop may go only 3000 km or as great as 7000 km depending on operating frequency, height of maximum ionization, thickness of the layers, and the retardation (bending) in the lower regions (section 7.2). Mixed layer MUFs are not included in this method; therefore, slight discrepancies may appear in extreme cases, e.g., mixed mode MUF (.55).

9.1. Empirical Distribution of F2(3000)MUF

An investigation of the distribution of daily values of MUF about their monthly median was carried out in order to provide information needed to estimate "circuit reliability" in the high frequency band. Three points on the distribution curve were considered, the values of daily MUF exceeded 0.90, 0.50, and 0.10 of the days within the month. The ratios of the decile values to the median value, were computed for comparison with the often used values of 0.85 and 1.15.

The data used in this study are values of the standard MUF, the product of the foF2 and M-3000 factor scaled from vertical-incidence records. Data were analyzed from 13 stations representing a range of geomagnetic latitudes from 71°S to 88°N. The temporal variations of the MUF-distribution were determined by considering observations at all 24 local time hours, each month of the year, and periods representing low, medium, and high solar activity.

The tables in Appendix B give the ratios of upper and lower decile MUFs to median MUF. Each table shows the values for a given season, a given solar activity, local time hours 00, 04, 08, etc., and each 10° of geographic latitude from 10° to 80°, north or south.

The study indicated that the distribution of MUFs is wider at night than in daytime, and wider at low latitudes than high latitudes in daytime. Again in daytime, the distribution is wider in summer than winter, except at high latitudes where the reverse is true. The sunspot number dependence is weaker, but in daytime the difference between the two ratios seems to increase with sunspot number at latitudes higher than 40° and to decrease with increasing sunspot number at latitudes below 40° [Davis and Groome 1965]. The study indicated that the distribution was mostly a function of the foF2 and not the M(3000)F2; therefore, the distributions are assumed valid for any oblique path.

9.2. Empirical Distribution of Transmission Loss (Y_p)

The day-to-day variations of signals on operating circuits of various lengths--55 to 15,689 km in the temperate region (below 40° geomagnetic latitude) and 1220 to 4470 km in the vicinity of the auroral zone (above 50° geomagnetic latitude)--have been analyzed. The paths were inspected at a given hour to best determine those signals being propagated by frequencies below the daily MUF. The results showed that the distributions were distinct functions of geomagnetic latitude, season, local time and length of path. The distributions of transmission loss are expressed in terms of the difference from the median of the lower decile (D_ℓ) and the upper decile (D_u). This was necessary because the distributions were not log-normal but were assumed to be log-normal on either side of the median values. The tables in Appendix C were condensed from the work of Davis and Groome [1964], Laitinen and Haydon [1962] and Haydon and Lucas [1966]. They show the separation from the median of the transmission loss exceeded 84 percent of the time ($S_\ell = D_\ell / 1.28$) and the transmission loss exceeded 16 percent of the time ($S_u = D_u / 1.28$).

A study of the distributions shows that the losses tend to be greater for paths in the region of 64° geomagnetic latitude and more widely

distributed with the diurnal maximum falling between 04-10 local mean time. The seasonal maximum loss occurs at equinox for both long and short paths, with the short path generally showing greater excess attenuation at high latitudes. The distributions are probably less reliable on paths near the geomagnetic equator since most of the temperate paths which were analyzed fell above 15° north geomagnetic latitude.

10. Reliability, $q(R_h)$

This section will be mainly concerned with suggesting a method of estimating the probability of an adequate signal-to-noise ratio at a given hour, i.e., the circuit reliability of HF sky-wave paths. "Circuit Reliability" is defined as the probability of successful communications at a given hour within the month at a specific operating frequency.

A consideration in the evaluation of a sky-wave circuit is the maximum frequency that will be supported at a given hour or conversely what is the probability that a chosen frequency will be propagated.

Tables of Appendix B show the distribution of the F2 region Maximum Usable Frequencies as a function of time of day, season, solar activity, and geomagnetic latitude of the circuit. These distributions of the F2 layer Maximum Usable Frequencies (MUF) are daily variations about the monthly median MUF as predicted by the Institute for Telecommunication Sciences and Aeronomy (formerly CRPL).

The distribution of the MUF on either side of the median is assumed to be log-normal; thus the probability of support at a chosen frequency propagated at a given elevation angle can be determined by

$$q_f = \frac{1}{\sqrt{2\pi}} \int_{\frac{f - MUF\,\Delta}{\sigma\ MUF\,\Delta}}^{\infty} e^{-\frac{1}{2}t^2} dt \quad , \tag{10.1}$$

where f = operating frequency - MHz

$\sigma_{MUF\ \Delta}$ = (9th or 1st decile)/ 1.28

$_{MUF\ \Delta}$ = frequency supported 0.50 of the time at angle Δ.

The above is only an approximation since the distribution is skewed as can be seen in the tables of Appendix B. In practice, however, the errors associated with the log-normal assumption (either side of the median) may be considered to be negligible in typical communication problems.

The frequency which has a 0.9 or a 0.1 probability of sky-wave propagation at a given hour within the month can be estimated by using the appropriate decile values with the predicted monthly median MUF provided the lower region retardation and depth of penetration into the reflecting region does not significantly change the takeoff angle (Δ).

The frequencies having a 0.9 and a 0.1 probability of sky-wave propagation correspond to the classically defined Optimum Traffic Frequency (FOT) and the Highest Probable Frequency (HPF).

The probability of a given frequency being propagated by a given sky-wave mode can be estimated from the distributions of the critical frequencies, layer heights, and semithicknesses of the ionospheric regions associated with the sky-wave mode.

Successful communications also depend upon an adequate signal-to-noise ratio at the receiver. Variations of the ionospheric and geophysical parameters result in a variation of the received signal. This variation can be expressed as a distribution about the monthly median. Tables of Appendix C show this distribution as a function of the season, the time of day, the geomagnetic latitude and the length of the circuit for frequencies below the daily MUF. The probability of successful HF sky-wave communications depends upon the probability of the operating frequency being

supported via the ionosphere and the probability that the signal-to-noise ratio will exceed some acceptable level.

These events are assumed to be independent; therefore, the combined probability is the product of the probability that the signal-to-noise ratio exceeds a given level and the probability that at least one mode will be present to produce the median available signal-to-noise. The total probability of ionospheric support at a given frequency f is taken to be the ray path producing the highest probability at a given hour. The probability $q_{s/N}$ is evaluated by the following integral assuming no correlation between the received signal and the received noise powers.

$$q_{s/N} = \frac{1}{\sqrt{2\pi}} \int_{\frac{R_h - (\bar{s} - \bar{N})}{\sqrt{\sigma_s^2 + \sigma_N^2}}}^{\infty} e^{-\frac{1}{2}t^2} dt \qquad (10.2)$$

where

R_h = minimum acceptable signal-to-noise ratio - dB

$\bar{s}$ = monthly median signal - dB

$\bar{N}$ = monthly median of the hourly median radio noise - dB

σ_N = standard deviation of radio noise - dB

σ_s = standard deviation of received signal - dB.

The resulting probability of exceeding a minimum required signal-to-noise ratio on a given day is then $q(R_h) = (q_f) \cdot (q_{s/N})$. This total probability is defined as the fraction of the days within the month at the given hour that the requirement (R_h) will be met (CIRCUIT RELIABILITY).

The median noise power ($\bar{N}$) and its associated distributions (σ_N) are calculated using numerical representations of CCIR 322 [Lucas and Harper 1965]. The median excess signal power ($\bar{S}$) above the quasi-maximum signal power and its distribution (σ_s) are found in Appendix C [Davis and Groome 1965] and [Laitinen and Haydon 1962].

The above method can be applied to propagation via the regular E, sporadic E or F1 layers as well as the F2 layer if sufficient knowledge of the distributions is available and independence can be assumed.

The variation of the regular E layer MUF's is very small and therfore a q_f of 1 can be assumed when f is less than the E-MUF and a q_f of 0 when f is greater than E-MUF. The signal distributions are assumed to be valid for both E layer and F2 layer propagation since in the empirically determined distributions no attempt was made at sorting out the individual ray paths of propagation. The contribution of each individual ray path of propagation is in part contained in the distributions about the median values.

It is possible using the above approach for the engineer or circuit planner to inspect the results of the above equations and extract much more useful information than in the past. For instance, one could look at $q_{s/N}$ and determine if a change in power, antenna or modulation would yield a better overall circuit reliability due to an increase in available signal-to-noise or a decrease in the basic required signal-to-noise ratio. The quantity q_f will dictate the frequency at which an increase of power, etc., would be advisable, since values of q_f dictate the overall circuit reliability at frequencies which yield low values of q_f.

Conversely, high values of q_f at a given frequency dictate that an increase of available signal-to-noise ratios or a decrease in required signal-to-noise may yield an increase in the overall circuit reliability.

A careful inspection of tables 10.1, 10.2 and 10.3 will show some possible effects of power and/or antenna changes at given frequencies on the overall "circuit reliability" of a typical high frequency communication circuit. (See section 15 for definition of variables appearing in the above tables.)

For example, at 0200 GMT using an operating frequency of 9 MHz a power increase to 30.00 kW (Table 10.1) from 1.00 kW (Table 10.2)

Table 10.1.

```
        I              JUN                  SSN= 75              MA  5.0ZI
    S.FRANCISCO        TO     HAWAII                    AZIMUTHS        N.MILES
  37.50N - 122.50W          21.00N - 158.00W     251.8  53.8          2088.1
 CURTAIN  23H  26L  2BAY  8STACK                  RHOMBIC  30H 180L  70DEG
 OFF AZIMUTH    0 DEG.     MIN. ANGLE=  0 DEG.     OFF AZIMUTH    0 DEG.
 PWR= 30.00KW          3 MC/S MAN. NOISE = -148 DBW          REQ.S/N= 50DB
                          OPERATING FREQUENCIES
GMT  MUF    3    5    7    9   11   13   15   17   19   21   23   26   30
2  22.4
      1F   2E   2E   3F   2E   2E   2X   2F   2F   2F   1F   1F   1F   -  MODE
       0    2    2   20    3    3    5   11   13   13    0    0    0   -  ANGLE
     138  136  136  148  136  136  137  141  143  143  138  138  138   -  DELAY
     .50  .99  .99  .99  .99  .99  .95  .76  .52  .23  .64  .43  .14   -  F.DAYS
      55 -220  -47   38   68   84   96   94   58   49   54   55   66   -  S/N..DB
     .40  .00  .00  .13  .98  .98  .95  .75  .46  .11  .46  .34  .14   -  REL.

4  22.6
      1F   4F   3F   2F   2F   2F   2F   2F   2F   2F   2F   1F   1F   -  MODE
       0   26   16    9    9    9    9   10   12   13   13    0    0   -  ANGLE
     138  154  144  139  139  140  140  141  142  143  143  138  138   -  DELAY
     .50  .99  .99  .99  .99  .97  .91  .78  .58  .30  .09  .46  .15   -  F.DAYS
      57    5   60   91  101   97   90   94   77   54   56   57   58   -  S/N..DB
     .42  .00  .94  .99  .99  .96  .90  .77  .58  .23  .08  .39  .13   -  REL.

6  20.2
      1F   2F   2F   2F   2F   2F   2F   2F   2F   1F   1F   1F   -    -  MODE
       1   10    9    9   10   10   11   13   14    0    1    1   -    -  ANGLE
     138  141  140  140  140  140  141  143  144  138  138  138   -    -  DELAY
     .50  .99  .99  .99  .98  .93  .80  .59  .28  .62  .40  .17   -    -  F.DAYS
      70   44   82  100  104   89   93   95   61   57   67   63   -    -  S/N..DB
     .50  .29  .99  .99  .95  .92  .80  .58  .26  .54  .39  .16   -    -  REL.

8  17.3
      1F   2F   2F   2F   2F   2F   2F   1F   1F   1F   1F   -    -    -  MODE
       1   11   10   10   11   12   14    0    1    1    1   -    -    -  ANGLE
     139  141  140  141  141  142  144  138  139  139  139   -    -    -  DELAY
     .50  .99  .99  .99  .96  .83  .54  .77  .54  .26  .08   -    -    -  F.DAYS
      90   46   83  100   96   86  101   72   90   74   77   -    -    -  S/N..DB
     .50  .37  .99  .99  .96  .82  .54  .76  .53  .26  .08   -    -    -  REL.

10  16.2
      1F   2F   2F   2F   2F   2F   2F   1F   1F   1F   -    -    -    -  MODE
       1   11   11   11   12   13   15    1    1    1   -    -    -    -  ANGLE
     139  141  141  141  142  143  145  138  139  139   -    -    -    -  DELAY
     .50  .99  .99  .99  .93  .73  .36  .66  .37  .13   -    -    -    -  F.DAYS
      99   46   84   99   89   93   95   91   95   75   -    -    -    -  S/N..DB
     .50  .37  .99  .99  .93  .72  .36  .65  .37  .13   -    -    -    -  REL.

12  14.9
      1F   2F   2F   2F   2F   2F   1F   1F   1F   1F   -    -    -    -  MODE
       1   11   11   11   12   14    0    1    1    1   -    -    -    -  ANGLE
     139  141  141  141  142  144  138  139  139  139   -    -    -    -  DELAY
     .50  .99  .99  .97  .84  .56  .73  .49  .28  .12   -    -    -    -  F.DAYS
     103   46   84   99   85  101   95  103   95   75   -    -    -    -  S/N..DB
     .49  .37  .99  .96  .84  .56  .73  .49  .28  .12   -    -    -    -  REL.
```

Sample Computer Print-Outs Using the Described Method of Prediction - Hawaii-San Francisco, June - SSN 75 - 30 kW - Curtain Array and Rhombic

Table 10.2.

```
        2              JUN                SSN=   75              HA  5.0?1
    S.FRANCISCO        TO     HAWAII                    AZIMUTHS        N.MILES
  37.50N - 122.50W          21.00N - 158.00W      51.8  53.8          2088.1
 CURTAIN  23H  26L  2RAY  8STACK                    RHOMBIC  30H 180L  70DEG
 OFF AZIMUTH    0 DEG.     MIN. ANGLE=  0 DEG.     OFF AZIMUTH    0 DEG.
 PWR=  1.00KW          3 MC/S MAN. NOISE = -148 DBW          REQ.S/N= 50DB
                              OPERATING FREQUENCIES
GMT  MUF    3    5    7    9   11   13   15   17   19   21   23   26   30
 2  22.4
      1F   2E   2E   3F   2E   2E   2X   2F   2F   2F   1F   1F   1F    -   MODE
       0    2    2   20    3    3    5   11   13   13    0    0    0    -   ANGLE
     13R  136  136  14R  136  136  137  141  143  143  138  138  13R    -   DELAY
     .50  .99  .99  .99  .99  .99  .95  .76  .52  .23  .64  .43  .14    -   F.DAYS
      41 -235  -62   24   54   69   81   79   43   35   39   40   51    -   S/N..DB
     .09  .00  .00  .00  .72  .98  .95  .75  .14  .01  .09  .07  .09    -   REL.

 4  22.6
      1F   4F   3F   2F   2F   2F   2F   2F   2F   2F   2F   1F   1F    -   MODE
       0   26   16    9    9    9    9   10   12   13   13    0    0    -   ANGLE
     13R  154  144  139  139  140  140  141  142  143  143  138  13R    -   DELAY
     .50  .99  .99  .99  .99  .97  .91  .78  .58  .30  .09  .46  .15    -   F.DAYS
      42   -9   45   77   87   82   75   79   62   40   41   42   43    -   S/N..DB
     .11  .00  .34  .99  .99  .96  .90  .77  .56  .05  .01  .10  .04    -   REL.

 6  20.3
      1F   2F   2F   2F   2F   2F   2F   2F   2F   1F   1F   1F    -    -   MODE
       1   10    9    9   10   10   11   13   14    0    1    1    -    -   ANGLE
     13R  141  140  140  140  140  141  143  144  138  138  138    -    -   DELAY
     .50  .99  .99  .99  .98  .93  .80  .59  .28  .62  .40  .17    -    -   F.DAYS
      55   29   27   86   90   74   78   80   46   43   52   48    -    -   S/N..DB
     .40  .02  .99  .99  .98  .92  .80  .58  .10  .15  .25  .07    -    -   REL.

 8  17.3
      1F   2F   2F   2F   2F   2F   2F   1F   1F   1F   1F    -    -    -   MODE
       1   11   10   10   11   12   14    0    1    1    1    -    -    -   ANGLE
     139  141  140  141  141  142  144  138  139  139  139    -    -    -   DELAY
     .50  .99  .99  .99  .96  .83  .54  .77  .54  .26  .08    -    -    -   F.DAYS
      75   31   68   86   82   71   86   57   75   60   62    -    -    -   S/N..DB
     .50  .05  .99  .99  .96  .82  .54  .66  .53  .24  .08    -    -    -   REL.

10  16.2
      1F   2F   2F   2F   2F   2F   2F   1F   1F   1F    -    -    -    -   MODE
       1   11   11   11   12   13   15    1    1    1    -    -    -    -   ANGLE
     139  141  141  141  142  143  145  138  139  139    -    -    -    -   DELAY
     .50  .99  .99  .99  .93  .73  .36  .66  .37  .13    -    -    -    -   F.DAYS
      85   31   69   85   75   78   80   76   80   61    -    -    -    -   S/N..DB
     .50  .05  .99  .99  .93  .72  .36  .65  .37  .12    -    -    -    -   REL.

12  14.9
      1F   2F   2F   2F   2F   2F   1F   1F   1F   1F    -    -    -    -   MODE
       1   11   11   11   12   14    0    1    1    1    -    -    -    -   ANGLE
     139  141  141  141  142  144  138  139  139  139    -    -    -    -   DELAY
     .50  .99  .99  .97  .84  .56  .73  .49  .28  .12    -    -    -    -   F.DAYS
      89   31   69   85   71   86   80   88   80   61    -    -    -    -   S/N..DB
     .50  .05  .99  .96  .84  .56  .73  .49  .28  .12    -    -    -    -   REL.
```

Sample Computer Print-Outs Using the Described Method of Prediction - Hawaii-San Francisco, June - SSN 75 - 1 kW - Curtain Array and Rhombic

Table 10.3.

```
        3              JUN                SSN=   75              HA  5.021
    S.FRANCISCO        TO     HAWAII                    AZIMUTHS       N.MILES
  37.50N - 122.50W          21.00N - 158.00W      251.8  53.8          2088.1
H-DIPOLE  30H -12L    0DEG                                          ANT=  5DB
OFF AZIMUTH    0 DEG.      MIN. ANGLE=   0 DEG.     OFF AZIMUTH    0 DEG.
PWR=  1.00KW          3 MC/S MAN. NOISE = -148 DBW        REQ.S/N= 50DB
                          OPERATING FREQUENCIES
GMT  MUF    3    5    7    9   11   13   15   17   19   21   23   26   30
 2  22.4
     1F   2E   2E   3F   2E   2E   2X   2F   2F   2F   1F   1F   1F   -  MODE
      0    2    2   20    3    3    5   11   13   13    0    0    0   -  ANGLE
    138  136  136  148  136  136  137  141  143  143  138  138  138   -  DELAY
    .50  .99  .99  .99  .99  .99  .95  .76  .52  .23  .64  .43  .14   -  F.DAYS
     53 -224  -72   20   35   48   55   59   60   57   52   53   54   -  S/N..DB
    .35  .00  .00  .00  .07  .45  .77  .70  .48  .20  .42  .31  .10   -  REL.

 4  22.6
     1F   4F   3F   2F   2F   2F   2F   2F   2F   2F   2F   1F   1F   -  MODE
      0   26   16    9    9    9    9   10   12   13   13    0    0   -  ANGLE
    138  154  144  139  139  140  140  141  142  143  143  138  138   -  DELAY
    .50  .99  .99  .99  .99  .97  .91  .78  .58  .30  .09  .46  .15   -  F.DAYS
     55   -6   33   50   58   62   66   68   68   64   57   55   57   -  S/N..DB
    .40  .00  .05  .51  .89  .94  .90  .77  .58  .30  .08  .36  .12   -  REL.

 6  20.3
     1F   2F   2F   2F   2F   2F   2F   2F   2F   1F   1F   1F   -    -  MODE
      1   10    9    9   10   10   11   13   14    0    1    1   -    -  ANGLE
    138  141  140  140  140  140  141  143  144  138  138  138   -    -  DELAY
    .50  .99  .99  .99  .98  .93  .80  .59  .28  .62  .40  .17   -    -  F.DAYS
     57   28   52   61   64   67   69   69   66   61   57   58   -    -  S/N..DB
    .43  .01  .62  .95  .97  .92  .80  .58  .28  .59  .35  .15   -    -  REL.

 8  17.3
     1F   2F   2F   2F   2F   2F   2F   1F   1F   1F   1F   -    -    -  MODE
      1   11   10   10   11   12   14    0    1    1    1   -    -    -  ANGLE
    139  141  140  141  141  142  144  138  139  139  139   -    -    -  DELAY
    .50  .99  .99  .99  .96  .83  .54  .77  .54  .26  .08   -    -    -  F.DAYS
     60   30   53   61   65   68   68   67   58   61   62   -    -    -  S/N..DB
    .47  .03  .68  .95  .95  .82  .54  .76  .47  .25  .08   -    -    -  REL.

10  16.2
     1F   2F   2F   2F   2F   2F   2F   1F   1F   1F   -    -    -    -  MODE
      1   11   11   11   12   13   15    1    1    1   -    -    -    -  ANGLE
    139  141  141  141  142  143  145  138  139  139   -    -    -    -  DELAY
    .50  .99  .99  .99  .93  .73  .36  .66  .37  .13   -    -    -    -  F.DAYS
     60   31   53   61   65   68   67   66   61   62   -    -    -    -  S/N..DB
    .47  .04  .68  .95  .92  .72  .36  .65  .35  .13   -    -    -    -  REL.

12  14.9
     1F   2F   2F   2F   2F   2F   1F   1F   1F   1F   -    -    -    -  MODE
      1   11   11   11   12   14    0    1    1    1   -    -    -    -  ANGLE
    139  141  141  141  142  144  138  139  139  139   -    -    -    -  DELAY
    .50  .99  .99  .97  .84  .56  .73  .49  .28  .12   -    -    -    -  F.DAYS
     66   31   53   61   65   68   67   66   61   62   -    -    -    -  S/N..DB
    .50  .04  .68  .92  .83  .56  .73  .49  .26  .12   -    -    -    -  REL.
```

Sample Computer Print-Outs Using the Described Method of Prediction - Hawaii-San Francisco June - SSN 75 - 1 kW - Horizontal Dipole and 5 dB Antenna

increases the circuit reliability from .72 to .98. An inspection of the same frequency at the same hour in Table 10.3 indicates that a change of antennas from curtains and rhombics to a horizontal dipole and an assumed gain of 5 dB lowers the circuit reliability to .07 when using 1 kW of power.

The prediction errors involved in the estimation of the radio noise levels and the available signal levels have been neglected in the calculation of the circuit reliability. It is, therefore, evident that any value of circuit reliability will under these circumstances be the most likely value of the parameter with actual values lying on either side with a like probability (.5) if the frequency has ionospheric support. The prediction errors associated with the expected time availability q_r are included in the following sections dealing with service probability (Q_r). The concept of service probability was originally developed by K. A. Norton in 1958 in connection with predicting the performance of tropospheric communication circuits.

11. Grade of Service (g_r) and Required Signal-To-Noise Ratios (R_h)

The "Grade of Service (g_r) refers to the degree of reliability over a short period of time (approximately a few minutes to an hour) during which the statistics of the signal-to-noise ratio may be considered to be stationary. It can be expressed for example as the percentage of error-free messages, the intelligibility achieved, or the percentage of satisfied observers." [CCIR Report 322]

The required signal-to-noise ratio (R_h) at the receiver for a given grade of service (g_r) will have some variation due to variations of the short-term noise and signal, multipath propagation, circuit equipments, etc. There is a prediction error σ_r in defining the required signal-to-noise ratio for any given grade of service. This report assumes that this prediction error is two decibels for all grades of service for the lack

of better information. If the circuit engineer has information on the prediction errors involved in the estimate of the required signal-to-noise, it should be used in lieu of the suggested two decibels.

12. Time Availability (q_r) and Service Probability (Q_r)

"The time availability refers to the percentage of the hours or other short periods of time used in defining the grade of service, during which the specified grade of service or better is achieved. The time involved should include all of the expected variations and may be an entire sunspot cycle, a year, a particular season or month, or certain hours of the day during a specified longer period." [CCIR Report 322] This specified longer period is the given hours of the day within a given month of the year. This means that when 0.90 time availability is specified a given grade of service (required signal-to-noise ratio) is expected to be exceeded 0.90 of the days within the month for the specified hours.

"Service Probability (Q_r) is defined as the probability that the specified grade of service (g_r) or better will be achieved for the specified time availability (q_r)." (CCIR Report 322) This combines statistically the uncertainties of the many parameters involved in the calculation of the performance of high frequency circuits.

The uncertainty (σ_R) of predicting a required signal-to-noise ratio for a specified grade of service has been explained in section 11. The uncertainties (σ_p, σ_{su} and $\sigma_{s\ell}$) of predicting the median, upper decile and lower decile respectively of system loss or conversely the available signal level at the receiver are shown in tables 1 through 3 of Appendix D. The values of prediction errors included in Appendix D were obtained from comparisons of predicted values of received signal with those observed on operating circuits. The comparisons include analyzed circuits ranging in great-circle distance from 250 km to 16,000 km and using frequencies ranging from 2.06 MHz to 20.0 MHz. A wide range

of latitudes was included in the circuits analyzed with most circuits lying between 12 and 80 degrees north geomagnetic latitude. Sufficient data were not available for high and low solar activity levels to attempt a correlation with solar activity. An attempt was made to include a frequency dependence in the uncertainties; however, no consistent variation was apparent. A distinct variation did appear as a function of local time of day and geomagnetic latitude of the circuit. The values of Appendix D are a function of these two variables and are assumed to be normally distributed either side of the median σ_p.

The uncertainties of predicting the radio noise level at the receiving site are contained in CCIR Report 322 as the error in predicting (1) the median 1 MHz atmospheric noise level (σ_{FAM}), (2) the lower decile value of the atmospheric noise level (σ_{DL}), and (3) the upper decile value of the atmospheric noise level (σ_{Du}). The three variables appearing above are evaluated using the numerical coefficients of tables 1 through 3 of Appendix E in the following equation

$$Y(x) = A_1 + A_2X + A_3X^2 + A_4X^3 + A_5X^4 \qquad (12.1)$$

where

$Y(x) = \sigma_{FAM}$, σ_{DL} or σ_{Du}

$X = \log_e (f)$, and

f = operating frequency - MHz

12.1 Calculation of the Protection Factor (C) for a Specified Time Availability (q_r)

The day-to-day variations of the hourly median signal levels ($\bar{S}$) and the hourly median noise levels ($\bar{N}$) are assumed to be normally distributed either side of the median values and can be described by the median values and the deviation $D_{S,N}$, of the value exceeded some specified fraction of the time, from the median. A protection factor (C)

needed to provide the required signal-to-noise ratio (R_h) for the specified time availability (q_r) can be determined--assuming no correlation--from

$$C^2 = D_N^2 + D_s^2 \tag{12.2}$$

D_N = values of the average noise power exceeded with probability $(1 - q_r)$

D_s = value of the average signal power exceeded with probability q_r.

The values D_N and D_s are evaluated using the values of tables 1 through 12 of Appendix C and the numerically represented values of F_{AM}, D_L, and D_u of CCIR Report 322 by the evaluation of the function

$$q_r = \frac{1}{\sqrt{2\pi}} \int_A^\infty e^{-\frac{1}{2}t^2} dt \tag{12.3}$$

q_r = given time availability $(0 \leq q_r \leq 1)$

A = standard normal deviate corresponding to a specified value of q_r

then

$$\begin{aligned} D_s &= A\, S_u \text{ and} \\ D_N &= A\, D_u \end{aligned} \tag{12.4}$$

The values of time availability are assumed to be between 0.50 and 1 in the above illustration; however, small changes in the above equations will allow the calculations to be performed for values of time availability less than 0.50.

12.2. Calculation of Service Probability (Q_T)

The service probability (Q_T) corresponding to the specified time availability (q_r) for a given required signal-to-noise ratio (R_h) can be calculated using the value of C calculated previously and the required signal-to-noise ratio (R_h) of section 11 and the total uncertainties (σ_t) to be explained later.

The median value of the expected required signal level $S(q_r)$ is evaluated by

$$S(q_r) = F_{AM} + C + R_h \text{ (dB < 1 watt)} \tag{12.5}$$

F_{AM} = median amplitude of the hourly median of the seasonal median prevailing radio noise level

C = required protection factor for the specified time availability (q_r).

R_h = required signal-to-noise ratio for the specified grade of service (g_r).

The total uncertainties (σ_t) involved in the prediction of circuit performance can be evaluated, on the assumption the prediction errors are uncorrelated, from

$$\sigma_t^2 = \sigma_r^2 + \sigma_p^2(s) + \sigma_c^2(n) + \sigma_c^2(s) + \sigma^2_{FAM}(dB)^2 \tag{12.6}$$

σ_r = standard error in decibels in predicting the required signal-to-noise ratio (R_h)

σ_p = root mean square error in decibels in predicting the median signal level (S)

σ_{FAM} = root mean square error in decibels in predicting the median radio noise level (N)

$\sigma_c(n)$ = additional standard error in decibels in predicting the radio noise level for a given median level, at the given value of time availability (q_r)

$\sigma_c(s)$ = additional standard error in decibels in predicting the signal level for a given median level, at the given value of time availability (q_r).

Since the value of the expected required signal level $S(q_r)$ has been evaluated along with the total uncertainties of the predictions (σ_t), the service probability can be evaluated for those frequencies having a probability of support (q_f) equal to 1 by

$$Q_T^* = \frac{1}{\sqrt{2\pi}} \int_{\frac{S(q_r) - \bar{S}}{\sigma_t}}^{\infty} e^{-\frac{1}{2}t^2} dt \qquad (12.7)$$

Q_T^* = service probability for frequencies sure of support via the ionosphere

$\bar{S}$ = predicted available median signal level-dB < 1 watt

$S(q_r)$ = the median value of the expected required signal power (for the given time availability-dB < 1 watt)

σ_t = total prediction uncertainties of the signal and noise levels-dB.

For those frequencies having a probability of support (q_f) less than one the total service probability would be

$$Q_T = Q_T^* \cdot q_f \qquad (12.8)$$

q_f = probability of ionospheric support of the operating frequency (f)

Q_T = service probability including the likelihood of support via the ionosphere.

During the hours at a given operating frequency when the atmospheric radio noise is not prevailing, the following values of the prediction errors for cosmic or man-made noise are recommended if more reliable information is not empirically available.

Cosmic Noise (dB)			Man-Made Noise (dB)		
σ_{FAM}	σ_{Du}	σ_{DL}	σ_{FAM}	σ_{Du}	σ_{DL}
0.5	0.2	0.2	3.0	1.5	1.5

Tables 12.1 and 12.2 show predictions of service probability for a chosen time availability of 0.90 and 0.80, respectively.

Table 12.1.

1 DEC SSN= 75 MD 1.007

LONDON	TO	MADRID	AZIMUTHS	N.MILES
52.37N - 1.18W		40.25N - 3.43W	188.1 6.5	733.1
RHOMBIC 20H 114L 70DEG			RHOMBIC 23H 120L 68DEG	
OFF AZIMUTH 64 DEG.	MIN. ANGLE= 0 DEG.		OFF AZIMUTH 47 DEG.	
PWR= 30.00KW	3 MC/S MAN. NOISE = -148 DBW		REQ.S/N= 45DB	

OPERATING FREQUENCIES — TIME AVAIL.=0.90

GMT	MUF	3	5	7	9	11	13	15	17	19	21	23	26	30	
14	18.7														
		1F	1F	2F	2F	1F	1F	1F	1F	1F	1F	-	-	-	MODE
		17	6	31	29	14	14	14	14	15	18	18	-	-	-	ANGLE
		54	51	59	58	53	53	53	53	53	54	54	-	-	-	DELAY
		.50	.99	.99	.99	.99	.99	.99	.94	.76	.44	.16	-	-	-	F.DAYS
		69	12	42	51	72	72	91	64	71	70	70	-	-	-	S/N..DB
		.50	.00	.01	.33	.99	.99	.99	.92	.76	.44	.16	-	-	-	S.PROB
16	17.0														
		1F	3F	2F	1F	1F	1F	1F	1F	1F	1F	-	-	-	-	MODE
		18	42	29	14	14	14	15	16	18	18	-	-	-	-	ANGLE
		54	68	58	53	53	53	53	53	54	54	-	-	-	-	DELAY
		.50	.99	.99	.99	.99	.99	.97	.82	.49	.17	-	-	-	-	F.DAYS
		64	26	56	69	75	75	92	64	64	70	-	-	-	-	S/N..DB
		.49	.00	.65	.99	.99	.99	.96	.80	.48	.17	-	-	-	-	S.PROB
18	11.8														
		1F	1F	1F	1F	1F	1F	1F	1F	-	-	-	-	-	-	MODE
		20	15	15	15	16	18	20	20	-	-	-	-	-	-	ANGLE
		55	53	53	53	53	54	55	55	-	-	-	-	-	-	DELAY
		.50	.99	.99	.99	.91	.65	.32	.11	-	-	-	-	-	-	F.DAYS
		70	48	71	71	77	72	85	64	-	-	-	-	-	-	S/N..DB
		.50	.11	.99	.99	.91	.64	.32	.11	-	-	-	-	-	-	S.PROB
20	8.6														
		1F	1F	1F	1F	1F	1F	-	-	-	-	-	-	-	-	MODE
		22	17	17	18	22	22	-	-	-	-	-	-	-	-	ANGLE
		56	54	54	54	56	56	-	-	-	-	-	-	-	-	DELAY
		.50	.99	.99	.86	.42	.11	-	-	-	-	-	-	-	-	F.DAYS
		74	49	72	70	75	69	-	-	-	-	-	-	-	-	S/N..DB
		.50	.22	.99	.86	.42	.11	-	-	-	-	-	-	-	-	S.PROB
22	7.4														
		1F	1F	1F	1F	1F	-	-	-	-	-	-	-	-	-	MODE
		24	19	20	23	24	-	-	-	-	-	-	-	-	-	ANGLE
		57	54	55	56	57	-	-	-	-	-	-	-	-	-	DELAY
		.50	.99	.99	.65	.17	-	-	-	-	-	-	-	-	-	F.DAYS
		60	51	73	65	74	-	-	-	-	-	-	-	-	-	S/N..DB
		.40	.35	.99	.61	.17	-	-	-	-	-	-	-	-	-	S.PROB
24	7.0														
		1F	1F	1F	1F	1F	-	-	-	-	-	-	-	-	-	MODE
		25	20	21	25	25	-	-	-	-	-	-	-	-	-	ANGLE
		57	55	55	58	58	-	-	-	-	-	-	-	-	-	DELAY
		.50	.99	.99	.49	.10	-	-	-	-	-	-	-	-	-	F.DAYS
		63	51	73	62	74	-	-	-	-	-	-	-	-	-	S/N..DB
		.46	.38	.98	.44	.10	-	-	-	-	-	-	-	-	-	S.PROB

Sample Computer Print-Out Showing Service Probability for a Chosen Time Availability of 0.90 Using Described Prediction Model

Table 12.2

1 DEC SSN= 75 MD 1.007
LONDON TO MADRID AZIMUTHS N.MILES
52.37N - 1.18W 40.25N - 3.43W 188.1 6.5 733.1
RHOMBIC 20H 114L 70DEG RHOMBIC 23H 120L 68DEG
OFF AZIMUTH 64 DEG. MIN. ANGLE= 0 DEG. OFF AZIMUTH 47 DEG.
PWR= 30.00KW 3 MC/S MAN. NOISE = -148 DBW REQ.S/N= 45DB
OPERATING FREQUENCIES TIME AVAIL.=0.80

GMT	MUF	3	5	7	9	11	13	15	17	19	21	23	26	30	
14	18.7														
	1F	1F	2F	2F	1F	1F	1F	1F	1F	1F	1F	-	-	-	MODE
	17	6	31	29	14	14	14	14	15	18	18	-	-	-	ANGLE
	54	51	59	58	53	53	53	53	53	54	54	-	-	-	DELAY
	.50	.99	.99	.99	.99	.99	.99	.94	.76	.44	.16	-	-	-	F.DAYS
	69	-12	42	51	72	72	91	64	71	70	70	-	-	-	S/N..DB
	.50	.00	.04	.57	.99	.99	.99	.94	.76	.44	[illegible]	-	-	-	S.PROB
16	17.0														
	1F	3F	2F	1F	1F	1F	1F	1F	1F	1F	-	-	-	-	MODE
	18	42	29	14	14	14	15	16	18	18	-	-	-	-	ANGLE
	54	68	58	53	53	53	53	53	54	54	-	-	-	-	DELAY
	.50	.99	.99	.99	.99	.99	.97	.82	.49	.17	-	-	-	-	F.DAYS
	64	26	56	69	75	75	92	64	64	70	-	-	-	-	S/N..DB
	.50	.00	.86	.99	.99	.99	.96	.82	.49	.17	-	-	-	-	S.PROB
18	11.8														
	1F	1F	1F	1F	1F	1F	1F	1F	-	-	-	-	-	-	MODE
	20	15	15	15	16	18	20	20	-	-	-	-	-	-	ANGLE
	55	53	53	53	53	54	55	55	-	-	-	-	-	-	DELAY
	.50	.99	.99	.99	.91	.65	.32	.11	-	-	-	-	-	-	F.DAYS
	70	48	71	71	77	72	85	64	-	-	-	-	-	-	S/N..DB
	.50	.27	.99	.99	.91	.64	.32	.11	-	-	-	-	-	-	S.PROB
20	4.5														
	1F	1F	1F	1F	1F	1F	-	-	-	-	-	-	-	-	MODE
	22	17	17	18	22	22	-	-	-	-	-	-	-	-	ANGLE
	56	54	54	54	56	56	-	-	-	-	-	-	-	-	DELAY
	.50	.99	.99	.86	.42	.11	-	-	-	-	-	-	-	-	F.DAYS
	74	49	72	70	75	69	-	-	-	-	-	-	-	-	S/N..DB
	.50	.38	.99	.86	.42	.11	-	-	-	-	-	-	-	-	S.PROB
22	7.4														
	1F	1F	1F	1F	1F	-	-	-	-	-	-	-	-	-	MODE
	24	19	20	23	24	-	-	-	-	-	-	-	-	-	ANGLE
	57	54	55	56	57	-	-	-	-	-	-	-	-	-	DELAY
	.50	.99	.99	.65	.17	-	-	-	-	-	-	-	-	-	F.DAYS
	60	51	73	65	74	-	-	-	-	-	-	-	-	-	S/N..DB
	.45	.53	.99	.64	.17	-	-	-	-	-	-	-	-	-	S.PROB
24	7.0														
	1F	1F	1F	1F	1F	-	-	-	-	-	-	-	-	-	MODE
	25	20	21	25	25	-	-	-	-	-	-	-	-	-	ANGLE
	57	55	55	58	58	-	-	-	-	-	-	-	-	-	DELAY
	.50	.99	.99	.49	.10	-	-	-	-	-	-	-	-	-	F.DAYS
	63	51	73	62	74	-	-	-	-	-	-	-	-	-	S/N..DB
	.48	.55	.98	.47	.10	-	-	-	-	-	-	-	-	-	S.PROB

Sample Computer Print-Out Showing Service Probability for a Chosen Time Availability of 0.80 Using Described Prediction Model

An inspection of the above tables will show that the service probability (Q_T) will be dominated by the probability of support (q_f) at the higher frequencies; but will be controlled by the available signal-to-noise ratio and the prediction errors (σ_t) at the lower frequencies.

13. Multipath Considerations

The usual type of multipath which provides the greatest difference in propagation times results from two or more paths with a different number of hops. Multipath propagation such as this can occur a large percent of the time over a wide frequency range. It can, however, be minimized by operating at frequencies where the likelihood of multiple signals of comparable strength is small, e.g., as close to the MUF as practical.

It is assumed that an adequate signal-to-noise ratio will suffice to determine circuit reliability if the operator has an adequate choice of frequencies in the complement to permit operation where the likelihood of multiple signals is low. The multipath predictions are intended to be used as an aid to determine the likelihood of multipath at a given frequency at a specific hour. If the reliability or service probability of two frequencies is equal, but one possesses a greater likelihood of multipath, this will also assist in the choice of operating frequency.

The difference in propagation times for various ray paths is a function of frequency and transmission distance; therefore, the probability of multipath is also dependent upon these variables. The multipath which is predicted is based upon some discrete minimum difference in received power and maximum tolerable time delay between ray paths. The probability of multipath is assumed to be the probability that a secondary ray path will be present to produce minimum difference in received signal powers.

In addition to selecting the frequency which is less likely to be subject to multipath, the multipath predictions may also be applicable to antenna design or selection to minimize multipath.

It is likely that predictions of this type will become more important as higher data rate systems are employed. The predictions are designed to estimate multipath probability as a function of time delay and minimum permissible level of the delayed signal. Tables 15.2a and 15.2b show some typical predictions of frequencies which possess multipath. They have an asterisk above the mode designation and an associated multipath probability printed below the circuit reliability or service probability.

14. Comparisons of Predictions with Observations

Limited comparisons of the predictions with observations are shown to illustrate the type of results which can be expected (figures 14.1 through 14.8).

Absolute comparisons between predictions and observations are normally difficult because the observed field strengths are usually abbreviated, e.g., read on a receiver "S" meter. Also changes in system sensitivity with frequency and insufficient knowledge of the actual equipment (antennas, transmitter power, line losses, multicouplers, etc.) are common.

The checks shown have some of the difficulties mentioned above, and assumptions were required in many of the predictions. When the details of the equipment parameters and methods of recording were not sufficiently known, only relative values are shown.

Figure 14.1 shows the agreement of observed monthly median maximum observed frequency MOF (0.50) with the predicted monthly median MUF (0.50). While the curves depart somewhat at certain hours the diurnal shape is in quite good agreement. The root mean square error of the predicted curve in figure 14.1 was calculated to be 0.94 MHz.

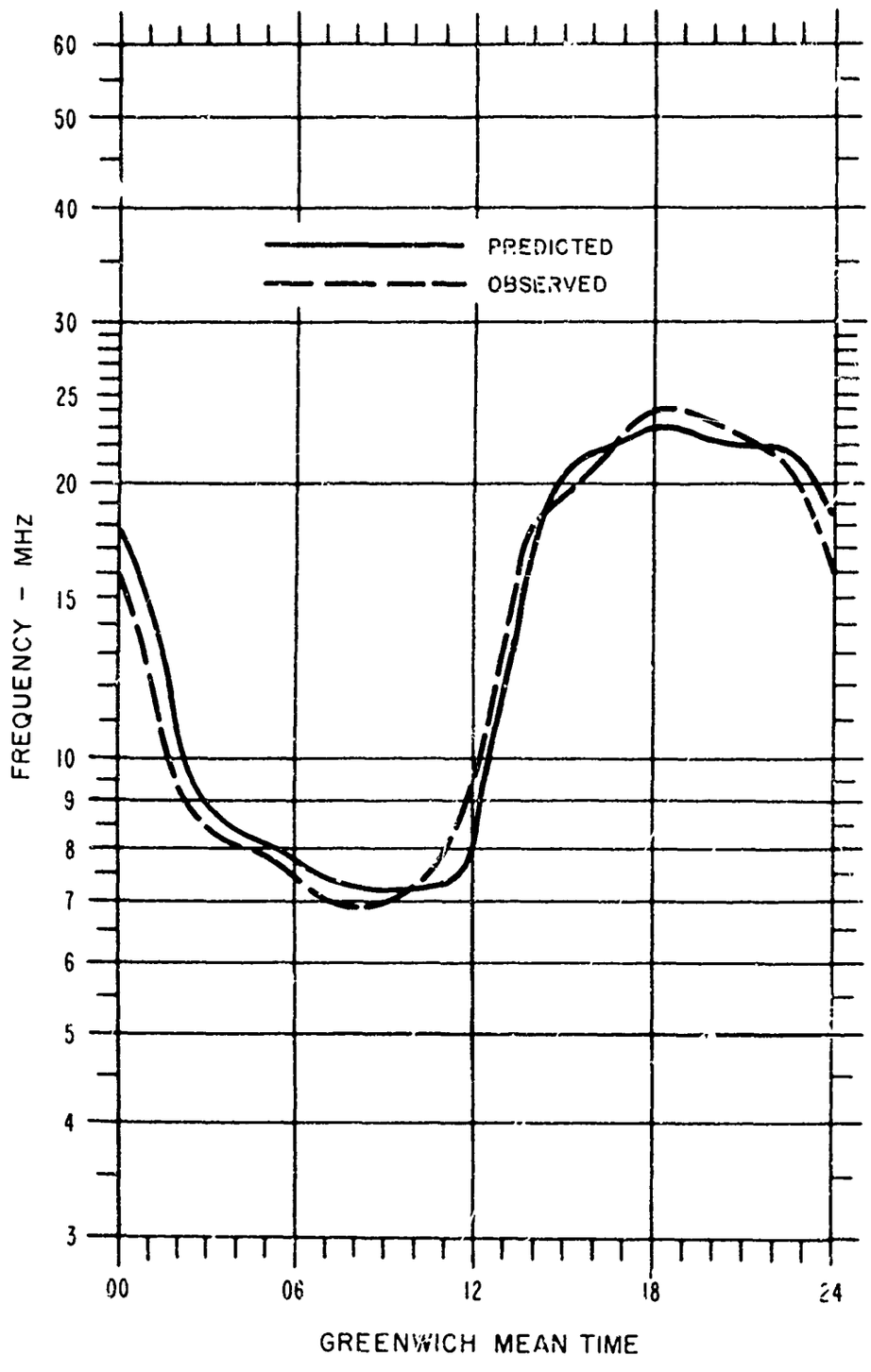

Figure 14.1. Fort Monmouth - Palo Alto Smooth MOF (0.50) Data Versus Predicted MUF (0.50) (November SSN 65)

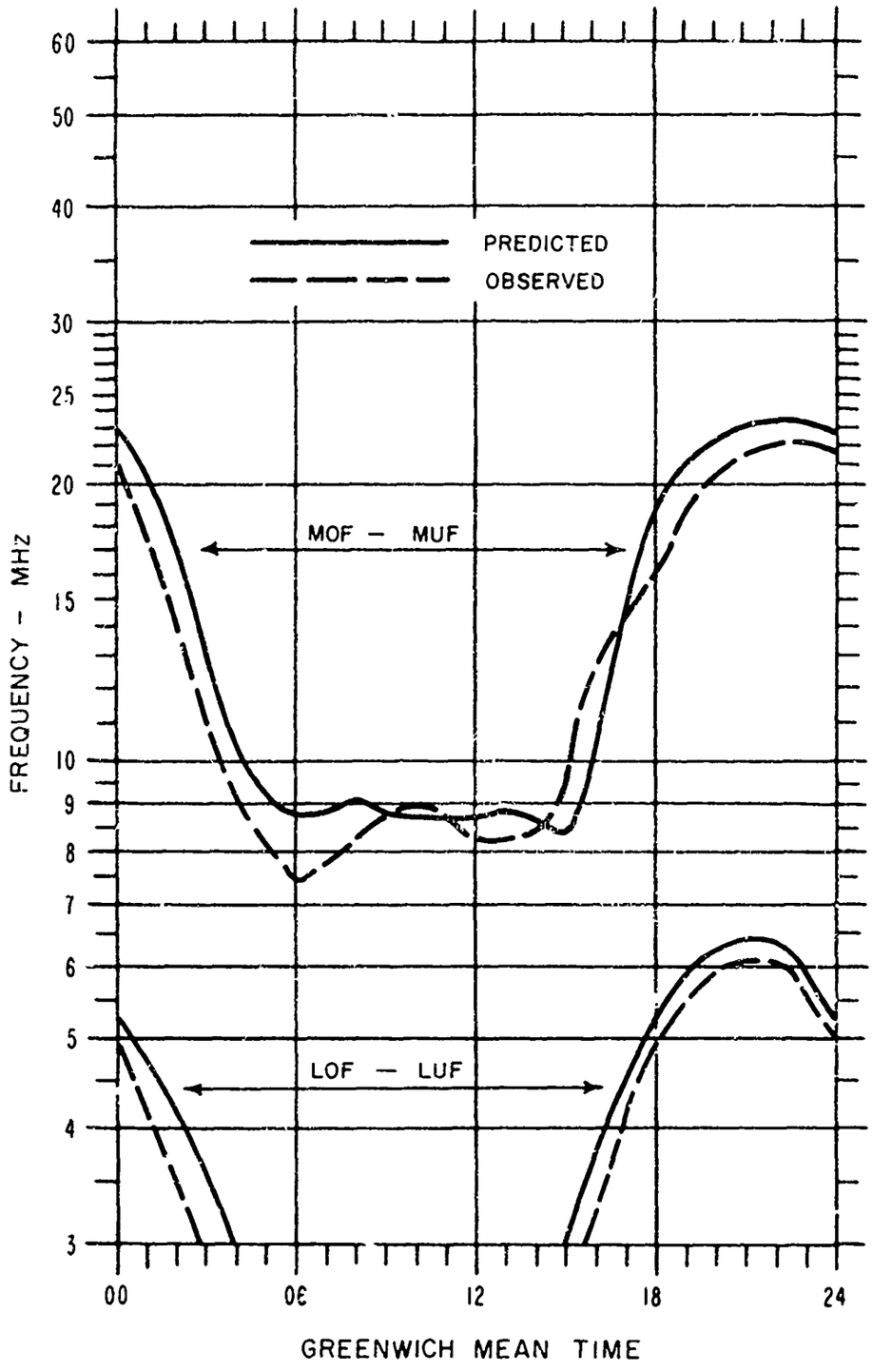

Figure 14.2. Predictions and Observations of the Elmendorf - McClellan Oblique Sounder January 1963 - 12 kW - SSN 29

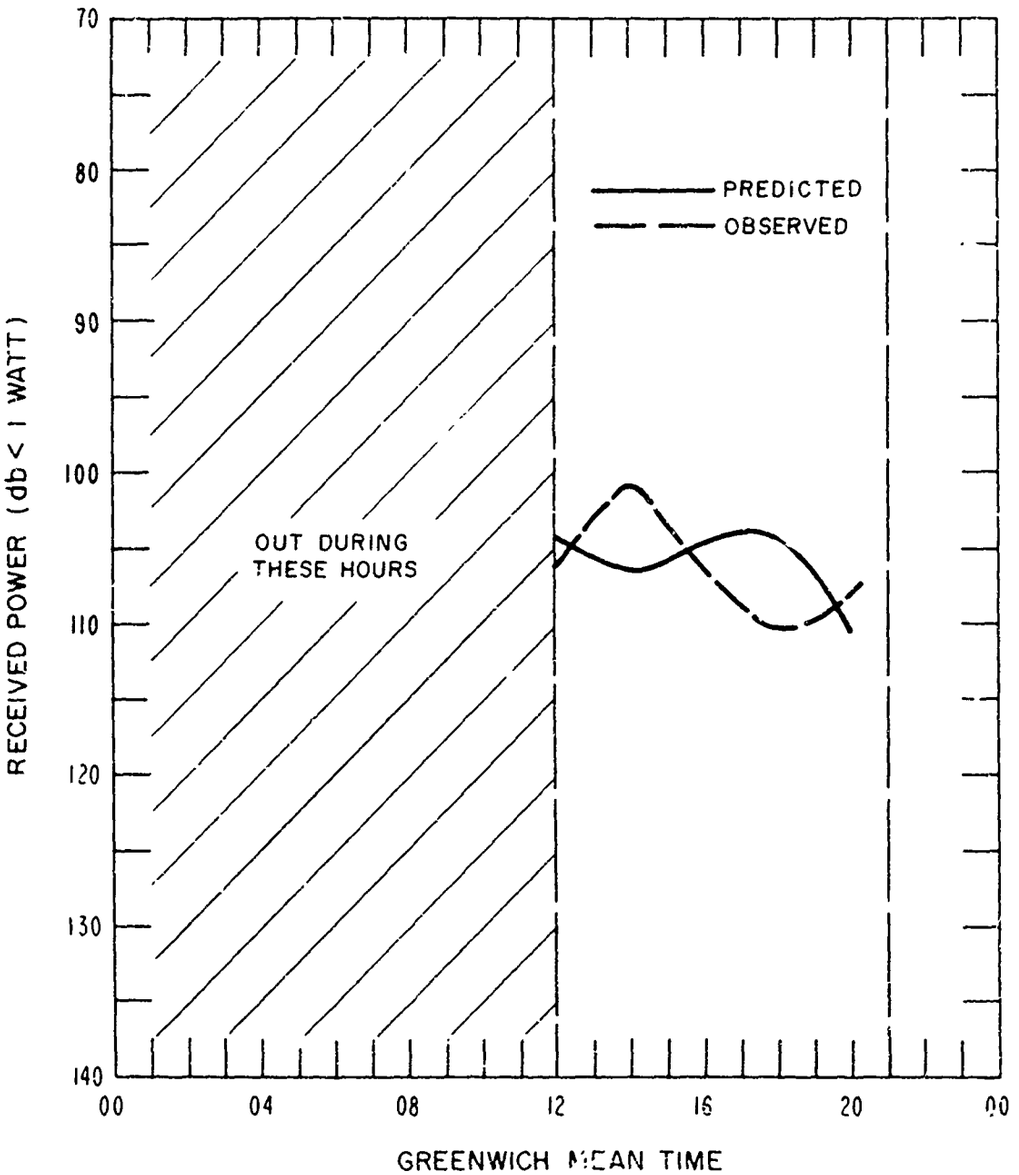

Figure 14.3. WWV Monitoring Versus Predictions Beltsville - Crowborough (December - SSN 12 - 15 MHz)

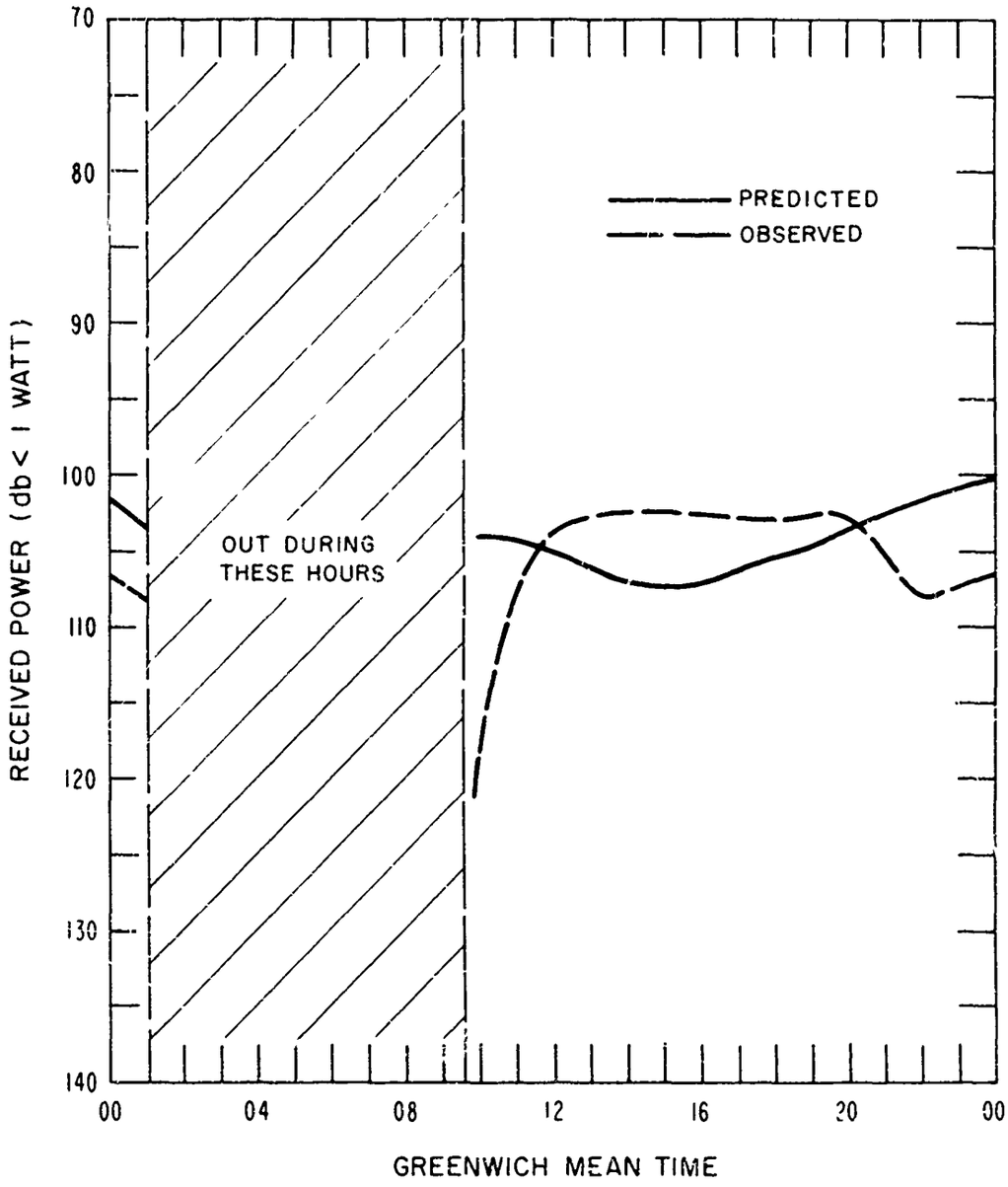

Figure 14.4. WWV Monitoring Versus Predictions Beltsville - Crowborough (December - SSN 180 - 20 MHz)

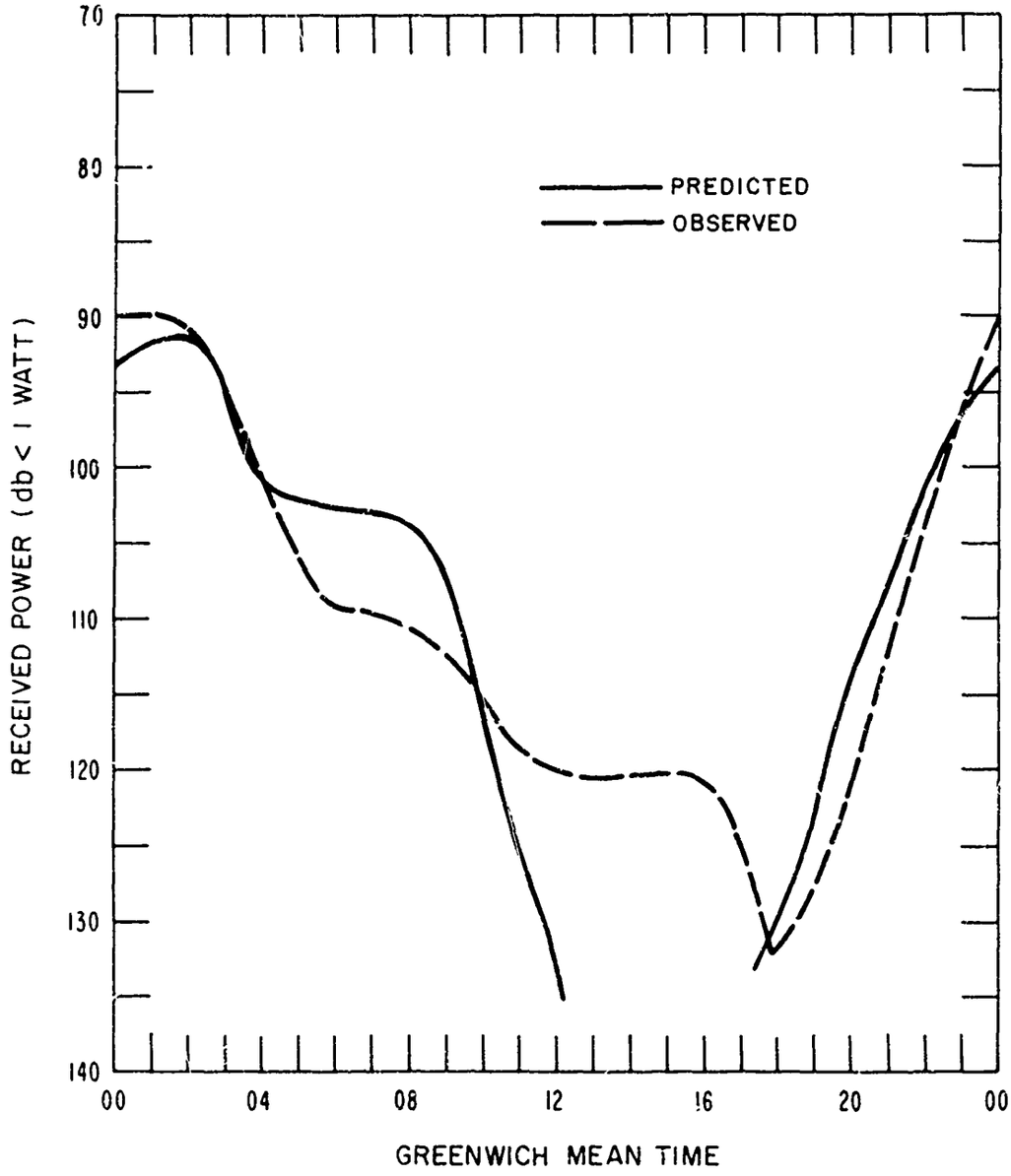

Figure 14.5. WWV Monitoring Versus Predictions Beltsville - Crowborough (June - SSN 14 - 10 MHz)

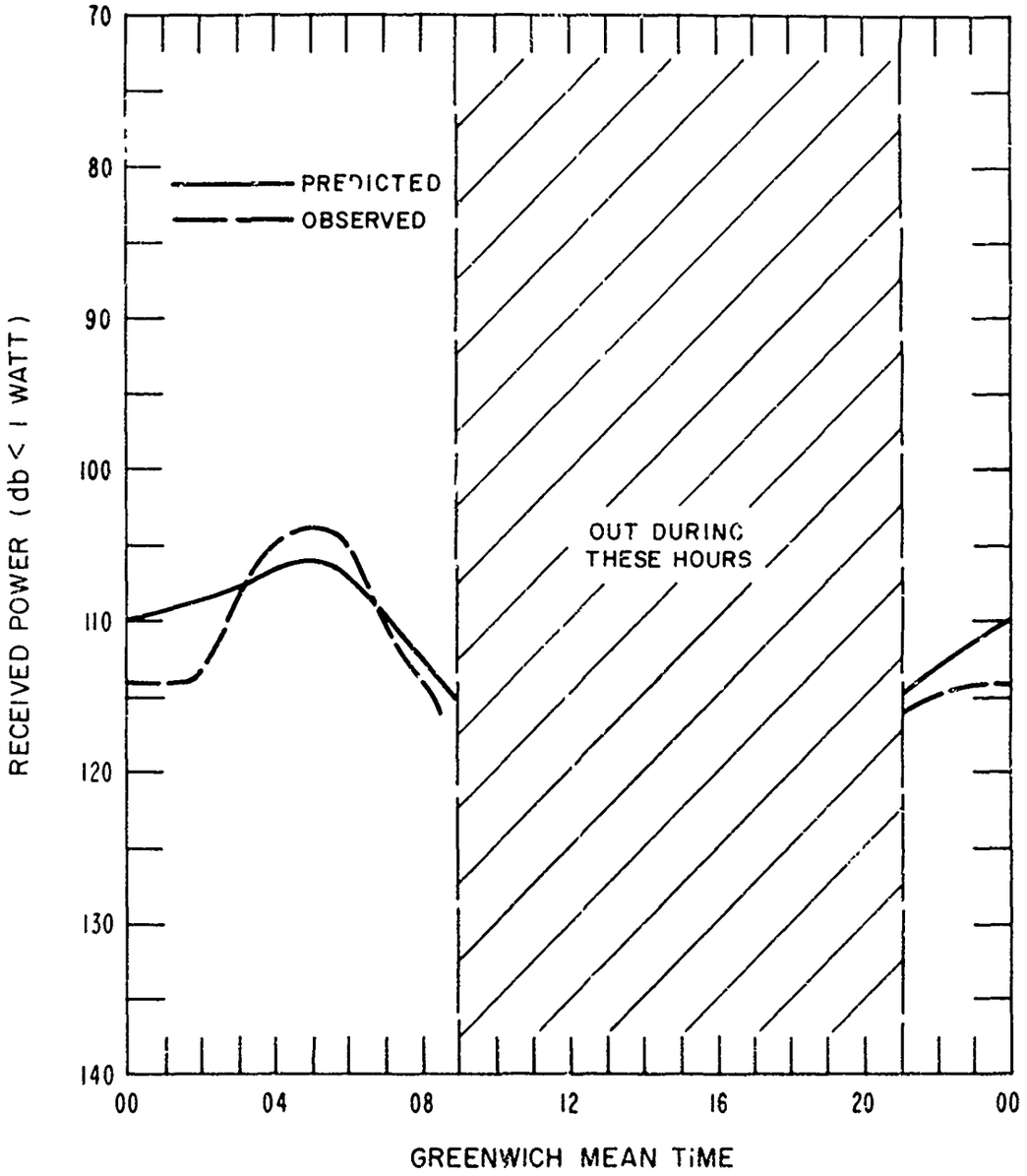

Figure 14.6. WWV Monitoring Versus Predictions Beltsville - Crowborough (March - SSN 201 - 5 MHz)

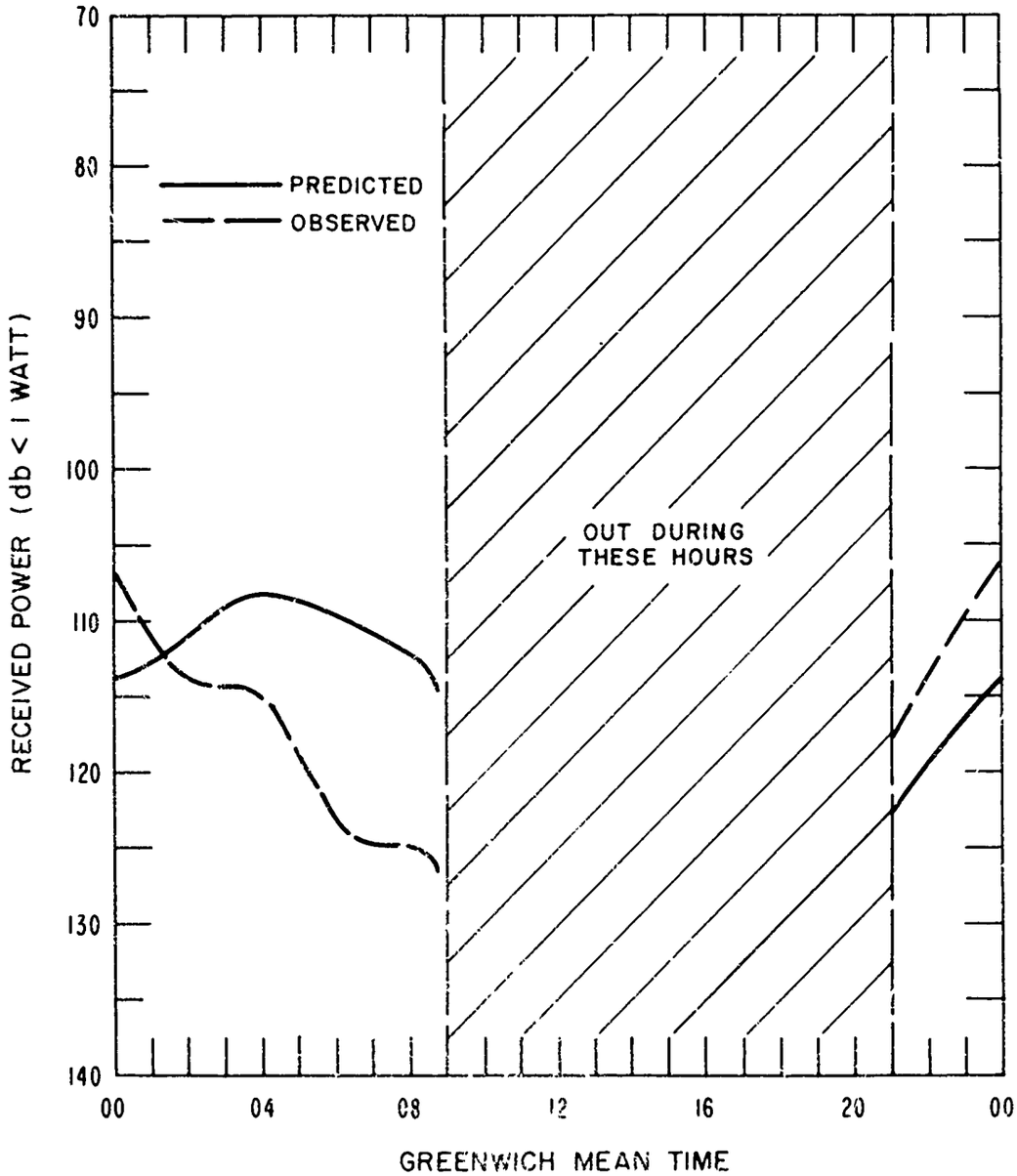

Figure 14.7. WWV Monitoring Versus Predictions Beltsville - Crowborough (March - SSN 19 - 5 MHz)

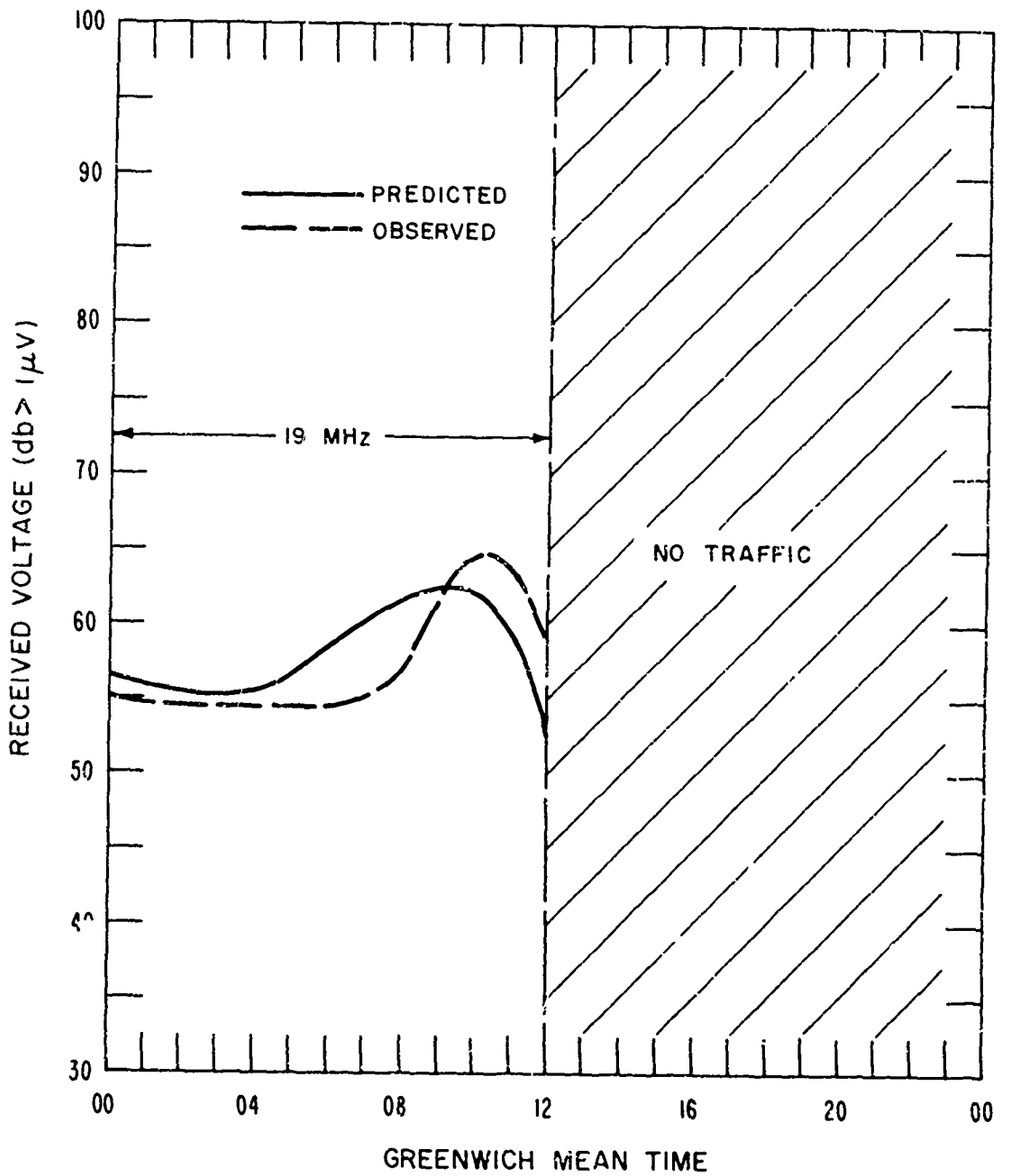

Figure 14.8. Predicted Versus Observed Relative Received Voltage Taipei - Tokyo - 1145 N.M. - June - SSN 161 - 200 Watts - Rhombics

Figure 14.2 shows a comparison of predicted MUF (0.5) and oblique sounder MOF (0.5) [Williams and Egan 1963]. The comparison may not be optimum since the predicted MUF should agree more closely with the junction frequency as recorded on the oblique sounder. The comparison was made, however, since both quantities are a measure of the upper limit of frequency. The root mean square error of the predicted MUF (0.5) was calculated to be 1.55 MHz. The root mean squared error of the predicted LUF (0.50) is .43 MHz.

Figures 14.3 through 14.8 are comparisons of observed received signal power with predicted received signal power. The figures shown are representative of many years of data analyzed at ITSA (formerly CRPL) and standard errors of the estimates have not been calculated for the specific figures shown. The agreement between observations and predictions appears good except for possibly figure 14.5, where the predicted received power for the middle of the day is in poor agreement with the observations. No really satisfactory explanation for this is currently available except that it is a high latitude path with a high probability of sporadic E and current prediction methods do not include sporadic E.

15. High Frequency Sky-Wave Computer Prediction Routine

The computer program is written primarily in Fortran 3600 for the CDC-3600 machine. The program is self-contained except for a few library subroutines which are assumed to be available on most machines. Comment cards are included throughout the program to provide easy stepping stones for those familiar with computer programming. All statements are intended to be simple and straightforward, utilizing no peculiarities of a specific monitor or machine. The basic Fortran should allow simplified conversion to other machines and languages if desired. All parameters which are evaluated many times are included as subprograms. The program is fast; yet ease of incorporating

changes and new knowledge is not sacrificed for speed alone. The program is intended to be a basic program on which to build as new knowledge and methods become available from basic research.

Tables 15.1 through 15.8 and figures 15.1 and 15.2 show the types of output possible using the basic concepts explained in preceding sections. Many items on the printed sheets are self-explanatory, but for the sake of completeness, the explanation is as follows:

A. Heading reading left to right

First Line

1. sequential number of circuit as entered into machine (X);
2. month of year (AAA);
3. solar activity level (SSN = XXX);
4. customer identification number derived from the great-circle distance and backward bearing (AA XX.XXX).

Second Line

1. transmitter and receiver locations;
2. azimuths (forward and backward);
3. nautical miles (N. Miles).

Third Line

1. geographic locations of transmitter and receiver in hundredths of degrees (XX.XXA-XXX.XXA);
2. azimuths (XXX.X XXX.X);
3. great-circle distance of path in nautical miles (XXXX.X).

Fourth Line

1. transmitting antenna and description;
2. receiving antenna and description.

Note: A minus number preceding any descriptive symbol denotes a parameter in wavelengths, i.e., $-12 = \lambda/2$, $-2 = 2\lambda$, $-14 = \lambda/4$. All other symbols are self-explanatory.

Fifth Line

1. off azimuth of transmitting antenna (XXX degrees);
2. minimum angle above the horizon for which any mode will be calculated (XX degrees);
3. off azimuth of receiving antenna (XXX degrees).

Sixth Line (if any)

1. output power of the transmitter at the antenna terminals;
2. (some options)
   measured or assumed man-made noise level at the receiving antenna site (dB < 1 watt at 3 MHz in a 1 Hz bandwidth);
3. (some options)
   the Lowest Useful Frequency (minimum operating frequency), i.e., 0.50 indicates lowest frequency having a circuit reliability of 0.50;
4. required signal-to-noise ratio (dB)
   a. the median signal power required in the occupied bandwidth relative to the noise power in a 1 Hz bandwidth;
   b. the signal power required must be the same type of power indicated at the transmitting antenna terminals.

Seventh Line (if any)

1. minimum tolerable difference in amplitude of received signal via two different ray paths, (M.P.PWR)
2. maximum tolerable delay time of two different ray paths (M.P.DELAY).

Note: The criteria of 1 and 2 above must both be met for the same two modes for detrimental multipath to be indicated.

Eighth Line (if any)

1. Greenwich mean time - hours;
2. monthly median Maximum Usable Frequency - MHz (XX.X);
3. operating frequency complement - MHz;
4. Time avail: specified time availability (fraction of days).

B. Body of print-outs

MODE: the sky-wave path contributing most to the overall probability or fraction of days a sky-wave path is expected, i.e., 1E = one hop via regular E, 2X = one hop via F2 and one hop via regular E;

ANGLE: the take off and arrival angle associated with the most probable sky-wave path;

F.DAYS: fraction of the days that at least one sky-wave mode is likely to be present to produce the quasi-minimum loss;

LOSS.DB: system loss as defined in section 5.3;

DBU: the incident field intensity at the receiving antenna site, dB relative to 1 uv/meter;

DBW: the power at the receiving antenna terminals, dB relative to 1 watt;

S/N: the signal-to-noise ratio at the receiving antenna terminals - dB;

REL: circuit reliability as explained in section 10;

S. PROB: service probability as explained in section 12;

FOT: Optimum Traffic Frequency based on empirical distributions of the MUF as explained in section 10;

DELAY: transmission time of most probable modes, tenths of milliseconds;

F.DAYS M.P.: probability of multipath or fraction of days multipath is expected (see section 13).

Additional Comments

1. A, -3, appearing in any LUF column or row denotes a LUF below 3 MHz.
2. An X appearing on the bottom line of any graphical print-out indicates a reliability, equal to or exceeding the required LUF level, did not exist at any frequency (3-30 MHz).
3. A column below any frequency containing all minus signs indicates that the probability of all sky-wave paths inspected fell below 0.05.

The computer program requires only one data tape for all needed data and one auxiliary tape for "scratch" purposes. Appendix F containing the program and instructions is available from ITSA. The following items are either included or available:

1. Data tape written in high (556 ch/in) or low (200 ch/in) density in either the binary coded decimal or binary format.
2. Hollerith deck of complete program including all subprograms and machine binary library routines if necessary.
3. Compiled listing and sample circuits run from compiled deck.
4. Complete explanation of all input and output requirements.
5. Machine listing and compiled program if necessary.
6. Pictorial views of input decks and output.
7. Arrangement of coefficients on data tape.
8. Complete listing of data tape.
9. The appendix will always contain latest improvements with complete explanation of same.

The program can be obtained by writing:

Frequency Utilization Section
Ionospheric Telecommunications Laboratory
Institute for Telecommunication Sciences and Aeronomy
ESSA/NBS Laboratories
Boulder, Colorado 80302

Table 15.1.

1			DEC			SSN=	75		MD	1.007	
LONDON			TO	MADRID			AZIMUTHS			N.MILES	
52.37N -		1.18W		+0.25N -		3.43W	188.1	6..		733.1	
GMT	MUF	FOT	GMT	MUF	FOT	GMT	MUF	FOT	GMT	MUF	FOT
1	6.9	5.8	7	7.8	6.5	13	18.9	15.3	19	9.7	7.6
2	7.1	5.8	8	12.7	10.5	14	18.7	15.7	20	8.6	6.7
3	7.0	5.8	9	17.3	14.4	15	18.2	15.3	21	7.8	6.1
4	7.0	5.7	10	19.4	15.7	16	17.0	14.2	22	7.4	6.2
5	6.5	5.3	11	19.4	16.0	17	14.6	12.3	23	7.2	6.0
6	6.0	4.9	12	19.4	15.7	18	1[illegible]8	9.2	24	7.0	5.8

Note: Updating of input va es is constantly taking place; therefore, values in this table and tables to follow are only tentative. Absolute values to be checked will always appear in Appendix F.

Sample Computer Print-Out of MUF (0.50) and FOT Only Using Described Prediction Model

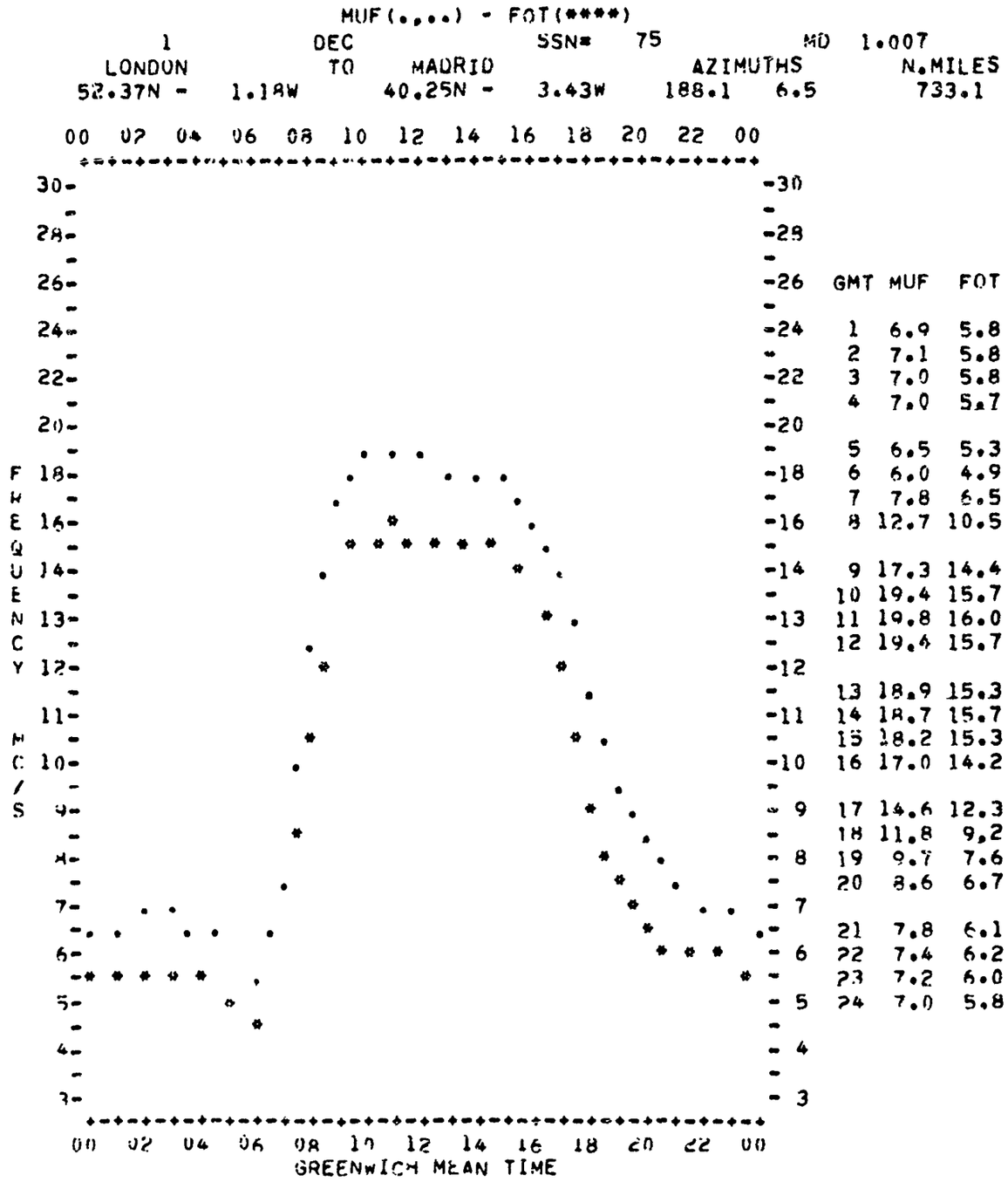

Figure 15.1. Sample Graphical Computer Print-Out of MUF (0.50) and FOT Using Described Prediction Model (London-Madrid. December - SSN 75)

Table 15.2a.

```
        1               OFC                    SSN=   75              MD   1.007
   LONDON               TO       MADRID                        AZIMUTHS         N.MILES
 52.37N -    1.18W         40.25N -     3.43W     188.1     6.5             733.1
RHOMBIC  20H 114L   70DEG                        RHOMBIC   23H 120L   68DEG
OFF AZIMUTH  64 DEG.      MIN. ANGLE=  0 DEG.      OFF AZIMUTH  47 DEG.
PWR= 30.00KW             3 MC/S MAN. NOISE = -148 DBW          REQ.S/N= 45DB
M.P. PWR= 10.0 DB                                        M.P. DELAY= 0.85 MS.
```

GMT	MUF	3	5	7	9	11	13	15	17	19	21	23	26	30	
							OPERATING FREQUENCIES								
2	7.1		*												
	1F	1F	1F	1F	-	-	-	-	-	-	-	-	-	-	MODE
	25	19	20	24	-	-	-	-	-	-	-	-	-	-	ANGLE
	57	55	55	57	-	-	-	-	-	-	-	-	-	-	DELAY
	.50	.99	.98	.52	-	-	-	-	-	-	-	-	-	-	F.DAYS
	60	50	73	62	-	-	-	-	-	-	-	-	-	-	S/N..DB
	.49	.78	.98	.52	-	-	-	-	-	-	-	-	-	-	REL.
	-	-	.97	-	-	-	-	-	-	-	-	-	-	-	F.DAYS M.P.
4	7.0		*												
	1F	1F	1F	1F	-	-	-	-	-	-	-	-	-	-	MODE
	24	18	19	24	-	-	-	-	-	-	-	-	-	-	ANGLE
	57	54	55	57	-	-	-	-	-	-	-	-	-	-	DELAY
	.50	.99	.98	.49	-	-	-	-	-	-	-	-	-	-	F.DAYS
	64	51	74	63	-	-	-	-	-	-	-	-	-	-	S/N..DB
	.50	.81	.97	.48	-	-	-	-	-	-	-	-	-	-	REL.
	-	-	.99	-	-	-	-	-	-	-	-	-	-	-	F.DAYS M.P.
6	6.6	*													
	1F	1F	1F	1F	-	-	-	-	-	-	-	-	-	-	MODE
	22	17	19	22	-	-	-	-	-	-	-	-	-	-	ANGLE
	56	54	54	56	-	-	-	-	-	-	-	-	-	-	DELAY
	.50	.99	.89	.05	-	-	-	-	-	-	-	-	-	-	F.DAYS
	71	50	74	65	-	-	-	-	-	-	-	-	-	-	S/N..DB
	.50	.77	.88	.05	-	-	-	-	-	-	-	-	-	-	REL.
	-	.96	-	-	-	-	-	-	-	-	-	-	-	-	F.DAYS M.P.
8	12.7	*													
	1F	2F	1F	1F	1F	1F	1F	-	-	-	-	-	-	-	MODE
	18	33	17	14	15	16	19	-	-	-	-	-	-	-	ANGLE
	54	61	54	53	53	53	54	-	-	-	-	-	-	-	DELAY
	.50	.99	.99	.99	.99	.84	.41	-	-	-	-	-	-	-	F.DAYS
	86	33	69	69	75	73	86	-	-	-	-	-	-	-	S/N..DB
	.50	.16	.99	.99	.98	.84	.41	-	-	-	-	-	-	-	REL.
	-	.99	-	-	-	-	-	-	-	-	-	-	-	-	F.DAYS M.P.
10	19.4														
	1F	1E	2F	2F	1F	1F	1F	1F	1F	1F	1F	1F	-	-	MODE
	17	6	30	28	14	13	13	16	14	16	17	17	-	-	ANGLE
	54	51	59	58	53	52	52	53	53	53	54	54	-	-	DELAY
	.50	.99	.99	.99	.99	.99	.99	.94	.80	.56	.24	.06	-	-	F.DAYS
	72	-7	44	52	72	73	91	65	74	71	70	66	-	-	S/N..DB
	.50	.00	.48	.84	.99	.99	.98	.93	.79	.55	.24	.06	-	-	REL.
	-	-	-	-	-	-	-	-	-	-	-	-	-	-	F.DAYS M.P.
12	19.4														
	1F	1E	2F	2F	1F	1F	1F	1F	1F	1F	1F	1F	-	-	MODE
	17	6	32	29	15	13	13	14	15	16	17	17	-	-	ANGLE
	54	51	60	58	53	53	53	53	53	53	54	54	-	-	DELAY
	.50	.99	.99	.99	.99	.99	.99	.94	.80	.55	.24	.05	-	-	F.DAYS
	71	-26	37	47	70	71	90	64	73	70	70	66	-	-	S/N..DB
	.50	.00	.24	.64	.99	.99	.98	.93	.79	.55	.24	.05	-	-	REL.
	-	-	-	-	-	-	-	-	-	-	-	-	-	-	F.DAYS M.P.

Sample Computer Print-Out of MUF (0.50), Mode, Angle, Delay, Fraction of Days, Signal-to-Noise Ratio, Circuit Reliability and Fraction of Days Multipath Using Described Prediction Model

Table 15.2b.

1 DEC SSN= 75 MD 1.007

LONDON TO MADRID AZIMUTHS N.MILES

52.37N - 1.18W 40.25N - 3.43W 188.1 6.5 733.1

RHOMBIC 20H 114L 70DEG RHOMBIC 23H 120L 68DEG

OFF AZIMUTH 64 DEG. MIN. ANGLE= 0 DEG. OFF AZIMUTH 47 DEG.

PWR= 30.00KW 3 MC/S MAN. NOISE = -148 DBW REQ.S/N= 45DB

M.P. PWR= 10.0 DB M.P. DELAY= 0.85 MS.

OPERATING FREQUENCIES

GMT	MUF	3	5	7	9	11	13	15	17	19	21	23	26	30	
14	18.7		*												
	1F	1E	2F	2F	1F	1F	1F	1F	1F	1F	1E	-	-	-	MODE
	17	6	31	29	14	14	14	14	15	18	18	-	-	-	ANGLE
	54	51	59	58	53	53	53	53	53	54	54	-	-	-	DELAY
	.50	.99	.99	.99	.99	.99	.99	.94	.76	.44	.16	-	-	-	F.DAYS
	69	-12	42	51	72	72	91	64	71	70	70	-	-	-	S/N..DB
	.50	.00	.40	.83	.99	.99	.99	.94	.76	.44	.16	-	-	-	REL.
	-	-	.99	-	-	-	-	-	-	-	-	-	-	-	F.DAYS M.P.
16	17.0														
	1F	3F	2F	1F	1F	1F	1F	1F	1F	1F	-	-	-	-	MODE
	18	42	29	14	14	14	15	16	18	18	-	-	-	-	ANGLE
	54	68	58	53	53	53	53	53	54	54	-	-	-	-	DELAY
	.50	.99	.99	.99	.99	.99	.97	.82	.49	.17	-	-	-	-	F.DAYS
	64	26	56	69	75	75	92	64	64	70	-	-	-	-	S/N..DB
	.50	.04	.93	.99	.99	.99	.96	.82	.49	.17	-	-	-	-	REL.
	-	-	-	-	-	-	-	-	-	-	-	-	-	-	F.DAYS M.P.
18	11.8														
	1F	1F	1F	1F	1F	1F	1F	1F	-	-	-	-	-	-	MODE
	20	15	15	15	16	18	20	20	-	-	-	-	-	-	ANGLE
	55	53	53	53	53	54	55	55	-	-	-	-	-	-	DELAY
	.50	.99	.99	.99	.91	.65	.32	.11	-	-	-	-	-	-	F.DAYS
	70	48	71	71	77	72	85	64	-	-	-	-	-	-	S/N..DB
	.50	.67	.99	.99	.91	.64	.32	.11	-	-	-	-	-	-	REL.
	-	-	-	-	-	-	-	-	-	-	-	-	-	-	F.DAYS M.P.
20	8.6		*												
	1F	1F	1F	1F	1F	1F	-	-	-	-	-	-	-	-	MODE
	22	17	17	18	22	22	-	-	-	-	-	-	-	-	ANGLE
	56	54	54	54	56	56	-	-	-	-	-	-	-	-	DELAY
	.50	.99	.99	.86	.42	.11	-	-	-	-	-	-	-	-	F.DAYS
	74	49	72	70	75	69	-	-	-	-	-	-	-	-	S/N..DB
	.50	.72	.99	.86	.42	.11	-	-	-	-	-	-	-	-	REL.
	-	-	.97	-	-	-	-	-	-	-	-	-	-	-	F.DAYS M.P.
22	7.4		*												
	1F	1F	1F	1F	1F	-	-	-	-	-	-	-	-	-	MODE
	24	19	20	23	24	-	-	-	-	-	-	-	-	-	ANGLE
	57	54	55	56	57	-	-	-	-	-	-	-	-	-	DELAY
	.50	.99	.99	.65	.17	-	-	-	-	-	-	-	-	-	F.DAYS
	80	51	73	65	74	-	-	-	-	-	-	-	-	-	S/N..DB
	.48	.81	.99	.65	.17	-	-	-	-	-	-	-	-	-	REL.
	-	-	.99	-	-	-	-	-	-	-	-	-	-	-	F.DAYS M.P.
24	7.0		*												
	1F	1F	1F	1F	1F	-	-	-	-	-	-	-	-	-	MODE
	25	20	21	25	25	-	-	-	-	-	-	-	-	-	ANGLE
	57	55	55	58	58	-	-	-	-	-	-	-	-	-	DELAY
	.50	.99	.99	.49	.10	-	-	-	-	-	-	-	-	-	F.DAYS
	83	51	73	62	74	-	-	-	-	-	-	-	-	-	S/N..DB
	.50	.83	.98	.49	.10	-	-	-	-	-	-	-	-	-	REL.
	-	-	.99	-	-	-	-	-	-	-	-	-	-	-	F.DAYS M.P.

Sample Computer Print-Out of MUF (0.50), Mode, Angle, Delay, Fraction of Days, Signal-to-Noise Ratio, Circuit Reliability and Fraction of Days Multipath Using Described Prediction Model

Table 15.3a.

1 DEC SSN= 75 MD 1.007

LONDON TO MADRID AZIMUTHS N.MILES
52.37N - 1.18W 40.25N - 3.43W 188.1 6.5 733.1
VERTICAL 35H 0L 0DEG VERTICAL -12H 0L 0DEG
OFF AZIMUTH 0 DEG. MIN. ANGLE= 0 DEG. OFF AZIMUTH 0 DEG.
PWR= 30.00KW LUF= 90 PERCENT REQ.S/N= 45DB
3 MC/S MAN. NOISE = -148 DBW

GMT	LUF	FOT	GMT	LUF	FOT	GMT	LUF	FOT	GMT	LUF	FOT
1	-3.0	5.8	7	-3.0	6.5	13	6.4	15.3	19	-3.0	7.6
2	-3.0	5.8	8	4.4	10.5	14	5.8	15.7	20	-3.0	6.7
3	-3.0	5.8	9	5.5	14.4	15	5.2	15.3	21	-3.0	6.1
4	-3.0	5.7	10	5.8	15.7	16	4.7	14.2	22	-3.0	6.2
5	-3.0	5.3	11	6.4	16.0	17	3.2	12.3	23	-3.0	6.0
6	-3.0	4.9	12	6.7	15.7	18	-3.0	9.2	24	-3.0	5.8

2 DEC SSN= 75 MD 1.007

LONDON TO MADRID AZIMUTHS N.MILES
52.37N - 1.18W 40.25N - 3.43W 188.1 6.5 733.1
H-YAGI 35H -12L 0DEG H-YAGI -12H -12L 0DEG
OFF AZIMUTH 64 DEG. MIN. ANGLE= 0 DEG. OFF AZIMUTH 47 DEG.
PWR= 30.00KW LUF= 90 PERCENT REQ.S/N= 45DB
3 MC/S MAN. NOISE = -148 DBW

GMT	LUF	FOT	GMT	LUF	FOT	GMT	LUF	FOT	GMT	LUF	FOT
1	-3.0	5.8	7	-3.0	6.5	13	4.7	15.3	19	-3.0	7.6
2	-3.0	5.8	8	-3.0	10.5	14	4.4	15.7	20	-3.0	6.7
3	-3.0	5.8	9	3.5	14.4	15	3.5	15.3	21	-3.0	6.1
4	-3.0	5.7	10	4.1	15.7	16	-3.0	14.2	22	-3.0	6.2
5	-3.0	5.3	11	4.7	16.0	17	-3.0	12.3	23	-3.0	6.0
6	-3.0	4.9	12	4.7	15.7	18	-3.0	9.2	24	-3.0	5.8

Sample Computer Print-Out of LUF and FOT Using Described Prediction Model

Table 15.3b.

1 DEC SSN= 75 MD 1.007

LONDON TO MADRID AZIMUTHS N.MILES
52.37N - 1.18W 40.25N - 3.43W 188.1 6.5 733.1
LOG PER. -14H 0L 0DEG LOG PER. -14H 0L 0DEG
OFF AZIMUTH 0 DEG. MIN. ANGLE= 0 DEG. OFF AZIMUTH 0 DEG.
PWR= 30.00KW LUF= 90 PERCENT REQ.S/N= 45DB
3 MC/S MAN. NOISE = -148 DBW

GMT	LUF	FOT	GMT	LUF	FOT	GMT	LUF	FOT	GMT	LUF	FOT
1		5.8	7		6.5	13		15.3	19		7.6
2	-3.0	5.8	8	-3.0	10.5	14	4.4	15.7	20	-3.0	6.7
3		5.8	9		14.4	15		15.3	21		6.1
4	-3.0	5.7	10	4.4	15.7	16	2.9	14.2	22	-3.0	6.2
5		5.3	11		16.0	17		12.3	23		6.0
6	-3.0	4.9	12	4.7	15.7	18	-3.0	9.2	24	-3.0	5.8

2 DEC SSN= 75 MD 1.007

LONDON TO MADRID AZIMUTHS N.MILES
52.37N - 1.18W 40.25N - 3.43W 188.1 6.5 733.1
CURTAIN 23H 46L 2BAY 8STACK CURTAIN 22H 45L 2BAY 8STACK
OFF AZIMUTH 64 DEG. MIN. ANGLE= 0 DEG. OFF AZIMUTH 47 DEG.
PWR= 30.00KW LUF= 90 PERCENT REQ.S/N= 45DB
3 MC/S MAN. NOISE = -148 DBW

GMT	LUF	FOT	GMT	LUF	FOT	GMT	LUF	FOT	GMT	LUF	FOT
1		5.8	7		6.5	13		15.3	19		7.6
2	-3.0	5.8	8	4.7	10.5	14	5.5	15.7	20	-3.0	6.7
3		5.8	9		14.4	15		15.3	21		6.1
4	-3.0	5.7	10	5.5	15.7	16	4.9	14.2	22	-3.0	6.2
5		5.3	11		16.0	17		12.3	23		6.0
6	-3.0	4.9	12	6.9	15.7	18	-3.0	9.2	24	-3.0	5.8

Sample Computer Print-Out of LUF and FOT Using Described Prediction Model

Table 15.4a.

1 DEC SSN= 75 MD 1.007

LONDON TO MADRID AZIMUTHS N.MILES

52.37N - 1.18W 40.25N - 3.43W 188.1 6.5 733.1

SL. VEE 35H 125L 20DEG SL. VEE 25H 120L 20DEG

OFF AZIMUTH 64 DEG. MIN. ANGLE= 0 DEG. OFF AZIMUTH 47 DEG.

GMT	MUF	OPERATING FREQUENCIES 3	5	7	9	11	13	15	17	19	21	23	26	30	
2	7.1														
	1F	1F	1F	1F	-	-	-	-	-	-	-	-	-	-	MODE
	25	19	20	24	-	-	-	-	-	-	-	-	-	-	ANGLE
	57	55	55	57	-	-	-	-	-	-	-	-	-	-	DELAY
	.50	.99	.98	.52	-	-	-	-	-	-	-	-	-	-	F.DAYS
	139	137	136	139	-	-	-	-	-	-	-	-	-	-	LOSS.DB
4	7.0														
	1F	1F	1F	1F	-	-	-	-	-	-	-	-	-	-	MODE
	24	18	19	24	-	-	-	-	-	-	-	-	-	-	ANGLE
	57	54	55	57	-	-	-	-	-	-	-	-	-	-	DELAY
	.50	.99	.98	.49	-	-	-	-	-	-	-	-	-	-	F.DAYS
	139	138	135	139	-	-	-	-	-	-	-	-	-	-	LOSS.DB
6	6.0														
	1F	1F	1F	1F	-	-	-	-	-	-	-	-	-	-	MODE
	22	17	19	22	-	-	-	-	-	-	-	-	-	-	ANGLE
	56	54	54	56	-	-	-	-	-	-	-	-	-	-	DELAY
	.50	.99	.89	.05	-	-	-	-	-	-	-	-	-	-	F.DAYS
	138	138	135	138	-	-	-	-	-	-	-	-	-	-	LOSS.DB
8	12.7														
	1F	2F	1F	1F	1F	1F	1F	-	-	-	-	-	-	-	MODE
	18	33	17	14	15	16	19	-	-	-	-	-	-	-	ANGLE
	54	61	54	53	53	53	54	-	-	-	-	-	-	-	DELAY
	.50	.99	.99	.99	.99	.84	.41	-	-	-	-	-	-	-	F.DAYS
	145	154	139	140	142	139	144	-	-	-	-	-	-	-	LOSS.DB
10	19.4														
	1F	1E	2F	2F	1F	1F	1F	1F	1F	1F	1F	1F	-	-	MODE
	17	6	30	28	14	13	13	14	14	16	17	17	-	-	ANGLE
	54	51	59	58	53	52	52	53	53	53	54	54	-	-	DELAY
	.50	.99	.99	.99	.99	.99	.99	.94	.80	.56	.24	.06	-	-	F.DAYS
	148	197	162	151	145	139	141	145	144	148	149	146	-	-	LOSS.DB
12	19.4														
	1F	1E	2F	2F	1F	1F	1F	1F	1F	1F	1F	1F	-	-	MODE
	17	6	32	29	15	13	13	14	15	16	17	17	-	-	ANGLE
	54	51	60	58	53	53	53	53	53	53	54	54	-	-	DELAY
	.50	.99	.99	.99	.99	.99	.99	.94	.80	.55	.24	.05	-	-	F.DAYS
	149	216	171	156	147	141	142	146	144	149	149	146	-	-	LOSS.DB

Sample Computer Print-Out of MUF (0.50), Mode, Angle, Fraction of Days and System Loss Using **Prediction Model**

Table 15.4b.

1 DEC SSN= 75 MD 1.007

LONDON TO MADRID AZIMUTHS N.MILES

52.37N - 1.18W 40.25N - 3.43W 188.1 6.5 733.1

SL. VEE 35H 125L 20DEG SL. VEE 25H 120L 20DEG

OFF AZIMUTH 64 DEG. MIN. ANGLE= 0 DEG. OFF AZIMUTH 47 DEG.

OPERATING FREQUENCIES

GMT	MUF	3	5	7	9	11	13	15	17	19	21	23	26	30	
14	18.7														
	1F	1E	2F	2F	1F	1F	1F	1F	1F	1F	1F	-	-	-	MODE
	17	6	31	29	14	14	14	14	15	18	18	-	-	-	ANGLE
	54	51	59	58	53	53	53	53	53	54	54	-	-	-	DELAY
	.50	.99	.99	.99	.99	.99	.99	.94	.76	.44	.16	-	-	-	F.DAYS
	148	202	165	152	145	140	142	145	144	148	149	-	-	-	LOSS.DB
16	17.0														
	1F	3F	2F	1F	1F	1F	1F	1F	1F	1F	-	-	-	-	MODE
	18	42	29	14	14	14	15	16	18	18	-	-	-	-	ANGLE
	54	68	58	53	53	53	53	53	54	54	-	-	-	-	DELAY
	.50	.99	.99	.99	.99	.99	.97	.82	.49	.17	-	-	-	-	F.DAYS
	145	164	148	140	141	137	141	143	145	149	-	-	-	-	LOSS.DB
18	11.8														
	1F	1F	1F	1F	1F	1F	1F	1F	-	-	-	-	-	-	MODE
	20	15	15	15	16	18	20	20	-	-	-	-	-	-	ANGLE
	55	53	53	53	53	54	55	55	-	-	-	-	-	-	DELAY
	.50	.99	.99	.99	.91	.65	.32	.11	-	-	-	-	-	-	F.DAYS
	143	140	136	137	140	139	143	140	-	-	-	-	-	-	LOSS.DB
20	8.6														
	1F	1F	1F	1F	1F	1F	-	-	-	-	-	-	-	-	MODE
	22	17	17	18	22	22	-	-	-	-	-	-	-	-	ANGLE
	56	54	54	54	55	56	-	-	-	-	-	-	-	-	DELAY
	.50	.99	.99	.86	.42	.11	-	-	-	-	-	-	-	-	F.DAYS
	143	139	136	138	144	142	-	-	-	-	-	-	-	-	LOSS.DB
22	7.4														
	1F	1F	1F	1F	1F	-	-	-	-	-	-	-	-	-	MODE
	24	19	20	23	24	-	-	-	-	-	-	-	-	-	ANGLE
	57	54	55	56	57	-	-	-	-	-	-	-	-	-	DELAY
	.50	.99	.99	.65	.17	-	-	-	-	-	-	-	-	-	F.DAYS
	139	137	135	138	144	-	-	-	-	-	-	-	-	-	LOSS.DB
24	7.0														
	1F	1F	1F	1F	1F	-	-	-	-	-	-	-	-	-	MODE
	25	20	21	25	25	-	-	-	-	-	-	-	-	-	ANGLE
	57	55	55	58	58	-	-	-	-	-	-	-	-	-	DELAY
	.50	.99	.99	.49	.10	-	-	-	-	-	-	-	-	-	F.DAYS
	139	137	136	139	144	-	-	-	-	-	-	-	-	-	LOSS.DB

Sample Computer Print-Out of MUF (0.50), Mode, Angle, Fraction of Days and System Loss Using Prediction Model

Table 15.5a.

```
        1            DEC              SSN=    75            MD  1.007
   LONDON              TO    MADRID                AZIMUTHS          N.MILES
  52.37N -    1.18W      40.25N -    3.43W    188.1    6.5          733.1
INVERT.L  30H  30L   0DEG                     INVERT.L -12H -12L     0DEG
OFF AZIMUTH  64 DEG.     MIN. ANGLE=  0 DEG.     OFF AZIMUTH  47 DEG.
PWR= 30.00KW             OPERATING FREQUENCIES          FIELD STRENGTH
```

GMT	MUF	3	5	7	9	11	13	15	17	19	21	23	26	30	
2	7.1														
	1F	1F	1F	1F	-	-	-	-	-	-	-	-	-	-	MODE
	25	19	20	24	-	-	-	-	-	-	-	-	-	-	ANGLE
	57	55	55	57	-	-	-	-	-	-	-	-	-	-	DELAY
	.50	.99	.98	.52	-	-	-	-	-	-	-	-	-	-	F.DAYS
	48	41	47	49	-	-	-	-	-	-	-	-	-	-	DBU
	70	70	67	69	-	-	-	-	-	-	-	-	-	-	-DBW
4	7.0														
	1F	1F	1F	1F	-	-	-	-	-	-	-	-	-	-	MODE
	24	18	19	24	-	-	-	-	-	-	-	-	-	-	ANGLE
	57	54	55	57	-	-	-	-	-	-	-	-	-	-	DELAY
	.50	.99	.98	.49	-	-	-	-	-	-	-	-	-	-	F.DAYS
	49	41	48	49	-	-	-	-	-	-	-	-	-	-	DBU
	69	69	66	69	-	-	-	-	-	-	-	-	-	-	-DBW
6	6.9														
	1F	1F	1F	1F	-	-	-	-	-	-	-	-	-	-	MODE
	22	17	19	22	-	-	-	-	-	-	-	-	-	-	ANGLE
	56	54	54	56	-	-	-	-	-	-	-	-	-	-	DELAY
	.50	.99	.89	.05	-	-	-	-	-	-	-	-	-	-	F.DAYS
	49	41	48	48	-	-	-	-	-	-	-	-	-	-	DBU
	67	69	66	69	-	-	-	-	-	-	-	-	-	-	-DBW
8	12.7														
	1F	2F	1F	1F	1F	1F	1F	-	-	-	-	-	-	-	MODE
	18	33	17	14	15	16	19	-	-	-	-	-	-	-	ANGLE
	54	61	54	53	53	53	54	-	-	-	-	-	-	-	DELAY
	.50	.99	.99	.99	.99	.84	.41	-	-	-	-	-	-	-	F.DAYS
	55	28	44	45	45	53	56	-	-	-	-	-	-	-	DBU
	66	78	67	71	73	67	66	-	-	-	-	-	-	-	-DBW
10	19.4														
	1F	1E	2F	2F	1F	1F	1F	1F	1F	1F	1F	1F	-	-	MODE
	17	6	30	28	14	13	13	14	14	16	17	17	-	-	ANGLE
	54	51	59	58	53	52	52	53	53	53	54	54	-	-	DELAY
	.50	.99	.99	.99	.99	.99	.99	.94	.80	.56	.24	.06	-	-	F.DAYS
	55	-11	27	35	41	51	57	59	54	54	59	61	-	-	DBU
	70	113	84	78	76	68	63	63	69	70	66	65	-	-	-DBW
12	19.4														
	1F	1E	2F	2F	1F	1F	1F	1F	1F	1F	1F	1F	-	-	MODE
	17	6	32	29	15	13	13	14	15	16	17	17	-	-	ANGLE
	54	51	60	58	53	53	53	53	53	53	54	54	-	-	DELAY
	.50	.99	.99	.99	.99	.99	.99	.94	.80	.55	.24	.05	-	-	F.DAYS
	54	-30	17	30	41	49	55	58	53	54	58	61	-	-	DBU
	71	137	93	83	77	70	65	64	70	70	67	65	-	-	-DBW

Sample Computer Print-Out of MUF (0.50), Mode, Angle, Delay, Fraction of Days, Field Strength and Received Power Using Described Prediction Model

Table 15.5b.

```
        1          DEC          SSN=   75          MD  1.007
     LONDON          TO     MADRID                AZIMUTHS      N.MILES
   52.37N -   1.18W      40.25N -   3.43W     188.1   6.5        733.1
 INVERT.L  30H  30L   0DEG                  INVERT.L -12H -12L   0DEG
 OFF AZIMUTH  64 DEG.     MIN. ANGLE=  0 DEG.     OFF AZIMUTH  47 DEG.
 PWR= 30.00KW          OPERATING FREQUENCIES          FIELD STRENGTH
GMT  MUF    3   5   7   9  11  13  15  17  19  21  23  25  30
14  18.7
      1F  1E  2F  2F  1F  1F  1F  1F  1F  1F  1F   -   -   -  MODE
      17   6  31  29  14  14  14  14  15  18  18   -   -   -  ANGLE
      54  51  59  58  53  53  53  53  53  54  54   -   -   -  DELAY
     .50 .99 .99 .99 .99 .99 .99 .94 .76 .44 .16   -   -   -  F.DAYS
      55 -16  25  34  42  50  57  58  53  55  58   -   -   -  DBU
      69 123  86  79  76  69  64  64  70  70  67   -   -   -  -DBW

16  17.0
      1F  3F  2F  1F  1F  1F  1F  1F  1F  1F  1F   -   -   -  MODE
      1B  42  29  14  14  14  15  16  18  18  18   -   -   -  ANGLE
      54  68  58  53  53  53  53  53  54  54  54   -   -   -  DELAY
     .50 .99 .99 .99 .99 .99 .97 .82 .49 .17   -   -   -  F.DAYS
      55  21  42  44  44  53  58  59  55  55  55   -   -   -  DBU
      69  85  69  70  73  66  63  63  69  70   -   -   -   -  -DBW

18  11.8
      1F  1F  1F  1F  1F  1F  1F  1F   -   -   -   -   -   -  MODE
      20  15  15  15  16  18  20  20   -   -   -   -   -   -  ANGLE
      55  53  53  53  53  54  55  55   -   -   -   -   -   -  DELAY
     .50 .99 .99 .99 .91 .65 .32 .11   -   -   -   -   -   -  F.DAYS
      5A  40  48  48  47  54  57  58   -   -   -   -   -   -  DBU
      67  69  65  68  71  66  65  65   -   -   -   -   -   -  -DBW

20   8.6
      1F  1F  1F  1F  1F  1F   -   -   -   -   -   -   -   -  MODE
      22  17  17  18  22  22   -   -   -   -   -   -   -   -  ANGLE
      56  54  54  54  56  56   -   -   -   -   -   -   -   -  DELAY
     .50 .99 .99 .85 .42 .11   -   -   -   -   -   -   -   -  F.DAYS
      48  40  48  48  48  53   -   -   -   -   -   -   -   -  DBU
      71  70  66  69  71  68   -   -   -   -   -   -   -   -  -DBW

22   7.4
      1F  1F  1F  1F  1F   -   -   -   -   -   -   -   -   -  MODE
      24  19  20  23  24   -   -   -   -   -   -   -   -   -  ANGLE
      57  54  55  56  57   -   -   -   -   -   -   -   -   -  DELAY
     .50 .99 .99 .65 .17   -   -   -   -   -   -   -   -   -  F.DAYS
      48  42  48  48  50   -   -   -   -   -   -   -   -   -  DBU
      70  69  66  69  70   -   -   -   -   -   -   -   -   -  -DBW

24   7.0
      1F  1F  1F  1F  1F   -   -   -   -   -   -   -   -   -  MODE
      25  20  21  25  25   -   -   -   -   -   -   -   -   -  ANGLE
      57  55  55  58  58   -   -   -   -   -   -   -   -   -  DELAY
     .50 .99 .99 .49 .10   -   -   -   -   -   -   -   -   -  F.DAYS
      49  41  49  49  50   -   -   -   -   -   -   -   -   -  DBU
      69  70  66  69  70   -   -   -   -   -   -   -   -   -  -DBW
```

Sample Computer Print-Out of MUF (0.50), Mode, Angle, Delay, Fraction of Days, Field Strength and Received Power Using Described Prediction Model

Table 15.6.

1 DEC SSN= 75 MD 1.007

LONDON TO MADRID AZIMUTHS N.MILES

52.37N - 1.18W 40.25N - 3.43W 188.1 6.5 733.1

SL.RHUM. 35H 125L 70DEG SL.RHUM. 25H 130L 70DEG

OFF AZIMUTH 64 DEG. MIN. ANGLE= 0 DEG. OFF AZIMUTH 47 DEG.

PWR= 20.00KW 3 MC/S MAN. NOISE = -148 DBW REQ.S/N= 45DB

RELIABILITIES

GMT	MUF	3	5	7	9	11	13	15	17	19	21	23	26	30	MCS
2	7.1	.85	.98	.52	-	-	-	-	-	-	-	-	-	-	
4	7.0	.85	.97	.48	-	-	-	-	-	-	-	-	-	-	
6	6.0	.81	.88	.05	-	-	-	-	-	-	-	-	-	-	
8	12.7	.98	.99	.99	.98	.84	.41	-	-	-	-	-	-	-	
10	19.4	.00	.87	.99	.99	.99	.98	.93	.79	.55	.24	.06	-	-	
12	19.4	.00	.58	.99	.99	.99	.98	.93	.79	.55	.24	.05	-	-	
14	18.7	.00	.82	.99	.99	.99	.99	.92	.76	.44	.16	-	-	-	
16	17.0	.05	.99	.99	.99	.99	.96	.82	.49	.17	-	-	-	-	
18	11.6	.67	.99	.99	.91	.64	.32	.11	-	-	-	-	-	-	
20	8.6	.72	.99	.86	.42	.11	-	-	-	-	-	-	-	-	
22	7.4	.85	.99	.65	.17	-	-	-	-	-	-	-	-	-	
24	7.0	.46	.98	.49	.10	-	-	-	-	-	-	-	-	-	

Sample Computer Print-Out of MUF (0.50) and Circuit Reliability Using Deacribed Prediction Model

Table 15.7a.

1 DEC SSN= 75 MD 1.007

LONDON TO MADRID AZIMUTHS N.MILES

52.37N - 1.18W 40.25N - 3.43W 188.1 6.5 733.1

ANT= 6DB ANT= 10DB

OFF AZIMUTH 0 DEG. MIN. ANGLE= 0 DEG. OFF AZIMUTH 0 DEG.

PWR= 30.00KW 3 MC/S MAN. NOISE = -148 DBW REQ.S/N= 45DB

GMT	MUF	OPERATING FREQUENCIES 3	5	7	9	11	13	15	17	19	21	23	26	30	
2	7.1														
		1F	1F	1F	-	-	-	-	-	-	-	-	-	-	MODE
		25	19	20	24	-	-	-	-	-	-	-	-	-	ANGLE
		57	55	55	57	-	-	-	-	-	-	-	-	-	DELAY
		.50	.99	.98	.52	-	-	-	-	-	-	-	-	-	F.DAYS
		96	84	91	95	-	-	-	-	-	-	-	-	-	S/N..DB
		64	64	63	64	-	-	-	-	-	-	-	-	-	-DBW
4	7.0														
		1F	1F	1F	1F	-	-	-	-	-	-	-	-	-	MODE
		24	18	19	24	-	-	-	-	-	-	-	-	-	ANGLE
		57	54	55	57	-	-	-	-	-	-	-	-	-	DELAY
		.50	.99	.98	.49	-	-	-	-	-	-	-	-	-	F.DAYS
		95	85	92	95	-	-	-	-	-	-	-	-	-	S/N..DB
		64	64	63	64	-	-	-	-	-	-	-	-	-	-DBW
6	6.0														
		1F	1F	1F	1F	-	-	-	-	-	-	-	-	-	MODE
		22	17	19	22	-	-	-	-	-	-	-	-	-	ANGLE
		56	54	54	56	-	-	-	-	-	-	-	-	-	DELAY
		.50	.99	.99	.05	-	-	-	-	-	-	-	-	-	F.DAYS
		94	85	92	95	-	-	-	-	-	-	-	-	-	S/N..DB
		63	64	63	64	-	-	-	-	-	-	-	-	-	-DBW
8	12.7														
		1F	2F	1F	1F	1F	1F	1F	-	-	-	-	-	-	MODE
		18	33	17	14	15	16	19	-	-	-	-	-	-	ANGLE
		54	61	54	53	53	53	54	-	-	-	-	-	-	DELAY
		.50	.99	.99	.99	.99	.84	.41	-	-	-	-	-	-	F.DAYS
		98	68	88	92	96	97	98	-	-	-	-	-	-	S/N..DB
		69	81	67	67	67	68	69	-	-	-	-	-	-	-DBW
10	19.4														
		1F	1E	2F	2F	1F	1F	1F	1F	1F	1F	1F	1F	-	MODE
		17	6	30	28	14	13	13	14	14	16	17	17	-	ANGLE
		54	51	59	58	53	52	52	53	53	53	54	54	-	DELAY
		.50	.99	.99	.99	.99	.99	.99	.94	.80	.56	.24	.06	-	F.DAYS
		101	28	67	82	92	95	97	99	100	101	102	102	-	S/N..DB
		71	121	88	77	71	70	70	70	70	71	71	72	-	-DBW
12	19.4														
		1F	1E	2F	2F	1F	1F	1F	1F	1F	1F	1F	1F	-	MODE
		17	6	32	29	15	13	13	14	15	16	17	17	-	ANGLE
		54	51	60	58	53	53	53	53	53	53	54	54	-	DELAY
		.50	.99	.99	.99	.99	.99	.99	.94	.80	.55	.24	.05	-	F.DAYS
		100	9	60	77	91	93	96	98	99	101	101	102	-	S/N..DB
		72	140	95	82	72	72	71	71	71	71	72	72	-	-DBW

Sample Computer Print-Out of MUF (0.50), Mode, Angle, Delay, Fraction of Days, Signal-to-Noise Ratio and Received Power Using Described Prediction Model

Table 15.7b.

1 DEC SSN= 75 MO 1.007

LONDON TO MADRID AZIMUTHS N.MILES

52.37N - 1.18W 40.25N - 3.43W 188.1 6.5 733.1

ANT= 6DB ANT= 10DB

OFF AZIMUTH 0 DEG. MIN. ANGLE= 0 DEG. OFF AZIMUTH 0 DEG.

PWR= 30.00KW 3 MC/S MAN. NOISE = -148 DBW REQ.S/N= 45DB

OPERATING FREQUENCIES

GMT	MUF	3	5	7	9	11	13	15	17	9	21	23	26	30	
14	18.7														
	1F	1E	2F	2F	1F	1F	1F	1F	1F	1F	1F	-	-	-	MODE
	17	6	31	29	14	14	14	14	15	18	18	-	-	-	ANGLE
	54	51	59	58	53	53	53	53	53	54	54	-	-	-	DELAY
	.50	.99	.99	.99	.99	.99	.99	.94	.76	.44	.16	-	-	-	F.DAYS
	100	23	65	80	92	96	97	99	99	101	101	-	-	-	S/N..DB
	71	126	90	79	71	70	70	70	71	71	72	-	-	-	-DBW
16	17.0														
	1F	3F	2F	1F	1F	1F	1F	1F	1F	1F	-	-	-	-	MODE
	18	42	29	14	14	14	15	16	18	18	-	-	-	-	ANGLE
	54	68	58	53	53	53	53	53	54	54	-	-	-	-	DELAY
	.50	.99	.99	.99	.99	.99	.97	.82	.49	.17	-	-	-	-	F.DAYS
	100	62	82	92	96	97	98	100	100	101	-	-	-	-	S/N..DB
	70	87	73	67	67	68	69	69	70	71	-	-	-	-	-DBW
18	11.8														
	1F	1F	1F	1F	1F	1F	1F	1F	-	-	-	-	-	-	MODE
	20	15	15	15	16	18	20	20	-	-	-	-	-	-	ANGLE
	55	53	53	53	53	54	55	55	-	-	-	-	-	-	DELAY
	.50	.99	.99	.99	.91	.65	.32	.11	-	-	-	-	-	-	F.DAYS
	99	83	91	95	98	98	99	100	-	-	-	-	-	-	S/N..DB
	67	66	64	64	65	67	68	69	-	-	-	-	-	-	-DBW
20	8.6														
	1F	1F	1F	1F	1F	1F	-	-	-	-	-	-	-	-	MODE
	22	17	17	18	22	22	-	-	-	-	-	-	-	-	ANGLE
	56	54	54	54	56	56	-	-	-	-	-	-	-	-	DELAY
	.50	.99	.99	.86	.42	.11	-	-	-	-	-	-	-	-	F.DAYS
	96	84	91	94	97	98	-	-	-	-	-	-	-	-	S/N..DB
	66	65	64	65	66	67	-	-	-	-	-	-	-	-	-DBW
22	7.4														
	1F	1F	1F	1F	1F	-	-	-	-	-	-	-	-	-	MODE
	24	19	20	23	24	-	-	-	-	-	-	-	-	-	ANGLE
	57	54	55	56	57	-	-	-	-	-	-	-	-	-	DELAY
	.50	.99	.99	.65	.17	-	-	-	-	-	-	-	-	-	F.DAYS
	96	85	91	95	98	-	-	-	-	-	-	-	-	-	S/N..DB
	64	64	63	64	65	-	-	-	-	-	-	-	-	-	-DBW
24	7.0														
	1F	1F	1F	1F	1F	-	-	-	-	-	-	-	-	-	MODE
	25	20	21	25	25	-	-	-	-	-	-	-	-	-	ANGLE
	57	55	55	58	58	-	-	-	-	-	-	-	-	-	DELAY
	.50	.99	.99	.49	.10	-	-	-	-	-	-	-	-	-	F.DAYS
	95	85	91	95	98	-	-	-	-	-	-	-	-	-	S/N..DB
	64	64	63	64	65	-	-	-	-	-	-	-	-	-	-DBW

Sample Computer Print-Out of MUF (0.50), Mode, Angle, Delay, Fraction of Days, Signal-to-Noise Ratio and Received Power Using Described Prediction Model

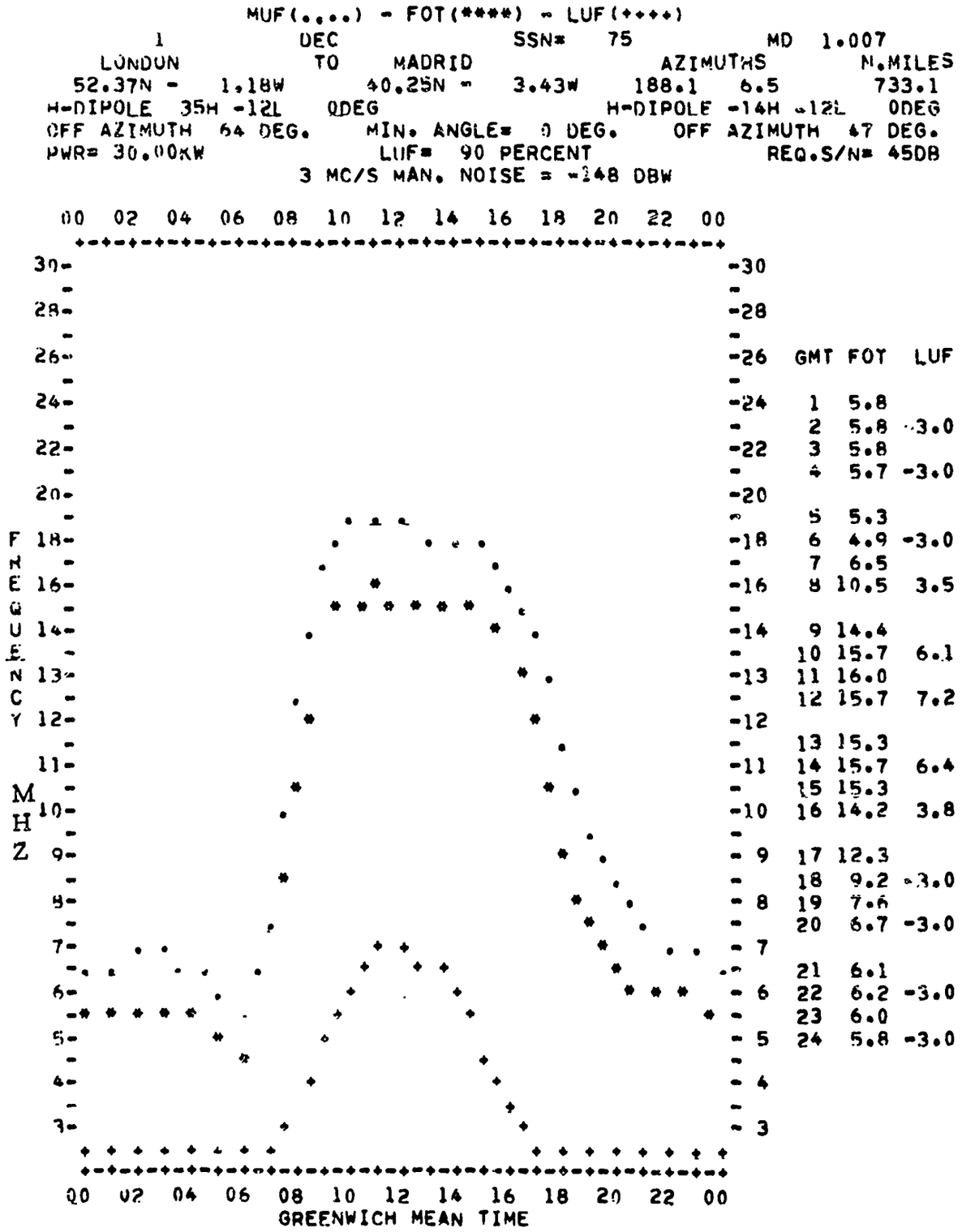

Figure 15.2. Sample Graphical Computer Print-Out of MUF (0.50) and LUF (0.90) Using Described Prediction Model (London-Madrid, December - SSN 75)

Table 15.8a.

3 DEC SSN= 75 MO 1.007

LONDON TO MADRID AZIMUTHS N.MILES

52.37N - 1.18W 40.25N - 3.43W 188.1 6.5 733.1

H-DIPOLE 10M -12L 0DEG ANT= 5DB

OFF AZIMUTH 64 DEG. MIN. ANGLE= 0 DEG. OFF AZIMUTH 47 DEG.

PWR= 30.00KW 3 MC/S MAN. NOISE = -148 DBW REQ.S/N= 45DB

OPERATING FREQUENCIES TIME AVAIL.=0.90

GMT	MUF	3	5	7	9	11	13	15	17	19	21	23	26	30	
2	7.1														
	1F	1F	1F	1F	-	-	-	-	-	-	-	-	-	-	MODE
	25	19	20	24	-	-	-	-	-	-	-	-	-	-	ANGLE
	57	55	55	57	-	-	-	-	-	-	-	-	-	-	DELAY
	.50	.99	.98	.52	-	-	-	-	-	-	-	-	-	-	F.DAYS
	79	63	71	79	-	-	-	-	-	-	-	-	-	-	S/N..DB
	.50	.90	.98	.52	-	-	-	-	-	-	-	-	-	-	S.PROB
4	7.0														
	1F	1F	1F	1F	-	-	-	-	-	-	-	-	-	-	MODE
	24	18	19	24	-	-	-	-	-	-	-	-	-	-	ANGLE
	57	54	55	57	-	-	-	-	-	-	-	-	-	-	DELAY
	.50	.99	.98	.49	-	-	-	-	-	-	-	-	-	-	F.DAYS
	79	63	72	79	-	-	-	-	-	-	-	-	-	-	S/N..DB
	.50	.91	.97	.48	-	-	-	-	-	-	-	-	-	-	S.PROB
6	6.0														
	1F	1F	1F	1F	-	-	-	-	-	-	-	-	-	-	MODE
	22	17	19	22	-	-	-	-	-	-	-	-	-	-	ANGLE
	56	54	54	56	-	-	-	-	-	-	-	-	-	-	DELAY
	.50	.99	.89	.05	-	-	-	-	-	-	-	-	-	-	F.DAYS
	77	62	72	79	-	-	-	-	-	-	-	-	-	-	S/N..DB
	.50	.89	.88	.05	-	-	-	-	-	-	-	-	-	-	S.PROB
8	12.7														
	1F	2F	1F	1F	1F	1F	1F	-	-	-	-	-	-	-	MODE
	18	33	17	14	15	16	19	-	-	-	-	-	-	-	ANGLE
	54	61	54	53	53	53	54	-	-	-	-	-	-	-	DELAY
	.50	.99	.99	.99	.99	.84	.41	-	-	-	-	-	-	-	F.DAYS
	82	52	67	72	76	79	82	-	-	-	-	-	-	-	S/N..DB
	.50	.35	.99	.99	.98	.84	.41	-	-	-	-	-	-	-	S.PROB
10	19.4														
	1F	1F	2F	2F	1F	1F	1F	1F	1F	1F	1F	1F	-	-	MODE
	17	6	30	28	14	13	13	14	14	16	17	17	-	-	ANGLE
	54	51	59	58	53	52	52	53	53	53	54	54	-	-	DELAY
	.50	.99	.99	.99	.99	.99	.99	.94	.80	.56	.24	.06	-	-	F.DAYS
	86	5	50	62	72	76	79	82	84	86	87	88	-	-	S/N..DB
	.50	.00	.24	.92	.99	.99	.98	.93	.79	.55	.24	.06	-	-	S.PROB
12	19.4														
	1F	1F	2F	2F	1F	1F	1F	1F	1F	1F	1F	1F	-	-	MODE
	17	6	32	29	15	13	13	14	15	16	17	17	-	-	ANGLE
	54	51	60	58	53	53	53	53	53	53	54	54	-	-	DELAY
	.50	.99	.99	.99	.99	.99	.99	.94	.80	.55	.24	.05	-	-	F.DAYS
	86	-13	45	58	71	74	78	81	83	86	87	88	-	-	S/N..DB
	.50	.00	.04	.74	.99	.99	.98	.93	.79	.55	.24	.05	-	-	S.PROB

Sample Computer Print-Out of MUF (0.50), Mode, Angle, Delay, Fraction of Days, Signal-to-Noise Ratio and Service Probability Using Described Prediction Model

Table 15.8b.

```
        3              DEC                    SSN=   75              MD  1.007
    LONDON              TO      MADRID                      AZIMUTHS      N.MILES
  52.37N -   1.18W          40.25N -   3.43W     188.1   6.5            733.1
H-DIPOLE  10H -12L    0DEG                                              ANT=  5DB
OFF AZIMUTH  64 DEG.     MIN. ANGLE=  0 DEG.     OFF AZIMUTH  47 DEG.
PWR= 30.00KW          3 MC/S MAN. NOISE = -148 DBW          REQ.S/N= 45DB
                        OPERATING FREQUENCIES                TIME AVAIL.=0.90
GMT  MUF     3    5    7    9   11   13   15   17   19   21   23   26   30
14  18.7
      1F   1F   2F   2F   1F   1F   1F   1F   1F   1F   1F    -    -    -   MODE
      17    6   31   29   14   14   14   14   15   18   18    -    -    -   ANGLE
      54   51   59   58   53   53   53   53   53   54   54    -    -    -   DELAY
     .50  .99  .99  .99  .99  .99  .99  .94  .76  .44  .16    -    -    -   F.DAYS
      85    0   49   61   72   76   79   82   84   87   87    -    -    -   S/N..DB
     .50  .00  .21  .91  .99  .99  .99  .94  .76  .44  .16    -    -    -   S.PROB

16  17.0
      1F   3F   2F   1F   1F   1F   1F   1F   1F   1F    -    -    -    -   MODE
      18   42   29   14   14   14   15   16   18   18    -    -    -    -   ANGLE
      54   68   58   53   53   53   53   53   54   54    -    -    -    -   DELAY
     .50  .99  .99  .99  .99  .99  .97  .82  .49  .17    -    -    -    -   F.DAYS
      85   39   61   71   75   78   81   83   85   87    -    -    -    -   S/N..DB
     .50  .00  .92  .99  .99  .99  .96  .82  .49  .17    -    -    -    -   S.PROB

18  11.8
      1F   1F   1F   1F   1F   1F   1F   1F    -    -    -    -    -    -   MODE
      20   15   15   15   16   18   20   20    -    -    -    -    -    -   ANGLE
      55   53   53   53   53   54   55   55    -    -    -    -    -    -   DELAY
     .50  .99  .99  .99  .91  .65  .32  .11    -    -    -    -    -    -   F.DAYS
      83   60   68   75   79   81   84   85    -    -    -    -    -    -   S/N..DB
     .50  .98  .99  .99  .91  .64  .32  .11    -    -    -    -    -    -   S.PROB

20   8.6
      1F   1F   1F   1F   1F   1F    -    -    -    -    -    -    -    -   MODE
      22   17   17   18   22   22    -    -    -    -    -    -    -    -   ANGLE
      56   54   54   54   56   56    -    -    -    -    -    -    -    -   DELAY
     .50  .99  .99  .86  .42  .11    -    -    -    -    -    -    -    -   F.DAYS
      80   61   70   76   81   82    -    -    -    -    -    -    -    -   S/N..DB
     .50  .85  .99  .86  .42  .11    -    -    -    -    -    -    -    -   S.PROB

22   7.4
      1F   1F   1F   1F   1F    -    -    -    -    -    -    -    -    -   MODE
      24   19   20   23   24    -    -    -    -    -    -    -    -    -   ANGLE
      57   54   55   56   57    -    -    -    -    -    -    -    -    -   DELAY
     .50  .99  .99  .65  .17    -    -    -    -    -    -    -    -    -   F.DAYS
      79   64   72   78   82    -    -    -    -    -    -    -    -    -   S/N..DB
     .50  .94  .99  .65  .17    -    -    -    -    -    -    -    -    -   S.PROB

24   7.0
      1F   1F   1F   1F   1F    -    -    -    -    -    -    -    -    -   MODE
      25   20   21   25   25    -    -    -    -    -    -    -    -    -   ANGLE
      57   55   55   58   58    -    -    -    -    -    -    -    -    -   DELAY
     .50  .99  .99  .49  .10    -    -    -    -    -    -    -    -    -   F.DAYS
      79   64   72   80   82    -    -    -    -    -    -    -    -    -   S/N..DB
     .50  .91  .98  .49  .10    -    -    -    -    -    -    -    -    -   S.PROB
```

Sample Computer Print-Out of MUF (0.50), Mode, Angle, Delay, Fraction of Days, Signal-to-Noise Ratio and Service Probability Using Described Prediction Model

16. Conclusions

16.1. Long Term Predictions

World-wide prediction of the necessary ionospheric and geophysical parameters is not considered to be available currently in sufficient detail to merit sophisticated ray tracing solution to typical problems in the long term prediction of the performance of ionospheric telecommunications circuits. The philosophy of basing high frequency predictions on the equivalence theorem, secant law, and typical electron density profiles generated from available ionospheric predictions is generally superior to simple ray path geometry between the earth and concentric ionospheric shells using the classical control point methods.

The empirical relationships included in this report should be considered as interim pending the development of more refined relationships by basic researchers. It is, therefore, apparent that more confidence should be placed in relative values produced by prediction methods such as the one described than in the absolute magnitudes of these predictions.

Caution should always be taken when using values produced by any prediction routine based on morphology of prediction parameters. The predictions are considered to be especially useful for long term plannin such as circuit design, siting, antenna considerations, and frequenc assignments. Additional work on the correlation of past circuit performance with "numerically" mapped parameters scaled from vertical ionograms on a world-wide basis is considered essential to further improvement of long-term predictions.

As the correlation between ionospheric parameters and circuit performance becomes better established, and as the ability to predict ionospheric characteristics in greater detail becomes available (e.g., through the use of topside sounding), it may prove useful to have prediction methods at several levels of sophistication, the choice depending upon the

knowledge of the circuit parameters involved, the importance of the communication link and the funds available to make the predictions.

16.2. Short Term Predictions

For established circuits with an operating history, it is often advantageous to combine operational experience with predictions of the type described in this report to optimize hour-to-hour frequency scheduling, e.g., if frequencies begin to fail earlier than normal or if the available signal-to-noise ratio is lower than normal, the prediction may be used to anticipate if this trend is likely to continue. It may also prove useful to monitor selected frequencies on nearby circuits to establish the time these frequencies become available, the available signal-to-noise ratio, etc. A comparison between these observations and the corresponding predictions may yield data to adjust the long term predictions for the circuit of interest. This approach is especially recommended where operational history of the circuit of interest is not available. For high priority operations, the use of auxiliary propagation path monitors such as oblique ionospheric sounders can be used to estimate the useful frequency limits and the trends established from the long term predictions. In such applications, it may prove useful to have predictions made for both the sounder circuit and the operational circuit to assist in the translation of the sounder information to expected trends on the operating circuit, e.g., the useful frequency range on the sounder may differ from that of the operational circuit due to differences in transmitter power, receiver sensitivity, antenna systems, etc. Predictions for both the sounder path and the operational path are expected to be especially desirable if it is necessary to translate oblique ionosonde data to operating circuits with paths differing from that of the sounder.

For particularly difficult communication paths, it might prove useful to prepare predictions for various solar activity levels and

attempt an estimate of the appropriate solar activity level on a given day. It may be possible to further refine the long range predictions by assigning different levels of effective solar activity to the different ionospheric regions, e.g., E and F2 to produce a family of predictions from which to make selections on given days.

17. Recommendations

The prediction method outlined in this report should be extensively compared with the observed performance of high frequency sky-wave communication circuits to establish areas where modification or extension of the prediction method is required. It is anticipated that the following areas may merit particular attention.

1. Nighttime propagation losses. Limited observations indicate seasonal and solar activity variations in the nighttime fields. The ability to predict these variations may be closely associated with predictions of ionization levels in the lower ionospheric regions, e.g., nighttime D and E region ionization including sporadic E.

2. Atmospheric noise levels for directive antennas. Current atmospheric noise levels are based on observations made with vertically polarized and essentially omnidirectional antennas. Adjustments for directive antennas may require a translation of current noise maps into noise source maps and the use of propagation predictions to anticipate atmospheric noise levels when directive antennas are used. This translation to noise sources could yield a badly needed solar activity dependence of the atmospheric noise levels which could be especially important at the higher frequencies.

3. Correlation coefficients between the several variables used in the prediction method. Correlation coefficients between signal levels and noise levels are especially needed, but other correlation coefficients could also materially add to the prediction method, e.g., sporadic E and F2 critical frequencies, F2 critical frequencies and noise, etc.

4. Short term correlation coefficients of system loss and likelihood of propagation as a function of frequency separation. A typical problem is the expected overall performance of a given complement of frequencies or the relative value of various frequencies in a given complement.

5. Practical antenna patterns at very low vertical angles. Terrain and atmosphere may be important factors in the space wave radiation of antennas at very low angles. Low angle paths are often the only possible paths. Practical estimates of antenna gain at these low angles could improve predictions.

6. Ground reflection losses. Although ground reflection losses are not normally a major factor in system loss calculations, the problem of multiple hop propagation when the ground reflection involves extreme terrain conditions such as tropical rain forest, deep arctic ice, or mountains, could merit further investigation. Side scatter from the earth's surface is part of this problem.

7. Ionospheric scatter losses. Ionospheric scatter may be important on certain paths when regular ionospheric reflection no longer takes place. The combination of ionospheric scatter and sporadic-E predictions to establish a floor in system loss predictions is a possible approach.

8. Ground wave and troposcatter losses. Loss estimates for use in calculations of transmitter and receiver site separation and multipath between ground and sky waves would be a useful addition to computer routine.

9. Improved circuit performance criteria. Performance is now estimated as a function of available signal-to-noise ratio. Although available signal-to-noise is a basic criteria, other factors such as multipath and doppler frequency spreads may be very significant especially for high data rate systems. Comparisons between multipath predictions

and circuit performance, and the development of required signal-to-noise ratios both as a function of multipath and type of interfering noise could be significant.

10. Daily predictions. The prediction method of this report is based on monthly median ionospheric predictions and system losses and the expected variation about these values within the month. The month is an arbitrary time increment, and the possibility of predictions continuous in time could merit investigation.

The development of D, E and F2-region predictions on this basis could be a first step. A parallel effort could be the development of semiempirical loss predictions from daily observed values in lieu of the monthly median observed values.

11. Path geometry. All basic inputs to estimating path geometry require improvement, e.g., F2 critical frequency, F2 heights, regular E criticals, sporadic E, F1 critical frequency and heights, plus other appropriate information to describe the height profile of ionization. Ray paths based on average ionospheric characteristics could be compared with more sophisticated ray tracing methods where ionospheric characteristics are known in detail, e.g., along the path of the topside sounder, to determine what adjustments would be profitable.

12. Extension to lower frequencies. Current methods have a lower limit of 3 MHz. An extension to lower frequencies including a computer program for the medium frequency band is desirable.

13. Inclusion of path antenna gain (G_p) in lieu of the obvious approximation ($G_t + G_r$) for G_p. [Norton 1959].

18. References

Al'pert, Ya. L. (1960), Radio wave propagation and the ionosphere (Authorized translation from the Russian by Consultants Bureau Enterprises, Inc., New York, New York).

Appleton, E. V., and W. J. G. Beynon (January 1947), The application of ionospheric data to radio communication problems, Part II, Proc. Phys. Soc. 59, 58-76.

Barsis, A. P., K. A. Norton, P. L. Rice and P. H. Elder (August 1961), Performance predictions for single tropospheric communication links and for several links in tandem, NBS Technical Note 102, U. S. Department of Commerce (U. S. Government Printing Office, Washington, D. C.).

Bibl, K. (1950), Le parcous d'un rayon dans une couche ionospherique courbes, Rev. Sci. 88, 27-29.

CCIR (1964), World distribution and characteristics of atmospheric radio noise, Report 322, Document of the Xth Plenary Assembly, Geneva, 1963 (International Telecommunication Union).

Cottony, H. V., and J. R. Johler (September 1952), Cosmic radio noise intensities in the VHF band, Proc. I.R.E. 40, No. 9, 1054-1060.

Crichlow, W. Q., and A. D. Spaulding (1965), (private communication).

Davies, K. (April 1965), Ionospheric radio propagation, NBS Monograph 80, U. S. Department of Commerce, (U. S. Government Printing Office, Washington, D. C.).

Davis, R. M., Jr., and Nancy L. Groome (1964), Variations of the 3000-km MUF in time and space (private communication).

Davis, R. M., Jr., and Nancy L. Groome (1965), The effect of auroral zone absorption on high frequency system loss, (private communication).

Haydon, G. W., and D. L. Lucas (1966), Technical considerations in the selection of optimum frequencies for high frequency sky-wave communication services, ESSA Monograph (to be published).

Jones, W. B., and R. M. Gallet (July-August 1962a), The representation of diurnal and geographic variations of ionospheric data by numerical methods, J. Res. NBS 66D (Radio Propagation), No. 4, 419-438. The same paper appears in English, French and Spanish in Telecommunication Journal 29, No. 5, 129-149 (May 1962b).

Jones, William B., Ronald P. Graham and Margo Leftin (May 1966), Advances in ionospheric mapping by numerical methods, NBS Technical Note 337, U. S. Department of Commerce, (U. S. Government Printing Office, Washington, D. C.).

Kelso, J. M. (1964), Radio ray propagation in the ionosphere, (McGraw-Hill Book Co., New York, N. Y.).

Knecht, R. W. (Summer 1962), The disturbed ionosphere, Lecture No. 24, NBS Radio Propagation Course.

Kobayashi, T. (November 1961), Transmission curves for the curved ionosphere, J. Radio Res. Labs. Japan 8, No. 40, 395-411.

Laitinen, P. O. (October 1957), Linear communication antennas, Technical Report No. 7, revised, U. S. Signal Radio Propagation Agency, Fort Monmouth, New Jersey.

Laitinen, P. O., and G. W. Haydon (October 1962), Analysis and prediction of sky-wave field intensities in the high frequency band, Technical Report No. 9, Revised (RPU 203), U. S. Army Signal Radio Propagation Agency, Fort Monmouth, New Jersey.

Lucas, D. L., and J. D. Harper, Jr. (July 6, 1965), A numerical representation of CCIR Report 322 high frequency (3-30 Mc/s) atmospheric radio noise data, NBS Technical Note 318, U. S. Department of Commerce, (U. S. Government Printing Office, Washington, D. C.).

Lucas, D. L., and O. D. Remmler (1966), Charts for estimating the ratio of the height of maximum ionization of the F2-region to its parabolic semithickness, (to be published).

Mitra, S. K. (1952). The upper atmosphere, 2nd ed. (The Asiatic Society, Calcutta).

Norton, K. A. (June 1959) Transmission loss in radio propagation, NBS Technical Note 12, U. S. Department of Commerce (U. S. Government Printing Office, Washington, D. C.).

Norton, K. A. (April 1962), Efficient use of the radio spectrum, NBS Technical Note 158, U. S. Department of Commerce (U. S. Government Printing Office, Washington, D. C.).

Ostrow, S. M. (December 1962), Handbook for CRPL ionospheric predictions based on numerical methods of mapping, NBS Handbook 90, U. S. Department of Commerce (U. S. Government Printing Office).

Ramo, S., and J. R. Whinnery (1960), Fields and waves in modern radio, (John Wiley and Sons, Inc., New York, New York).

Rawer, K. (1948), Optique geometrique de l'ionosphere, Rev. Scientifique 86, 585-600.

Rawer, K. (August 19, 1950), Geometrical optics of ionospheric propagation, Nature 166, No. 4216, 316.

Rawer, K. (1960), Radio propagation between a space vehicle and the earth in the presence of the ionosphere, in Space Research, Proceedings of the First International Space Science Symposium, Nice, January 11-16, 1960. Edited by H. K. Kallman Bijl., 245-271 (North-Holland Publishing Co., Amsterdam).

Remmler, O. D. (1965), Private Communication.

Rice, P. L., A. G. Longley, K. A. Norton and A. P. Barsis (May 1965) Transmission loss predictions for tropospheric communication circuits, NBS Technical Note 101, Two vols., U. S. Department of Commerce (U. S. Government Printing Office, Washington, D. C.)

Schelkunoff, S. A., and H. T. Friis (1952), Antennas--theory and practice (John Wiley and Sons, Inc., New York, New York).

Shimazaki, T. (January 1955), World-wide daily variations in the height of the maximum electron density of the ionospheric F2 layer, J. Radio Res. Labs., Japan, 2, No. 7, 85-97.

Smith, N. (May 1939), The relation of radio sky-wave transmission to ionospheric measurements, Proc. I. R. E. 27, No. 5, 332-347.

Spaulding, A. D. (1965), Private communication.

Wait, J. R., and A. M. Conda (October 1958), Pattern of an antenna on a curved glossy surface, I. R. E. Trans. on Antennas & Propagation, AP-6, No. 4, 348-359.

Wakai, N. (May 1961), Non-deviative absorption at night, J. Radio Res. Labs. 8, No. 37, 213-218.

Waterman, A. T., Jr. (March 1952), Ray theory applied to a spherical ionosphere, Technical Report No. 142, Cruft Laboratory, Harvard University, Cambridge, Massachusetts.

Watts, J. M., and J. N. Brown (March 1954), Some results of sweep-frequency investigation in the low frequency band, J. Geophys. Res. 59, No. 1, 71-86.

Williams, R. D., and R. D. Egan (1963), Elmendorf-McClellan ionospheric sounder program, Final Report, Granger Associates.

Woyk, E. (Chvojkova) (1959), The refraction of radio waves by a spherical ionized layer, J. Atmospheric and Terrest. Phys. 16, 124-135.

Wright, J. W., and R. E. McDuffie (July 1960), The relation of H_{max} F2 to M(3000)F2 and H_p F2, J. Radio Res. Labs., Japan, 7, No. 32, 409-420.

Wright, J. W., and A. K. Paul (October 1, 1963), Some results of the new method for obtaining ionospheric N_h profiles and their bearing on the structure of the lower F-region, Journal of Geophysical Research 68, No. 9.

Wright, J. W., L. R. Wescott, and D. J. Brown (1960-1963), Mean electron density variations of the quiet ionosphere, NBS Technical Notes 40-1 through 40-13, U. S. Department of Commerce, (U. S. Government Printing Office, Washington, D. C.).

19. Bibliography

Appleton, E. V. (1947), The investigation and forecasting of ionospheric conditions, J. I. E. E., 94, Part IIIA, No. 11, 186-199.

Appleton, E. V., and W. J. G. Beynon (July 1940), The application of ionospheric data to radio communication problems, Part I, Proc. Phys. Soc. 52, 518-533.

Appleton, E. V., and W. J. G. Beynon (July 1955), Radio communication on frequencies exceeding predicted values, Proc. I. E. E. 100, Part III.

Bibl, K., A. Paul, and K. Rawer (December 1961), Absorption in the D and E regions and its time variation, J. Atmospheric and Terrest. Phys. 23, 244-259.

Bibl, K., and K. Rawer (1952), Les contributions des regions D et E dans les mesures de l'absorption ionospherique, J. Atmospheric and Terrest. Phys 2, No. 1, 51-65.

Bibl, K., K. Rawer, and E. Theissen (January 26, 1952), An improved method for the calculation of the field-strength of waves reflected by the ionosphere, Nature 169, No. 4291, 147-148.

Booker, H. G., and S. L. Seaton (January 1940) Relation between actual and virtual ionospheric heights, Phy. Rev. 57, No. 2, 87-94.

Bremmer, H. (1949), Terrestrial Radio Waves (Elsevier Publishing Co., New York, New York).

Central Radio Propagation Laboratory Ionospheric Predictions (Monthly-three months in advance), NBS, U. S. Department of Commerce, (U. S. Government Printing Office, Washington, D. C.).

Crichlow, W. Q., D. F. Smith, R. N. Morton, and W. R. Corliss (1955) Worldwide radio noise levels expected in the frequency band 10 kilocycles to 100 megacycles, NBS Circular 557, U. S. Department of Commerce (Government Printing Office, Washington, D. C.).

Crichlow, W. Q., and A. D. Spaulding (1965), (private communication).

Chrisman, Mary E., and Charles O. Stearns (March 1962), Computation and plotting of rhombic antenna gains using electronic digital computers, (private communication).

Davies, K. (June 1958), Some studies of the transmission of high frequency radio waves via the ionosphere at oblique incidence, Air Force Cambridge Research Center, Scientific Report AF 2066/2.

Duncan, D. B., and J. F. Kenny (1946), On the solution of the normal equation and related topics, (Edwards Bros., Inc., Ann Arbor, Michigan).

Haydon, G. W. (Summer 1962), Ionospheric predictions and disturbance forecasts, Lecture No. 47, NBS Radio Propagation Course.

Jones, W. B., and R. M. Gallet (November-December, 1962), Methods for applying numerical maps of ionospheric characteristics, J. Res. NBS 66D, No. 6, 649-662.

Jordan, E. C. (1950), Electromagnetic waves and radiating systems, (Prentice-Hall, New York, New York).

JTAC (1964), Radio spectrum utilization a program for the administration of the radio spectrum. A report of the Joint Technical Advisory Committee of the Institute of Electrical and Electronics Engineers and Electronic Industries Association (Copyright 1965 by I. E. E. E.).

McCracken, D. D. (April 1962), A guide to Fortran programming (Wiley and Sons, New York, New York).

Manning, L. A. (November 1947), The determination of ionospheric electron distribution, Proc. I. R. E. 35, No. 11, 1203-1208.

Manning, L. A. (June 1949), The reliability of ionospheric height determination, Proc. I. R. E. 37, No. 6, 599-603.

NBS Circular No. 462 (June 1948), Ionospheric radio propagation, U. S. Department of Commerce, (U. S. Government Printing Office).

Ostrow, S. M., and M. PoKempner (December 1952), The difference in the relationship between ionospheric critical frequencies and sunspot number for different sunspot cycles, J. Geophys. Res. 57, No. 4, 473-480.

Phillips, K. L. (October 1961), Theory of radiation patterns and gains for horizontal rhombic antennas adapted to electronic computers, (private communication).

Piggott, W. R. (March 1953), The reflection and absorption of radio waves in the ionosphere, Proc. I. E. E. 100, Part III, No. 64, 61-72.

Rawer, K. (November 1952), Calculation of sky-wave field strength, Wireless Engineer 29, 287-301.

Rawer, K. (1957), The ionosphere (Frederick Ungar Publishing Co., New York, New York).

Rawer, K. (1958), Intercomparison of different calculation methods of the sky-wave field-strength, in Electromagnetic Wave Propagation, ed. by Desirant and Michiels, 647-659 (Academic Press, London and New York, 1960).

Rawer, K. (1961), Propagation of decameter waves (HF band). Chapter 11 in Meteorological and Astronomical Influences on Radio Wave Propagation, Proceedings of NATO Advanced Study Institute, Corfu 1961, Edited by B. Landmark, pp. 221-250, MacMillan, New York, 1963.

Silberstein, R. (August 1952), Interpretation of high-frequency C-W field-intensity records with the aid of simultaneous pulse data, Proc. I. R. E. 40 No. 8, 974-976.

Stratton, J. A. (1941), Electromagnetic theory, 1st ed. (McGraw-Hill Book Co., New York, New York.).

Terman, F. E. (1943), Radio engineer's handbook, (McGraw-Hill Book Co., New York, New York).

U. S. Army Signal Radio Propagation Agency (May 1958), Radiation from antennas in the 2 to 30 megacycle band, Technical Report No. 2.

Utlaut, W. F. (March-April 1961), Effect of antenna radiation angles upon HF radio signals propagated over long distances, J. Res. NBS 65D (Radio Propagation), No. 2, 167-174.

Watson, G. N. (1922), Theory of Bessel Functions, (Cambridge University Press, London, England).

Wieder, B. (1955), Some results of a sweep-frequency propagation experiment over a 1100 km east-west path, J. Geophys. Res. 60, 395.

Wilkins, A. F. (December 1960), H. F. propagation - its present and future use for communication purposes, J. Brit. I. R. E. 20, 939-951.

Wilkins, A. F., and C. M. Minnis (May 1951), Comparison of ionospheric radio transmission forecasts with practical results, Proc. I. E. E. 98, Part III, No. 53.

Wilkins, A. F., and C. M. Minnis (May 1952), Comparison of ionospheric radio transmission forecasts with practical results, Proc. I. E. E. 99, Part III, No. 59.

Woyk, E. (March 1965), Analytical formulas for radio paths in spherically stratified ionospheres, Radio Sci. J. Res. NBS 69D, No. 3, 453-458.

Wright, J. W. (1964), Private communication.

Wright, J. W., and R. W. Knecht (Summer 1962), The quiet ionosphere, Lecture No. 23, NBS Radio Propagation Course.

Appendix A. Theoretical Antenna Power Gain Equations

1. Horizontal Rhombic Antenna

Combining (8.21), (8.22) and (8.23) and assuming the antenna sufficiently high for R = 600 ohms, the gain, g, of a horizontal rhombic is given by

$$g = 3.2\left\{\frac{\cos\alpha \sin\left(\frac{k\ell}{2}\cdot U_1\right)\cdot \sin\left(\frac{k\ell}{2}\cdot U_2\right)}{U_1\cdot U_2}\right\}^2 \qquad \text{(A-1)}$$

$$\cdot \left\{K_v \sin^2\phi \sin^2\Delta + K_H(\cos\phi - \cos\Delta\cdot\sin\alpha)^2\right\},$$

where ℓ is the leg length of the rhombic in meters

α is half the obtuse angle of the rhombic

ϕ is the azimuthal angle of arrival measured counter-clockwise from major axis of the rhombic

$U_1 = 1 - \cos\Delta\cdot\sin(\alpha+\phi)$

$U_2 = 1 - \cos\Delta\cdot\sin(\alpha-\phi)$.

2. Horizontal Dipole Antenna

Using the same approach as followed for the horizontal rhombic antenna the gain, g, of a horizontal dipole of arbitrary length, ℓ, is given by

$$g = \frac{120}{R}\left\{\frac{\cos\left(\frac{k\ell}{2}\cdot\sin\phi\cdot\cos\Delta\right) - \cos\frac{k\ell}{2}}{1-\sin^2\phi\cos^2\Delta}\right\}^2 \qquad \text{(A-2)}$$

$$\cdot \left\{K_v\cdot\sin^2\phi\sin^2\Delta + K_H\cdot\cos^2\phi\right\}$$

where

$$R = 30 \left\{ \left(1 - \cot^2 \frac{k\ell}{2}\right) \mathrm{Cin}(2k\ell) + 4 \cot^2 \frac{k\ell}{2} \mathrm{Cin}(k\ell) \right. \tag{A-3}$$

$$\left. + 2 \cdot \cot \frac{k\ell}{2} \left[\mathrm{Si}(2k\ell) - 2\,\mathrm{Si}(k\ell) \right] \right\},$$

where

$$\mathrm{Cin}(x) = 0.577 + \ln(x) - \mathrm{Ci}(x)$$

$$\mathrm{Ci}(x) = \int_{\infty}^{x} \frac{\cos u}{u}\, du$$

$$\mathrm{Si}(x) = \int_{0}^{x} \frac{\sin u}{u}\, du .$$

3. Ground Based Vertical Antenna

For the vertical antenna we will define P_r in terms of the electric field, E_θ, and the magnetic field, H_ϕ, by

$$P_r = \tfrac{1}{2} |E_\theta| \cdot |H_\phi|, \tag{A-4}$$

where E_θ, as given by Laitinen [1957], is

$$E_\theta = \eta H_\phi = j \frac{30 I (\cos(k\ell \sin\Delta) - \cos k\ell)}{r \cos\Delta \cos b'} \tag{A-5}$$

$$\cdot \left\{ K_v^2 + 1 + 2K_v \cos(\psi_v - 2b') \right\}^{\frac{1}{2}},$$

which implies

$$g = \frac{30}{R} \left\{ \frac{\cos(k\ell \sin\Delta) - \cos(k\ell)}{\cos\Delta \cos b'} \right\}^2 \cdot H_{vh}, \tag{A-6}$$

where

$$K_{vh} = \left\{ K_v^2 + 1 + K_v^2 \cos \left[\psi_v - 2b' \right] \right\} \qquad \text{(A-7)}$$

$$R = 30 \left\{ -0.5 \cos [k\ell] \, \mathrm{Cin} [2k\ell] + (1 + \cos [k\ell]) \, \mathrm{Cin} [k\ell] + \sin [k\ell] \left(0.5 \, \mathrm{Si} [2k\ell] - \mathrm{Si} [k\ell] \right) \right\}$$

$$b' = \tan^{-1} \left\{ \frac{\sin (k\ell \sin \Delta) - \sin \Delta \sin k\ell}{\cos (k\ell \sin \Delta) - \cos k\ell} \right\} , \qquad \text{(A-8)}$$

where ℓ is the height of the vertical antenna in meters.

4. Inverted L Antenna

For the inverted L antenna:

$$g = \frac{30}{R} \left\{ \left[2c \, K_H^{\frac{1}{2}} \cos \phi \right]^2 + \left[\frac{a \, K_v^{\frac{1}{2}}}{\cos b' \cos \Delta} \right]^2 \right\} \qquad \text{(A-9)}$$

$b' = \tan^{-1} \left[\frac{b}{a} \right]$

$a = \cos [khv] \cos [k\ell] - v \sin [khv] \sin [k\ell] - \cos [k(h + \ell)]$

$b = v \cos [khv] \sin [k\ell] + \sin [khv] \cos [k\ell] - v \sin [k(h + \ell)]$

$c = \frac{1}{1 - u^2} \left\{ 1 - \cos [k\ell u] \cos [k\ell] - u \sin [k\ell u] \sin [k\ell] - 0.5 \cdot \sin^2 [k\ell] \cdot (1 - u^2) \right\}$

$u = \cos \Delta \sin \phi$

$v = \sin \Delta$

h = length of vertical portion of inverted L

ℓ = length of horizontal portion of inverted L

$$R = 60\{\ln[k\ell] - Ci[k\ell] - \frac{\sin[2k\ell]}{2k\ell} - 0.423\}$$
$$+ 30\{-0.5\cos[kh]\,Cin[2kh] + (1+\cos[kh])\,Cin[kh]$$
$$+ \sin[kh]\,(0.5\,Si[2kh] - Si[kh])\}$$

ϕ = 0 is broadside to the horizontal portion of the inverted L.

The reflection factors K_H and K_v are defined in (8.23b) and (8.23a) respectively. The vertically polarized field of the horizontal portion of the inverted L is omitted in (A-9). Its combination with the vertical portion of the inverted L to obtain the component N_θ of the radiation vector is unweildy. This is not a serious omission since its contribution is small near $\phi = 0$.

5. Sloping V Antenna

For sloping V antenna:

$$g = .05\Big\{\cos^2\Delta'\Big\{\Big[\frac{Y_2\cdot Z_1 - Y_1\cdot Z_2}{U_1\cdot U_2} - \frac{K_H}{U_3\cdot U_4}\Big(Y_4(W_1\cdot Z_3 + W_2\cdot V_3)$$
$$- Y_3(W_1\cdot Z_4 + W_2\cdot V_4)\Big)\Big]^2 + \Big[-\frac{Y_2\cdot V_1 + Y_1\cdot V_2}{U_1\cdot U_2} - \frac{K_H}{U_3\ U_4}$$
$$\Big(Y_4(W_2\cdot Z_3 - W_1\cdot V_3) - Y_3(W_2\cdot Z_4 - W_1\cdot V_4)\Big)\Big]^2\Big\} + \Big[\frac{UC_{27}\cdot Z_1}{U_1\cdot U_2}$$
$$- \frac{UC_{18}\cdot Z_2}{U_1\cdot U_2} - \frac{K}{U_3\cdot U_4}\Big(W_3(UC_{45}\cdot Z_3 - UC_{36}\cdot Z_4) + W_4(UC_{45}\cdot V_3$$
$$- UC_{36}\cdot V_4)\Big)\Big]^2 + \Big[\frac{-UC_{27}\cdot V_1 + UC_{18}\cdot V_2}{U_1\cdot U_2} - \frac{K_v}{U_3\cdot U_4}$$
$$\Big(W_3(-UC_{45}\cdot V_3 + UC_{36}\cdot V_4) + W_4(UC_{45}\cdot Z_3 - UC_{36}\cdot Z_4)\Big)\Big]^2\Big\}, \quad \text{(A-10)}$$

where

$U_1 = 1 - \cos\Psi_1$ $\qquad$ $U_3 = 1 - \cos\Psi_3$

$U_2 = 1 - \cos \Psi_2$ $\quad$ $U_4 = 1 - \cos \Psi_4$

$UC_{18} = U_1 \cdot \cos \Psi_8$ $\quad$ $UC_{36} = U_3 \cdot \cos \Psi_6$

$UC_{27} = U_2 \cdot \cos \Psi_7$ $\quad$ $UC_{45} = U_4 \cdot \cos \Psi_5$

$$\cos \Psi_1 = \sin \Delta \sin \Delta' + \cos \Delta \cos \Delta' \cos (\phi - \alpha)$$
$$\cos \Psi_2 = \sin \Delta \sin \Delta' + \cos \Delta \cos \Delta' \cos (\phi + \alpha)$$
$$\cos \Psi_3 = -\sin \Delta \sin \Delta' + \cos \Delta \cos \Delta' \cos (\phi - \alpha)$$
$$\cos \Psi_4 = -\sin \Delta \sin \Delta' + \cos \Delta \cos \Delta' \cos (\phi + \alpha)$$
$$\cos \Psi_5 = \cos \Delta \sin \Delta' + \sin \Delta \cos \Delta' \cos (\phi - \alpha)$$
$$\cos \Psi_6 = \cos \Delta \sin \Delta' + \sin \Delta \cos \Delta' \cos (\phi + \alpha)$$
$$\cos \Psi_7 = -\cos \Delta \sin \Delta' + \sin \Delta \cos \Delta' \cos (\phi - \alpha)$$
$$\cos \Psi_8 = -\cos \Delta \sin \Delta' + \sin \Delta \cos \Delta' \cos (\phi + \alpha)$$

$Z_1 = \cos (k\ell U_1) - 1$ $\quad$ $Z_3 = \cos (k\ell U_3) - 1$

$Z_2 = \cos (k\ell U_2) - 1$ $\quad$ $Z_4 = \cos (k\ell U_4) - 1$

$V_1 = \sin (k\ell U_1)$ $\quad$ $V_3 = \sin (k\ell U_3)$

$V_2 = \sin (k\ell U_2)$ $\quad$ $V_4 = \sin (k\ell U_4)$

$Y_1 = U_1 \cdot \sin (\phi + \alpha)$ $\quad$ $Y_3 = U_3 \cdot \sin (\phi + \alpha)$

$Y_2 = U_2 \cdot \sin (\phi - \alpha)$ $\quad$ $Y_4 = U_4 \cdot \sin (\phi - \alpha)$

$W_1 = \cos (\Psi_H - 2kH \sin \Delta)$ $\quad$ $W_3 = \cos (\Psi_v - 2kH \sin \Delta)$

$W_2 = \sin (\Psi_H - 2kH \sin \Delta)$ $\quad$ $W_4 = \sin (\Psi_v - 2kH \sin \Delta)$

H = height of feed end of sloping wire above ground.

HT = height of terminated end of sloping wire above ground

$$\Delta' = \sin^{-1} \left[\frac{HT - H}{\ell} \right]$$ valid for negative or positive slope, Δ'

$$\alpha = \sin^{-1} \left[\frac{\sin \gamma}{\cos \Delta'} \right]$$ projection of γ, the half angle between the wires, onto the horizontal plane.

6. Curtain Arrays

$$g = \frac{960}{R} \left\{ \frac{\cos [\pi \ell \sin \phi \cos \Delta] - \cos [\pi \ell]}{1 - \sin^2 \phi \cos^2 \Delta} \right\}^2$$

$$\cdot \left\{ \epsilon + 2 \sum_{n=1}^{\frac{N-\epsilon}{2}} \cos \left[\frac{\pi D (2n - 1 + \epsilon)}{\lambda} \cos \Delta \sin \phi \right] \right\}^2$$

$$\cdot \left\{ \left| \sum_{m=1}^{M} \Big(\cos a - K_H \cos [a - \Psi_H] + i \{ \sin a + K_H \sin [a - \Psi_H] \} \Big) \right|^2 \right\} \cos^2 \phi + \left\{ \left| \sum_{m=1}^{M} \Big(\cos a - K_v \cos [a - \Psi_v] + i \{ \sin a + K_v \sin [a - \Psi_v] \} \Big) \right|^2 \sin^2 \phi \sin^2 \Delta \right\}$$

$$\cdot \sin^2 [KC \cos \phi \cos \Delta] , \qquad \text{(A-11)}$$

where $a = [E + (m - 1) F] k \sin \Delta$

E = height of 1st element above ground

F = vertical separation between horizontal dipoles

D = horizontal separation between feed points of horizontal dipoles

N = the number of bays in the array

M = the number of elements in each bay

C = distance to reflecting screen

ϵ = 0 for N even

1 for N odd

$R = r_1 + r_2 + \ldots + r_{M \cdot N}$

$$r_i = R_{i1} + R_{i2} + \ldots R_{ij} + \ldots R_{i\,M\cdot N}$$

R_{ij} = mutual resistance of the elements in the array and is given by

$$R_{ij} = -15 \cos [kh] (- 2 Ci A - 2 Ci A' + Ci B + Ci B' + Ci C + Ci C') + 15 \sin [kh] (2 Si A - Si A' - Si B + Si B' - Si C + Si C') \text{ ohms}$$

$$A = k \{ (d^2 + h^2)^{\frac{1}{2}} + h \}$$
$$A' = k \{ (d^2 + h^2)^{\frac{1}{2}} - h \}$$
$$B = k \{ (d^2 + (h - \ell)^2)^{\frac{1}{2}} + (h - \ell) \}$$
$$B' = k \{ (d^2 + (h - \ell)^2)^{\frac{1}{2}} - (h - \ell) \}$$
$$C = k \{ (d^2 + (h - \ell)^2)^{\frac{1}{2}} + (h + \ell) \}$$
$$C' = k \{ (d^2 + (h + \ell)^2)^{\frac{1}{2}} - (h + \ell) \},$$

where ℓ = length of antenna element

h = horizontal distance between the ith and jth elements

d = vertical distance between the ith and jth elements

R is given by (A-3).

7. Interlaced Horizontal Rhombics

The gain equation for two interlaced rhombic antennas such that they are fed end-fire is given by (A-1) where

$$K_{\substack{V \\ H}} = \left[1 + \cos X - K_{\substack{V \\ H}} \left\{ \cos Y_{\substack{V \\ H}} (1 + \cos Z) - \sin Y_{\substack{V \\ H}} \sin Z \right\} \right]^2$$

$$+ \left[- \sin X - K_{\substack{V \\ H}} \left\{ - \sin Y_{\substack{V \\ H}} (1 + \cos Z) - \cos Y_{\substack{V \\ H}} \sin Z \right\} \right]^2,$$

where

$$X = k \left[S - d \left\{ \sin \Delta \sin \Delta' + \cos \Delta \cos \Delta' \cos \phi \right\} \right]$$

$$Y_{\substack{v \\ H}} = \Psi_{\substack{v \\ H}} - 2\,kH \sin \Delta$$

$$Z = X - 2\,kh \sin \Delta$$

S = the horizontal displacement between feed points of the two rhombics in meters

h = the vertical displacement of the two rhombics in meters

H = the height of the lower rhombic in meters

$$d = (S^2 + h^2)^{\frac{1}{2}} .$$

Also replace the constant, 3.2, by 0.8.

8. Sloping Rhombic Antenna

For the sloping rhombic antenna:

$$g = .05 \left\{ \cos^2 \Delta' \left[\{X_1 W_1 - Y_1 K_H (\cos Z_1 W_2 - \sin Z_1 V_2)\}^2 \right.\right.$$

$$+ \left. \{X_1 V_1 - Y_1 K_H (\sin Z_1 W_2 + \cos Z_1 V_2)\}^2 \right]$$

$$+ \{X_2 W_1 - Y_2 K_v (\cos Z_2 W_2 - \sin Z_2 V_2)\}^2$$

$$+ \left. \{X_2 V_1 - Y_2 K_v (\sin Z_2 W_2 + \cos Z_2 V_2)\}^2 \right\} ,$$

where

$$X_1 = \frac{\sin [\phi + \alpha]}{u_1} - \frac{\sin [\phi - \alpha]}{u_2}$$

$$Y_1 = \frac{\sin[\phi + \alpha]}{u_4} - \frac{\sin[\phi - \alpha]}{u_3}$$

$$u_1 = 1 - \sin\Delta \sin\Delta' - \cos\Delta \cos\Delta' \cos(\phi + \alpha)$$

$$u_2 = 1 - \sin\Delta \sin\Delta' - \cos\Delta \cos\Delta' \cos(\phi - \alpha)$$

$$u_3 = 1 + \sin\Delta \sin\Delta' - \cos\Delta \cos\Delta' \cos(\phi - \alpha)$$

$$u_4 = 1 + \sin\Delta \sin\Delta' - \cos\Delta \cos\Delta' \cos(\phi + \alpha)$$

$$X_2 = \frac{\cos\Delta' \sin\Delta \cos(\phi+\alpha) - \sin\Delta' \cos\Delta}{u_1} - \frac{\cos\Delta' \sin\Delta \cos(\phi-\alpha) - \sin\Delta'\cos\Delta}{u_2}$$

$$Y_2 = \frac{\cos\Delta' \sin\Delta \cos(\phi+\alpha) + \sin\Delta' \cos\Delta}{u_4} - \frac{\cos\Delta' \sin\Delta \cos(\phi-\alpha) + \sin\Delta'\cos\Delta}{u_3}$$

$$Z_{12} = \Psi_H - 2kH \sin\Delta$$

$$W_{12} = 1 + \cos[k\ell(u_{13} + u_{24})] - \cos[k\ell u_{13}] - \cos[k\ell u_{24}]$$

$$V_{12} = -\sin[k\ell(u_{13} + u_{24})] + \sin[k\ell u_{13}] + \sin[k\ell u_{24}]$$

$$\Delta' = \sin^{-1}\left[\frac{HT - H}{2\ell}\right]$$

ϕ and α are the same as defined for the sloping V.

Appendix B. Tables of the Distribution of F2(3000) MUF

MUF EXCEEDED 0.10 AND 0.90 OF THE HOURS
(Ratio of MUF to Monthly Median)

Sunspot Number: High			No. Hemis: Jan., Feb., Nov., Dec.			
Season: Winter			So. Hemis: May, June, July, Aug.			
Geog. Lat.	LOCAL TIME					
(N or S)	00	04	08	12	16	20
			Upper Decile			
30°	1.36	1.27	1.41	1.42	1.40	1.43
70°	1.31	1.25	1.34	1.30	1.16	1.34
60°	1.26	1.23	1.24	1.18	1.11	1.26
50°	1.19	1.19	1.16	1.11	1.09	1.20
40°	1.15	1.14	1.13	1.09	1.09	1.14
30°	1.22	1.26	1.12	1.09	1.11	1.13
20°	1.32	1.35	1.12	1.12	1.14	1.20
10°	1.18	1.25	1.14	1.13	1.15	1.20
			Lower Decile			
80°	.62	.70	.74	.67	.64	.73
70°	.69	.74	.77	.72	.72	.78
60°	.77	.78	.81	.80	.79	.82
50°	.83	.80	.84	.87	.84	.86
40°	.86	.81	.87	.90	.87	.87
30°	.83	.76	.89	.90	.88	.86
20°	.78	.70	.89	.89	.89	.83
10°	.83	.76	.89	.90	.89	.84

Table B. 1

MUF EXCEEDED 0.10 AND 0.90 OF THE HOURS
(Ratio of MUF to Monthly Median)

Sunspot Number:	High					
Season:	Equinox			March, April, September October		
Geog. Lat. (N or S)	LOCAL TIME 00	04	08	12	16	20
			Upper Decile			
80°	1.46	1.37	1.35	1.40	1.38	1.46
70°	1.42	1.31	1.30	1.31	1.33	1.37
60°	1.30	1.25	1.27	1.24	1.25	1.24
50°	1.18	1.20	1.25	1.20	1.16	1.17
40°	1.15	1.16	1.17	1.16	1.12	1.14
30°	1.25	1.18	1.10	1.10	1.11	1.15
20°	1.31	1.32	1.11	1.11	1.12	1.20
10°	1.21	1.23	1.09	1.20	1.14	1.23
			Lower Decile			
80°	.66	.67	.75	.66	.70	.72
70°	.67	.71	.73	.70	.70	.72
60°	.69	.75	.71	.71	.71	.72
50°	.75	.78	.70	.72	.74	.73
40°	.79	.82	.75	.78	.80	.82
30°	.81	.82	.87	.87	.87	.86
20°	.81	.77	.89	.92	.90	.85
10°	.80	.79	.86	.90	.90	.82

Table B. 2

MUF EXCEEDED 0.10 AND 0.90 OF THE HOURS
(Ratio of MUF to Monthly Median)

Sunspot Number: High			No. Hemis: May, June, July, Aug.			
Season: Summer			So. Hemis: Jan., Feb., Nov., Dec.			
Geog. Lat.	LOCAL TIME					
(N or S)	00	04	08	12	16	20
			Upper Decile			
80°	1.30	1.27	1.17	1.15	1.23	1.24
70°	1.22	1.22	1.20	1.18	1.21	1.23
60°	1.16	1.18	1.26	1.21	1.19	1.21
50°	1.14	1.15	1.30	1.26	1.19	1.18
40°	1.14	1.14	1.30	1.27	1.19	1.16
30°	1.16	1.15	1.25	1.20	1.17	1.15
20°	1.21	1.22	1.18	1.15	1.18	1.19
10°	1.25	1.21	1.13	1.17	1.22	1.23
			Lower Decile			
80°	.73	.74	.82	.83	.79	.75
70°	.75	.75	77	.80	.80	.77
60°	.77	.76	.74	.77	.80	.80
50°	.79	.76	.73	.75	.80	.84
40°	.80	.76	.75	.75	.79	.84
30°	.81	.76	.82	.81	.79	.83
20°	.81	.77	.85	.86	.81	.80
10°	.80	.79	.86	.89	.85	.78

Table B.3

MUF EXCEEDED 0.10 AND 0.90 OF THE HOURS
(Ratio of MUF to Monthly Median)

Sunspot Number: Medium			No. Hemis: Jan., Feb., Nov., Dec.			
Season: Winter			So. Hemis: May, June, July, Aug.			
Geog. Lat. (N or S)	LOCAL TIME 00	04	08	12	16	20
			Upper Decile			
80°	1.45	1.39	1.44	1.40	1.33	1.45
70°	1.39	1.31	1.37	1.32	1.29	1.41
60°	1.33	1.24	1.25	1.21	1.22	1.33
50°	1.30	1.19	1.14	1.15	1.16	1.29
40°	1.27	1.17	1.12	1.14	1.14	1.28
30°	1.30	1.31	1.16	1.18	1.18	1.32
20°	1.33	1.38	1.17	1.22	1.26	1.40
10°	1.21	1.26	1.14	1.13	1.15	1.23
			Lower Decile			
80°	.76	.78	.68	.67	.62	.70
70°	.79	.81	.74	.70	.73	.73
60°	.82	.83	.79	.75	.80	.76
50°	.84	.82	.83	.81	.84	.78
40°	.83	.81	.85	.86	.86	.79
30°	.73	.76	.85	.85	.85	.78
20°	.74	.71	.85	.83	.82	.76
10°	.77	.69	.87	.86	.85	.78

Table B.4

MUF EXCEEDED 0.10 AND 0.90 OF THE HOURS
(Ratio of MUF to Monthly Median)

Sunspot Number: Medium Season: Equinox	March, April, September, October					
Geog. Lat. (N or S)	LOCAL TIME 00	04	08	12	16	20
	Upper Decile					
80°	1.45	1.31	1.27	1.28	1.30	1.47
70°	1.41	1.22	1.23	1.26	1.26	1.38
60°	1.35	1.17	1.20	1.23	1.18	1.29
50°	1.28	1.15	1.17	1.21	1.13	1.20
40°	1.22	1.16	1.16	1.18	1.12	1.17
30°	1.22	1.22	1.15	1.17	1.14	1.23
20°	1.32	1.30	1.13	1.15	1.17	1.37
10°	1.18	1.39	1.11	1.13	1.20	1.23
	Lower Decile					
80°	.64	.61	.73	.74	.74	.67
70°	.68	.71	.77	.74	.78	.70
60°	.70	.75	.80	.72	.78	.73
50°	.73	.77	.81	.74	.76	.75
40°	.75	.78	.82	.78	.76	.76
30°	.77	.76	.82	.83	.78	.72
20°	.75	.73	.84	.87	.81	.69
10°	.79	.68	.86	.89	.84	.80

Table B.5

MUF EXCEEDED 0.10 AND 0.90 OF THE HOURS
(Ratio of MUF to Monthly Median)

Sunspot Number: Medium Season: Summer			No. Hemis: May, June, July, Aug. So. Hemis: Jan., Feb., Nov., Dec.			
Geog. Lat. (N or S)	LOCAL TIME 00	04	08	12	16	20
			Upper Decile			
80°	1.27	1.23	1.20	1.18	1.25	1.23
70°	1.23	1.19	1.19	1.17	1.17	1.19
60°	1.20	1.18	1.19	1.17	1.14	1.17
50°	1.17	1.19	1.21	1.17	1.15	1.16
40°	1.17	1.22	1.23	1.18	1.17	1.17
30°	1.20	1.30	1.22	1.19	1.19	1.18
20°	1.26	1.38	1.17	1.23	1.23	1.28
10°	1.26	1.44	1.11	1.28	1.28	1.22
			Lower Decile			
80°	.82	.80	.82	.85	.80	.79
70°	.83	.82	.79	.82	.82	.82
60°	.83	.82	.77	.79	.82	.83
50°	.81	.81	.76	.77	.81	.82
40°	.78	.78	.75	.78	78	.78
30°	.77	.73	.75	.79	.77	.74
20°	.77	.69	.78	.82	.78	.73
10°	.79	.63	.84	.85	.81	.77

Table B.6

MUF EXCEEDED 0.10 AND 0.90 OF THE HOURS

(Ratio of MUF to Monthly Median)

Sunspot Number: Low			No. Hemis: Jan. Feb., Nov., Dec.			
Season: Winter			So. Hemis: May, June, July, Aug.			
Geog. Lat.	LOCAL TIME					
(N or S)	00	04	08	12	16	20
			Upper Decile			
80°	1.44	1.34	1.45	1.32	1.33	1.40
70°	1.37	1.29	1.38	1.23	1.24	1.35
60°	1.30	1.24	1.27	1.15	1.17	1.30
50°	1.25	1.21	1.16	1.12	1.12	1.25
40°	1.23	1.20	1.13	1.11	1.11	1.23
30°	1.28	1.30	1.15	1.17	1.15	1.28
20°	1.34	1.37	1.19	1.20	1.24	1.32
10°	1.27	1.38	1.18	1.15	1.14	1.20
			Lower Decile			
80°	.60	.65	.69	.72	.68	.67
70°	.68	.71	.75	.76	.75	.70
60°	.74	.76	.80	.80	.82	.73
50°	.79	.78	.83	.85	.84	.76
40°	.81	.79	.85	.87	.89	.77
30°	.81	.74	.86	.82	.85	.78
20°	.78	.67	.87	.75	.77	.79
10°	.71	.70	.88	.86	.87	.79

Table B.7

MUF EXCEEDED 0.10 AND 0.90 OF THE HOURS
(Ratio of MUF to Monthly Median)

Sunspot Number: Low Season: Equinox	March, April, September, October					
Geog. Lat.	LOCAL TIME					
(N or S)	00	04	08	12	16	20
			Upper Decile			
80°	1.42	1.32	1.29	1.26	1.33	1.48
70°	1.38	1.25	1.25	1.23	1.26	1.40
60°	1.32	1.21	1.22	1.20	1.20	1.31
50°	1.26	1.19	1.20	1.18	1.16	1.26
40°	1.22	1.20	1.19	1.16	1.16	1.25
30°	1.22	1.26	1.18	1.15	1.16	1.28
20°	1.30	1.32	1.16	1.14	1.18	1.33
10°	1.23	1.40	1.13	1.13	1.19	1.16
			Lower Decile			
80°	.67	.72	.74	.73	.80	.65
70°	.70	.75	.76	.74	.82	.69
60°	.73	.78	.80	.75	.81	.73
50°	.75	.80	.81	.76	.81	.76
40°	.77	.81	.81	.77	.80	.78
30°	.78	.80	.82	.78	.81	.74
20°	.77	.75	.83	.81	.83	.69
10°	.76	.66	.86	.89	.86	.75

Table B.8

MUF EXCEEDED 0.10 AND 0.90 OF THE HOURS
(Ratio of MUF to Monthly Median)

Sunspot Number: Low Season: Summer			No. Hemis: May, June, July, Aug. So. Hemis: Jan., Feb., Nov., Dec.			
Geog. Lat. (N or S)	LOCAL TIME 00	04	08	12	16	20
			Upper Decile			
80°	1.26	1.24	1.15	1.17	1.21	1.22
70°	1.22	1.18	1.14	1.15	1.16	1.18
60°	1.18	1.17	1.14	1.15	1.14	1.15
50°	1.17	1.20	1.15	1.16	1.14	1.15
40°	1.17	1.25	1.17	1.17	1.15	1.16
30°	1.18	1.30	1.17	1.20	1.19	1.20
20°	1.20	1.34	1.14	1.24	1.22	1.23
10°	1.20	1.37	1.12	1.30	1.27	1.20
			Lower Decile			
80°	.68	.79	.84	.87	.85	.76
70°	.70	.81	.83	.86	.86	.77
60°	.72	.84	.83	.84	.86	.81
50°	.75	.85	.82	.83	.85	.84
40°	.79	.85	.80	.82	.83	.85
30°	.79	.82	.78	.80	.81	.80
20°	.77	.78	.77	.79	.79	.73
10°	.74	.75	.80	.83	.82	.69

Table B.9

Appendix C. Tables of the Distribution of Transmission Loss

EXPECTED EXCESS SYSTEM LOSS ABOVE QUASI-MINIMUM (dB)
(Winter - Paths < 2500 km)

G. M. Lat.	01-04 LMT Med.	01-04 LMT S_ℓ	01-04 LMT S_u	04-07 LMT Med.	04-07 LMT S_ℓ	04-07 LMT S_u
0-40°	9.0	4.0	9.0	9.0	4.0	7.6
40-45°	9.4	4.3	9.0	9.3	4.3	8.3
45-50°	9.9	4.7	9.1	9.6	4.6	9.0
50-55°	10.3	5.1	9.2	10.0	5.0	9.7
55-60°	11.0	5.3	10.0	13.5	6.7	9.6
60-65°	16.0	8.0	13.5	25.0	12.7	13.0
65-70°	15.2	7.7	14.6	24.6	13.5	13.2
70-75°	12.4	6.3	9.4	17.3	8.9	15.2
75-80°	11.0	5.6	9.4	15.6	7.7	8.8
	07-10 LMT			10-13 LMT		
0-40°	9.0	4.0	7.6	9.0	4.0	6.4
40-45°	10.1	4.6	8.6	9.1	4.5	7.1
45-50°	11.2	5.2	9.6	9.2	5.1	7.8
50-55°	12.2	5.9	10.7	9.3	5.7	8.7
55-60°	15.6	8.2	14.6	10.4	5.0	10.6
60-65°	23.0	12.3	23.7	12.6	6.8	20.5
65-70°	21.8	11.8	22.5	11.3	6.0	22.0
70-75°	17.6	9.9	14.3	9.9	5.4	13.9
75-80°	15.2	8.4	10.2	10.5	6.3	10.7

Table C. 1

EXPECTED EXCESS SYSTEM LOSS ABOVE QUASI-MINIMUM (dB)
(Winter - Paths < 2500 km)

G. M. Lat.	13 - 16 LMT Med.	S_ℓ	S_u	16 - 19 LMT Med.	S_ℓ	S_u
0-40°	9.0	4.0	6.4	9.0	4.0	7.6
40-45°	9.1	4.2	6.2	9.6	4.6	8.1
45-50°	9.2	4.4	6.5	10.2	5.2	8.6
50-55°	9.4	4.6	6.9	10.8	5.8	9.1
55-60°	9.8	4.8	7.2	11.7	6.5	9.0
60-65°	11.0	5.8	8.7	15.8	8.3	14.1
65-70°	10.5	5.4	8.2	13.6	7.8	11.3
70-75°	9.5	4.8	7.5	11.5	6.5	10.5
75-80°	9.5	4.7	6.7	10.4	5.4	8.6
	19 - 22 LMT			22 - 01 LMT		
0-40°	9.0	4.0	7.6	9.0	4.0	9.0
40-45°	9.7	4.6	7.9	9.3	4.2	9.1
45-50°	10.5	5.2	8.3	9.6	4.5	9.2
50-55°	11.8	5.8	8.7	9.9	4.8	9.3
55-60°	12.0	5.4	10.6	11.0	5.1	9.5
60-65°	18.8	8.9	17.2	15.6	7.2	9.9
65-70°	16.0	7.8	18.6	14.0	6.8	11.5
70-75°	12.0	5.8	14.8	12.0	6.0	9.0
75-80°	10.5	4.9	11.5	10.0	5.4	8.5

Table C. 2

EXPECTED EXCESS SYSTEM LOSS ABOVE QUASI-MINIMUM (dB)
(Winter - Paths > 2500 km)

	01-04 LMT			04-07 LMT		
G. M. Lat.	Med.	S_ℓ	S_u	Med.	S_ℓ	S_u
0-40°	9.0	4.0	9.0	9.0	4.0	7.6
40-45°	9.3	4.2	9.1	9.3	4.3	7.8
45-50°	9.6	4.4	9.3	9.6	4.6	8.0
50-55°	9.9	4.6	9.5	10.0	5.0	8.2
55-60°	10.6	4.7	9.6	11.4	5.5	8.3
60-65°	14.3	5.7	11.4	16.0	6.8	9.5
65-70°	14.5	6.5	10.2	14.0	6.3	10.9
70-75°	11.5	3.4	9.7	13.5	6.5	7.8
75-80°	10.5	5.1	9.2	11.7	5.9	8.1
	07-10 LMT			10-13 LMT		
0-40°	9.0	4.0	7.6	9.0	4.0	6.4
40-45°	9.4	4.2	9.0	9.0	4.2	7.3
45-50°	9.8	4.5	10.4	9.1	4.4	8.2
50-55°	10.3	4.8	11.9	9.1	4.6	9.2
55-60°	11.7	5.6	12.4	9.6	5.2	10.4
60-65°	14.9	7.3	14.1	11.0	5.2	15.2
65-70°	16.0	8.3	14.2	10.9	4.4	15.8
70-75°	13.3	6.8	11.2	9.8	4.8	11.2
75-80°	11.5	5.7	10.?	9.8	4.8	9.2

Table C. 3

EXPECTED EXCESS SYSTEM LOSS ABOVE QUASI-MINIMUM (dB)
(Winter - Paths > 2500 km)

	13-16 LMT			16-19 LMT		
G. M. Lat.	Med.	S_ℓ	S_u	Med.	S_ℓ	S_u
0-40°	9.0	4.0	6.4	9.0	4.0	7.6
40-45°	9.0	4.0	6.5	9.3	4.3	7.7
45-50°	9.1	4.1	6.7	9.6	4.7	7.8
50-55°	9.1	4.1	6.9	10.0	5.1	7.9
55-60°	9.4	4.6	7.4	10.7	5.5	7.6
60-65°	9.7	4.1	8.3	13.0	6.7	8.0
65-70°	9.5	5.1	7.7	12.0	6.2	7.3
70-75°	9.3	4.7	7.1	10.6	5.4	7.4
75-80°	8.8	4.4	7.0	9.9	5.0	7.5
	19-22 LMT			22-01 LMT		
0-40	9.0	4.0	7.6	9.0	4.0	9.0
40-45°	9.5	4.3	7.6	9.4	4.3	9.2
45-50°	10.0	4.6	7.6	9.5	4.6	9.4
50-55°	10.5	4.9	9.6	10.4	4.9	9.6
55-60°	10.8	5.0	7.9	12.5	5.3	9.8
60-65°	13.5	5.6	8.9	19.0	7.8	13.8
65-70°	13.5	6.1	8.5	18.6	8.6	11.1
70-75°	11.0	5.1	8.6	13.8	6.5	9.2
75-80°	9.8	4.8	8.2	10.6	5.0	9.7

Table C. 4

EXPECTED EXCESS SYSTEM LOSS ABOVE QUASI-MINIMUM (dB)
(Equinox - Paths < 2500 km)

G. M. Lat.	01-04 LMT Med.	S_ℓ	S_u	04-07 LMT Med.	S_ℓ	S_u
0-40°	9.0	4.0	9.0	9.0	4.0	9.0
40-45°	9.5	4.5	10.0	9.6	4.4	11.5
45-50°	10.1	5.0	11.1	10.3	4.8	14.1
50-55°	10.7	5.6	12.2	11.0	5.2	16.6
55-60°	11.4	5.7	17.6	13.4	6.4	22.0
60-65°	15.7	7.7	30.3	20.2	9.5	29.3
65-70°	15.5	8.1	28.0	21.0	11.1	31.0
70-75°	12.3	7.0	21.7	20.0	13.8	20.8
75-80°	10.4	6.1	15.5	11.5	7.5	18.7
	07-10 LMT			10-13 LMT		
0-40°	9.0	4.0	7.6	9.0	4.0	6.4
40-45°	10.6	5.3	9.8	10.0	4.7	9.0
45-50°	12.3	6.6	12.0	11.0	5.4	11.6
50-55°	14.0	8.0	14.3	12.0	6.2	14.2
55-60°	16.5	8.3	15.3	14.0	7.6	18.3
60-65°	26.0	14.0	23.4	18.0	10.6	33.0
65-70°	30.4	18.2	26.9	17.5	10.0	27.9
70-75°	20.6	12.8	20.2	14.1	8.8	18.9
75-80°	16.4	9.7	14.4	12.8	7.5	13.6

Table C.5

EXPECTED EXCESS SYSTEM LOSS ABOVE QUASI-MINIMUM(dB)
(Equinox - Paths < 2500 km)

G. M. Lat.	13-16 LMT Med.	S_ℓ	S_u	16-19 LMT Med	S_ℓ	S_u
0-40°	9.0	4.0	6.4	9.0	4.0	7.6
40-45°	9.7	4.5	8.9	10.3	5.0	11.3
45-50°	10.4	5.0	11.4	11.6	6.0	15.0
50-55°	11.2	5.6	13.9	13.0	7.0	18.7
55-60°	11.6	5.6	15.5	13.8	7.5	20.2
60-65°	16.2	8.3	19.2	18.0	10.3	27.0
65-70°	13.8	7.0	18.0	15.0	8.4	24.0
70-75°	11.6	6.2	14.2	13.0	7.2	18.0
75-80°	10.0	5.4	12.0	11.4	6.2	14.1
	19-22 LMT			22-01 LMT		
0-40°	9.0	4.0	7.6	9.0	4.0	9.0
40-45°	10.0	4.8	10.0	10.3	4.7	10.0
45-50°	11.0	5.6	12.5	11.6	5.4	11.0
50-55°	12.0	6.4	15.0	13.0	6.2	12.0
55-60°	14.5	7.7	19.5	15.1	7.4	13.3
60-65°	19.9	11.3	29.0	24.0	13.0	26.7
65-70°	19.0	11.3	28.8	22.7	11.2	17.5
70-75°	15.0	8.6	22.0	16.0	8.0	16.5
75-80°	11.4	6.4	20.6	12.3	6.3	15.7

Table C.6

EXPECTED EXCESS SYSTEM LOSS ABOVE QUASI-MINIMUM (dB)

(Equinox - Paths > 2500 km)

	01-04 LMT			04-07 LMT		
G. M. Lat.	Med.	S_ℓ	S_u	Med.	S_ℓ	S_u
0-40°	9.0	4.0	9.0	9.0	4.0	7.6
40-45°	9.3	4.1	10.0	9.3	4.1	8.5
45-50°	9.6	4.2	11.0	9.6	4.2	9.4
50-55°	9.9	4.4	12.1	9.9	4.3	10.3
55-60°	10.4	4.5	13.2	11.0	4.6	10.6
60-65°	12.9	5.7	15.5	14.2	5.9	10.8
65-70°	12.7	5.7	14.3	14.6	6.6	10.6
70-75°	10.8	4.9	13.1	11.9	5.3	9.8
75-80°	10.0	4.8	11.0	10.2	4.6	9.0
	07-10 LMT			10-13 LMT		
0-40°	9.0	4.0	7.6	9.0	4.0	6.4
40-45°	9.6	4.2	8.3	9.6	4.4	7.9
45-50°	10.2	4.5	9.0	10.3	4.9	9.4
50-55°	10.8	4.8	9.7	11.0	5.4	11.0
55-60°	12.2	5.7	9.8	12.8	6.3	11.2
60-65°	16.6	7.9	11.4	18.0	9.4	15.7
65-70°	16.7	7.7	13.8	17.1	9.0	13.4
70-75°	13.1	6.1	10.9	14.7	7.7	12.4
75-80°	11.7	5.7	10.6	12.0	6.5	12.2

Table C.7

EXPECTED EXCESS SYSTEM LOSS ABOVE QUASI-MINIMUM (dB)
(Equinox - Paths > 2500 km)

	13-16 LMT			16-19 LMT		
G. M. Lat.	Med.	S_ℓ	S_u	Med	S_ℓ	S_u
0-40°	9.0	4.0	6.4	9.0	4.0	7.6
40-45°	9.4	4.3	8.8	10.0	4.5	9.0
45-50°	9.8	4.6	11.2	11.0	4.9	10.4
50-55°	10.3	5.0	13.7	12.1	5.4	11.9
55-60°	10.8	5.1	14.2	13.0	5.7	12.0
60-65°	14.0	6.5	17.2	16.5	7.5	14.2
65-70°	12.5	5.7	17.3	14.0	6.5	13.3
70-75°	10.5	4.9	15.9	12.2	5.8	12.5
75-80°	9.6	5.0	14.8	11.0	5.5	11.0
	19-22 LMT			22-01 LMT		
0-40°	9.0	4.0	7.6	9.0	4.0	9.0
40-45°	9.9	4.3	8.9	9.6	4.2	10.6
45-50°	10.8	4.6	10.2	10.3	4.4	12.3
50-55°	11.7	5.0	11.6	11.0	4.7	14.0
55-60°	14.4	6.2	12.4	12.4	5.1	17.5
60-65°	19.0	8.5	16.7	16.9	7.5	22.1
65-70°	18.5	8.5	16.0	16.3	7.1	17.5
70-75°	14.6	6.9	13.8	12.6	5.6	16.3
75-80°	11.3	5.5	13.7	10.6	4.9	15.6

Table C.8

EXPECTED EXCESS SYSTEM LOSS ABOVE QUASI-MINIMUM (dB)
(Summer - Paths < 2500 km)

G. M. Lat.	01-04 LMT Med.	S_ℓ	S_u	04-07 LMT Med.	S_ℓ	S_u
0-40°	9.0	4.0	9.0	9.0	4.0	7.6
40-45°	9.8	4.4	9.8	9.6	4.3	9.9
45-50°	10.6	4.8	10.6	10.2	4.7	12.2
50-55°	11.5	5.3	11.4	10.8	5.1	14.6
55-60°	12.2	5.5	17.8	11.7	5.5	16.1
60-65°	15.5	7.5	24.5	13.8	5.8	22.7
65-70°	13.9	6.5	22.1	13.2	6.2	21.8
70-75°	11.4	5.4	15.6	12.0	5.8	15.0
75-80°	11.2	5.7	12.8	11.7	6.0	11.3
	07-10 LMT			10-13 LMT		
0-40°	9.0	4.0	7.6	9.0	4.0	6.4
40-45°	9.8	4.7	9.1	9.7	4.5	7.2
45-50°	10.6	5.5	10.7	10.5	5.0	8.1
50-55°	11.4	6.3	12.3	11.3	5.5	9.0
55-60°	13.0	7.2	15.6	12.0	6.0	10.6
60-65°	18.0	10.7	26.0	15.0	7.8	18.8
65-70°	15.2	9.2	26.7	13.5	6.7	19.5
70-75°	11.8	6.8	18.2	12.0	6.2	12.0
75-80°	10.2	5.3	16.8	11.3	5.7	9.5

Table C.9

EXPECTED EXCESS SYSTEM LOSS ABOVE QUASI-MINIMUM (dB)
(Summer - Paths < 2500 km)

	13-16 LMT			16-19 LMT		
G. M. Lat.	Med.	S_ℓ	S_u	Med.	S_ℓ	S_u
0-40°	9.0	4.0	6.4	9.0	4.0	7.6
40-45°	9.8	4.5	8.1	10.6	5.1	8.6
45-50°	10.7	5.0	9.8	12.3	6.2	9.7
50-55°	11.6	5.5	11.6	14.0	7.3	10.8
55-60°	12.0	5.8	13.5	15.5	8.5	11.0
60-65°	13.8	6.2	19.9	18.1	9.1	14.2
65-70°	12.8	5.7	16.6	14.4	7.2	13.8
70-75°	11.7	5.5	13.3	13.2	6.9	11.1
75-80°	11.2	5.3	12.1	12.8	7.0	10.2
	19-22 LMT			22-01 LMT		
0-40°	9.0	4.0	7.6	9.0	4.0	9.0
40-45°	10.5	4.9	9.5	10.3	4.7	10.0
45-50°	12.1	5.9	11.4	11.6	5.4	11.0
50-55°	13.6	6.9	13.4	13.0	6.1	12.0
55-60°	15.7	7.8	14.1	14.0	6.4	15.0
60-65°	18.5	10.1	20.5	17.9	8.9	21.1
65-70°	16.7	7.9	21.9	16.2	7.8	19.0
70-75°	13.8	7.6	17.8	13.5	6.8	16.0
75-80°	13.2	7.2	11.8	12.8	6.8	12.7

Table C.10

EXPECTED EXCESS SYSTEM LOSS ABOVE QUASI-MINIMUM (dB)
(Summer - Paths > 2500 km)

	01-04 LMT			04-07 LMT		
G. M. Lat.	Med.	S_ℓ	S_u	Med.	S_ℓ	S_u
0-40°	9.0	4.0	9.0	9.0	4.0	7.6
40-45°	9.7	4.4	9.1	9.8	4.4	9.1
45-50°	10.4	4.8	9.2	10.6	4.9	10.6
50-55°	11.2	5.2	9.4	11.4	5.4	12.2
55-60°	11.8	5.4	9.6	12.8	6.2	13.0
60-65°	14.5	6.7	9.8	17.5	8.8	16.8
65-70°	13.4	6.1	10.0	15.3	7.4	16.7
70-75°	10.9	4.8	8.9	13.6	6.5	11.9
75-80°	10.8	5.3	8.2	12.8	6.0	10.0
	07-10 LMT			10-13 LMT		
0-40°	9.0	4.0	7.6	9.0	4.0	6.4
40-45°	9.7	4.5	8.1	9.3	4.2	6.9
45-50°	10.4	5.0	8.6	9.6	4.4	7.5
50-55°	11.2	5.6	9.2	10.0	4.7	8.1
55-60°	12.7	6.5	9.7	10.4	4.9	9.2
60-65°	16.6	9.3	13.8	11.6	5.6	13.1
65-70°	14.9	8.2	14.5	10.9	5.4	13.1
70-75°	11.9	5.9	11.1	10.3	5.0	10.1
75-80°	11.2	5.5	10.1	10.1	4.8	8.6

Table C.11

EXPECTED EXCESS SYSTEM LOSS ABOVE QUASI-MINIMUM (dB)
(Summer - Paths > 2500 km)

	13-16 LMT			16-19 LMT		
G. M. Lat.	Med.	S_ℓ	S_u	Med.	S_ℓ	S_u
0-40°	9.0	4.0	6.4	9.0	4.0	7.6
40-45°	9.7	4.5	7.6	9.4	4.2	8.1
45-50°	10.4	5.0	8.8	9.8	4.5	8.6
50-55°	11.2	5.6	10.1	10.2	4.8	9.1
55-60°	11.7	5.9	12.3	10.6	5.1	9.7
60-65°	13.2	6.8	17.4	12.2	6.1	11.3
65-70°	12.3	6.3	14.0	10.7	5.4	10.4
70-75°	11.2	5.5	12.2	10.3	5.1	9.0
75-80°	11.1	5.4	11.4	10.2	5.0	8.2
	19-22 LMT			22-01 LMT		
0-40°	9.0	4.0	7.6	9.0	4.0	9.0
40-45°	10.4	4.9	8.2	9.8	4.4	9.6
45-50°	11.9	5.8	8.9	10.6	4.9	10.3
50-55°	13.4	6.7	9.6	11.5	5.4	11.0
55-60°	13.5	6.8	11.8	12.2	5.7	13.4
60-65°	14.5	7.1	17.2	14.7	7.2	18.4
65-70°	13.4	6.4	15.2	13.5	6.4	15.1
70-75°	11.8	5.8	12.3	11.7	5.3	12.1
75-80°	11.3	5.6	9.9	11.4	5.5	10.3

Table C.12

Appendix D: Tables of Prediction Errors in Excess System Loss Above Quasi-Minimum (dB)

Winter Months

Geomag. Lat.	01-07 LMT σ_p	01-07 LMT σ_{su}	01-07 LMT $\sigma_{s\ell}$	07-13 LMT σ_p	07-13 LMT σ_{su}	07-13 LMT $\sigma_{s\ell}$
0-40°	5.60	.60	1.63	3.10	.80	1.89
40-45°	5.61	.62	1.65	3.13	.62	2.16
45-50°	5.71	.65	1.66	3.28	.68	2.25
50-55°	5.80	.68	1.67	3.30	.78	2.30
55-60°	5.75	.88	1.88	3.58	1.26	4.50
60-65°	6.75	2.48	2.05	5.15	2.48	5.48
65-70°	6.82	2.50	2.16	4.93	2.49	5.31
70-75°	5.93	1.85	2.92	4.10	1.80	2.96
75-80°	5.83	2.08	2.08	3.63	1.27	2.07
	13-19 LMT			19-01 LMT		
0-40°	3.10	.60	1.68	5.60	.60	1.66
40-45°	3.20	.85	1.78	5.62	.63	1.67
45-50°	3.32	.87	1.80	5.64	.65	1.70
50-55°	3.56	1.00	2.30	5.65	.72	1.75
55-60°	4.08	1.25	2.90	5.66	1.00	1.80
60-65°	7.43	2.65	3.62	5.97	1.35	3.65
65-70°	5.03	1.73	3.66	5.91	1.09	4.10
70-75°	4.12	1.25	6.06	5.80	.67	2.80
75-80°	3.45	1.23	2.05	5.63	.63	2.75

Table D.1

Prediction Errors in Excess System Loss
Above Quasi-Minimum (dB)

Summer Months

Geomag. Lat.	01-07 LMT σ_p	σ_{su}	σ_{sl}	07-13 LMT σ_p	σ_{su}	σ_{sl}
0-40°	5.60	.60	1.65	3.10	.60	1.61
40-45°	5.63	.65	1.68	3.21	.62	1.66
45-50°	5.70	.78	1.81	3.30	.73	1.80
50-55°	5.86	1.07	2.57	3.47	1.00	2.06
55-60°	5.88	1.35	3.01	3.94	1.52	2.67
60-65°	6.56	2.57	4.84	5.71	2.86	4.73
65-70°	6.42	2.05	4.51	4.87	2.16	6.38
70-75°	5.88	1.40	2.76	3.67	1.26	2.95
75-80°	5.85	1.25	2.01	3.55	1.24	2.90
	13-19 LMT			19-01 LMT		
0-40°	3.10	.60	1.68	5.60	.60	1.66
40-45°	3.25	.73	1.77	5.63	1.25	1.85
45-50°	4.52	1.22	1.92	6.10	2.28	2.34
50-55°	4.58	1.71	2.30	6.15	3.29	3.05
55-60°	5.15	2.27	2.62	8.02	3.31	3.40
60-65°	8.62	3.78	4.36	8.00	3.85	3.40
65-70°	5.22	2.09	3.22	7.80	2.25	2.95
70-75°	4.40	1.72	2.61	6.56	1.99	2.83
75-80°	4.25	1.65	2.57	6.32	1.72	2.05

Table D.2

Prediction Errors in Excess System Loss
Above Quasi-Minimum (dB)

Equinox Months

Geomag. Lat.	01-07 LMT σ_p	σ_{su}	$\sigma_{s\ell}$	07-13 LMT σ_p	σ_{su}	$\sigma_{s\ell}$
0-40°	5.60	.60	1.63	3.10	.60	1.60
40-45°	5.68	.62	1.71	3.28	.61	1.76
45-50°	5.69	.65	2.02	3.34	1.00	2.42
50-55°	5.92	1.24	2.61	3.75	1.52	3.08
55-60°	6.38	1.82	4.09	4.40	1.81	3.28
60-65°	9.05	3.28	6.45	5.70	7.65	7.35
65-70°	9.92	4.54	7.26	7.75	4.85	8.62
70-75°	7.10	3.05	4.98	4.93	2.49	5.48
75-80°	5.87	1.35	3.62	4.35	2.09	3.08
	13-19 LMT			19-01 LMT		
0-40°	3.10	.60	1.68	5.60	.60	1.66
40-45°	3.32	.72	1.77	5.63	.63	1.68
45-50°	3.87	1.25	2.38	5.70	.72	1.95
50-55°	4.98	1.73	2.84	5.78	.91	2.24
55-60°	5.63	1.75	2.85	6.27	1.35	2.96
60-65°	7.85	3.75	5.06	8.30	2.28	5.30
65-70°	6.45	2.69	4.50	7.81	2.29	5.71
70-75°	4.85	1.73	2.93	5.32	1.35	3.45
75-80°	3.89	1.25	2.61	5.92	1.07	2.78

Table D.3

APPENDIX E: TABLES OF THE PREDICTION ERRORS IN THE ATMOSPHERIC RADIO NOISE LEVELS

Numerical Coefficients for use in Evaluation of the
Standard Deviation of the Median Value of the Atmospheric Radio Noise (σ_{FAM})

DEC-JAN-FEB

LMT	A1	A2	A3	A4	A5
00-04	0.743378714E 00	0.184805028E 01	-0.890621021E 00	-0.199749105E 01	0.452507 41E 01
04-08	-0.428241640E-00	0.302301746E-00	0.742823556E 00	-0.160900280E 01	0.417567089E 01
08-12	-0.342594393E-00	0.585453220E 00	0.177053191E 01	-0.985735320E 00	0.445040822E 01
12-16	-0.109962426E 01	-0.410155922E-00	0.272162378E 01	-0.191081896E-00	0.466347449E 01
16-20	-0.225827657E-00	0.262166932E-00	0.212718993E-00	-0.114418842E 01	0.468955919E 01
20-24	0.735802598E 00	0.143983714E 01	-0.177913114E 01	-0.191274747E 01	0.529730834E 01

MAR-APR-MAY

00-04	0.168881863E-00	0.653290711E 00	0.919879317E-01	-0.640682638E 00	0.367957190E 01
04-08	0.136798099E 01	0.256033473E 01	-0.222543932E 01	-0.292736776E 01	0.497451954E 01
08-12	0.114860554E 01	0.282529637E 01	-0.154908501E 01	-0.383357443E 01	0.603194296E 01
12-16	0.557916760E 00	0.171872430E 01	-0.111953944E 01	-0.284309931E 01	0.663044795E 01
16-20	-0.719275042E-01	0.119483747E 01	0.787773415E 00	-0.246702715E 01	0.451285884E 01
20-24	-0.104107969E-00	0.258123524E-00	0.256637678E-00	-0.575033508E 00	0.388958767E 01

JUN-JUL-AUG

00-04	0.441078149E-00	0.754692435E 00	-0.149458855E 01	-0.123047307E 01	0.552806072E 01
04-08	0.179996520E 01	0.285386428E 01	-0.427601837E 01	-0.421216518E 01	0.702823602E 01
08-12	0.122893803E 01	0.264190425E 01	-0.285555728E 01	-0.389196001E 01	0.766424164E 01
12-16	0.975428268E 00	0.875660010E 00	-0.440645486E 01	-0.204496071E 01	0.902339548E 01
16-20	0.147046417E 01	0.320094123E 1	-0.152497672E 01	-0.313552327E 01	0.587586746E 01
20-24	0.193232499E-01	-0.494468227E-00	-0.143067203E 01	0.118104860E-00	0.482582383E 01

SEP-OCT-NOV

00-04	0.507301651E 00	0.168124154E 01	0.292957835E-01	-0.211237140E 01	0.387806118E 01
04-08	-0.111660779E-01	0.110631615E 01	0.733433887E 00	-0.185950108E 01	0.449588954E 01
08-12	0.279820472E-00	0.177786238E 01	0.746843509E 00	-0.243937045E 01	0.494175017E 01
12-16	0.212440260E-00	0.130495265E 01	-0.603454560E-02	-0.221374713E 01	0.604905583E 01
16-20	0.820952326E-01	0.142235264E 01	0.685795024E 00	-0.248459294E 01	0.444219068E 01
20-24	0.425375693E-00	0.118228056E 01	-0.472298205E-00	-0.142878741E 01	0.427190468E 01

Table E. 1

Numerical Coefficients for use in Evaluation of the
Standard Deviation of the Lower Decile Value of the Atmospheric Radio Noise (σ_{0L})

DEC-JAN-FEB

LMT	A1	A2	A3	A4	5
00-04	0.126903839E-00	0.268784523E-01	-0.770941772E 00	0.226284616E-01	0.248547509E 01
04-08	0.614280351E 00	0.571794346E 00	-0.235540621E 01	-0.100524604E 01	0.404069029E 01
08-12	-0.119744711E-00	-0.151770540E-01	-0.408071324E-00	-0.438921601E-00	0.347453326E 01
12-16	0.248158284E-00	0.202147439E-00	-0.149445355E 01	-0.538424484E 00	0.379969291E 01
16-20	0.511611715E 00	0.347771183E-00	-0.232742615E 01	-0.632404819E 00	0.429346301E 01
20-24	-0.343667753E-00	-0.414469182E-00	0.343420424E-00	0.494972602E-00	0.241308816E 01

MAR-APR-MAY

00-04	-0.794446878E-01	-0.421281464E-01	-0.106715105E-00	-0.450396530E-00	0.275694132E 01
04-08	0.400024898E-00	0.417995073E-00	-0.156035453E 01	-0.869965412E 00	0.369666651E 01
08-12	0.996029027E 00	0.112321563E 01	-0.368354186E 01	-0.221056826E 01	0.577246509E 01
12-16	0.795788229E 00	0.912118189E 00	-0.388409697E 01	-0.251609661E 01	0.719725356E 01
16-20	0.416648589E-00	0.821669541E 00	-0.199944861E 01	-0.223434053E 01	0.521205023E 01
20-24	0.137419797E-00	0.572643824E 00	-0.345254064E-00	-0.150924332E 01	0.284753665E 01

JUN-JUL-AUG

00-04	0.232037783E-00	0.183978885E-00	-0.116380252E 01	-0.550627425E 00	0.294488624E 01
04-08	0.686566405E 00	0.435190804E-00	-0.290795319E 01	-0.878486626E 00	0.455869719E 01
08-12	0.760253631E 00	0.494537182E-00	-0.318958737E 01	-0.969694585E 00	0.499248818E 01
12-16	0.956413560E 00	0.375092655E-00	-0.436183646E 01	-0.729335889E 00	0.636322550E 01
16-20	0.680901885E 00	0.331788123E-00	-0.308259986E 01	-0.609270409E 00	0.496306434E 01
20-24	0.302133366E-01	0.200020753E-00	-0.166200176E-00	-0.521769941E 00	0.197851606E 01

SEP-OCT-NOV

00-04	-0.104325563E-00	0.796536148E-01	-0.663267933E-01	-0.221127994E-00	0.244773269E 01
04-08	0.547741719E 00	0.505893320E 00	-0.187324695E 01	-0.747519873E 00	0.365203135E 01
08-12	0.927719198E 00	0.123640932E 01	-0.299950309E 01	-0.222165659E 01	0.514313728E 01
12-16	0.403634302E-00	0.695742287E 00	-0.198731989E 01	-0.177995436E 01	0.532870464E 01
16-20	0.148200716E-00	0.170572110E-00	-0.108537078E 01	-0.747056834E 00	0.383925848E 01
20-24	0.208183080E-01	0.125692286E-00	-0.290533783E-00	-0.662367195E 00	0.244939230E 01

Table E. 2

Numerical Coefficients for use in Evaluation of the
Standard Deviation of the Upper Decile Value of the Atmospheric Radio Noise (σ_{Du})

DEC-JAN-FEB

LMT	A1	A2	A3	A4	A5
00-04	0.586943351E 00	0.910162516E 00	-0.144566191E 01	-0.979272597E 00	0.320931919E 01
04-08	0.688151143E 00	0.149756305E 01	-0.147183307E 01	-0.217741162E 01	0.371525072E 01
08-12	0.667779170E 00	0.149890840E 01	-0.188272089E 01	-0.231266074E 01	0.518980362E 01
12-16	0.637561329E 00	0.154565722E 01	-0.159769915E 01	-0.217260964E 01	0.513590842E 01
16-20	0.272472672E-00	0.134363256E 01	-0.234189205E-00	-0.202113360E 01	0.372760497E 01
20-24	0.201482765E-00	0.709483206E 00	-0.493239917E-00	-0.963045754E 00	0.327556841E 01

MAR-APR-MAY

00-04	0.292769849E-00	0.588746786E 00	-0.399141528E-00	-0.827666216E 00	0.261711352E 01
04-08	0.121490076E 01	0.155130342E 01	-0.327356338E 01	-0.227473855E 01	0.483125739E 01
08-12	0.888090961E 00	0.104199968E 01	-0.334305115E 01	-0.175927393E 01	0.627552070E 01
12-16	0.510004684E 00	0.166034453E-00	-0.306647375E 01	-0.646327630E 00	0.690507919E 01
16-20	0.783328645E 00	0.768176310E 00	-0.290280811E 01	-0.155713499E 01	0.553902552E 01
20-24	0.239283971E-00	0.681584917E 00	-0.304963708E-00	-0.122300893E 01	0.269532323E 01

JUN-JUL-AUG

00-04	0.396174334E-00	0.566412203E 00	-0.116124064E 01	-0.792149663E 00	0.278699666E 01
04-08	0.787777245E 00	0.107464857E 01	-0.281629033E 01	-0.192216516E 01	0.480765678E 01
08-12	0.476864338E-00	0.300840043E-00	-0.257711329E 01	-0.614124849E 00	0.541122749E 01
12-16	0.294015385E-00	-0.609974310E 00	-0.290586174E 01	0.986588866E 00	0.631988645E 01
16-20	0.785735734E 00	0.705832422E 00	-0.332976483E 01	-0.124018416E 01	0.563061409E 01
20-24	0.576981798E 00	0.110841028E 01	-0.134596676E 01	-0.171088234E 01	0.270139502E 01

SEP-OCT-NOV

00-04	0.248493604E-00	0.485689573E-00	-0.744257100E 00	-0.847143218E 00	0.271591507E 01
04-08	0.846005708E 00	0.108394101E 01	-0.260228969E 01	-0.170797855E 01	0.439020723E 01
08-12	0.426887305E-00	0.161761276E-00	-0.255402632E 01	-0.525121868E 00	0.576006070E 01
12-16	0.350895122E-00	0.363107026E-02	-0.258306339E 01	-0.531404689E 00	0.598092720E 01
16-20	0.537617147E 00	0.877537653E 00	-0.189475365E 01	-0.172579959E 01	0.452223852E 01
20-24	0.160974182E-01	0.437416337E-00	-0.768397138E-02	-0.858681470E 00	0.262707986E 01

Table E.3

GPO 831-552